TECHNISCHE UNIVERSITÄT DRESDEN

Fakultät Forst-, Geo- und Hydrowissenschaften

Modelling reactive transport processes in porous media

Dissertation zur Erlangung des akademischen Grades
Doctor rerum naturalium (Dr. rer. nat.)

vorgelegt von
M.Sc. Haibing Shao
geboren am 20.07.1983 in Shanghai

Gutachter:

Herr Prof. Dr.-Ing. Olaf Kolditz
Technische Universität Dresden

Herr Prof. Dr. Sebastian Bauer
Christian-Albrechts-Universität zu Kiel

Leipzig, Dezember 2009

Erklärung des Promovenden

Die Übereinstimmung dieses Exemplars mit dem Original der Dissertation zum Thema:

„Modelling reactive transport processes in porous media"

wird hiermit bestätigt.

……………………………………..…
Ort, Datum

……………………………………..…
Unterschrift (Vorname Name)

Modelling reactive transport processes in porous media

Haibing Shao

Abstract

Reactive transport modelling has wide applications in geosciences. In the field of hydrogeology, it has been utilised to simulate the biogeochemical processes that disperse and degrade contaminants in the aquifer. For geotechnical applications, such as geological CO_2 sequestration, the reaction of CO_2 with the ambient saline aquifer determines the final success of storage. In a radioactive waste repository, scientists rely on reactive transport models to predict the mobilisation of hazardous radionuclides within space and time.

In this work, the multi-component mass transport code OpenGeoSys[1], was coupled with two geochemical solvers, the Gibbs Energy Minimization Selektor (GEM)[2] and the Biogeochemical Reaction Network Simulator (BRNS). Both coupled codes were verified against analytical solutions and simulation results from other numerical models. Moreover, the coupling interface was developed for parallel simulation. Test runs showed that the speed-up of reaction part had a very good linearity with number of nodes in the mesh. However, for three dimensional problems with complex geochemical reactions, the model performance was dominated by solving transport equations of mobile chemical components.

OpenGeoSys-BRNS was applied to a two dimensional groundwater remediation problem. Its calculated concentration profiles fitted very well with analytical solutions and numerical results from TBC. The model revealed that natural attenuation of groundwater contaminants is mainly controlled by the mixing of carbon source and electron donor. OpenGeoSys-GEM was employed to investigate the retardation mechanism of radionuclides in the near field of a nuclear waste repository. Radium profiles in an idealised bentonite column was modelled with varying clay/water ratios. When clay content is limited, Ba-Sr-Ra sulfate solid solutions have a very strong retardation effect on the aqueous radium. Nevertheless, when clay mineral is abundant, cation exchange sites also attract Sr and Ba, thus dominates the transport of Ra.

---

[1]http://www.opengeosys.net/
[2]http://gems.web.psi.ch/

Contents

List of abbreviations and mathematical symbols

a	activity of aqueous species	$[-]$
C	solute concentration	$[\text{kg m}^{-3}]$
C_s	concentration of sorbed species	$[\text{kg kg}^{-1}]$
D_d	molecular diffusion coefficient	$[\text{m}^2 \text{ s}^{-1}]$
D^*	effective diffusion coefficient	$[\text{m}^2 \text{ s}^{-1}]$
G°	standard Gibbs formation energy	$[\text{mol}]$
h	hydraulic head	$[\text{m}]$
K	in transport equations, hydraulic conductivity	$[\text{m s}^{-1}]$
K	in chemical reactions, equilibrium constant	$[-]$
K_D	distribution coefficient	$[\text{L kg}^{-1}]$
M	mass of fluid	$[\text{kg}]$
m	molality of a chemical component	$[\text{mol}]$
n	in transport equations, porosity	$[-]$
n	in chemical reactions, mole amount	$[\text{mol}]$
P	pressure, or partial pressure of a gas component	$[\text{Pa}]$
Q	flow rate	$[\text{m}^3 \text{ s}^{-1}]$
R	in transport equations, retardation coefficient	$[-]$
R	in chemical reactions, ideal gas constant	$[\text{J K}^{-1} \text{ mol}^{-1}]$
S	storativity	$[-]$
S_y	specific yield	$[\text{m}^{-1}]$
T	transmissivity	$[\text{m}^2 \text{ s}^{-1}]$
T_K	temperature in Kelvin	$[\text{K}]$
x	fugacity coefficient	$[-]$
α_L	longitudinal dispersivity	$[\text{m}]$
α_T	transverse dispersivity	$[\text{m}]$
γ	activity coefficient	$[-]$
μ	chemical potential	$[\text{J mol}^{-1}]$
ω	tortuosity factor	$[-]$
θ	symmetric interaction parameters	$[-]$
ρ	density	$[\text{kg m}^{-3}]$
χ	molar fraction of end member in solid solution phase	$[-]$

GEM	gibbs energy minimization
LMA	law of mass action
MPI	message parsing interface
REV	representative elementary volume
SI	sequential iterative
SNI	sequential non − iterative

1 Introduction

1.1 State of the art

In the subsurface, due to the low permeability of the porous media, the transport of geofluid is relatively slow (usually in a scale of meters per year), compared to the speed on the surface (meters per minute or second). At the mean time, the chemical components that transport with the fluid, are subject to the change of geochemical environment and also participates in the corresponding chemical reactions. Such processes, that fall into the time scale of both mass transport and chemical reactions, are referred to as reactive transport.

With the growing capacity of computational resources, reactive transport models have gained their influence in multiple application fields. For ground water contamination sites, modelling the microorganism activities, mainly biogeochemical reactions, are important for the remediation and natural attenuation of contaminants (Cirpka and Valocchi, 2007; Mayer et al., 2002). In nuclear waste repositories, the chemical reactions that fixes radionuclides in the buffering material, has a crucial effect on the risk assessment of such engineering design (Xie et al., 2006). For the geological sequestration of carbon dioxide, the reactions between CO_2 and aquifer minerals, determines whether CO_2 can be fixed as mineral form in a geological time scale (Xu et al., 2004; Pruess et al., 2004; Lagneau et al., 2005).

To simulate these processes, various models that couple chemistry with mass transport have been developed in the past. Based on the methodology used for simulation of chemical processes, they can be divided into two groups, Law of Mass Action (LMA) and Gibbs Energy Minimization (GEM) approach. Generally, they are complementary with advantages and disadvantages on both sides. The majority of coupled codes use the LMA approach (Bethke, 1996). Some known codes that use this approach are TBC (Schäfer et al., 1998), MIN3P (Mayer et al., 2002), TOUGHREACT (Xu and Pruess, 2001), PHT3D (Prommer, 2002), HYTEC (Van der Lee et al., 2003), SHEMAT (Clauser, 2003), CRUNCH (Steefel et al., 2005), and OpenGeoSys (Kolditz and Bauer, 2004). Only recently, the integration of GEM chemical solvers in coupled codes has been attempted (Cleverley et al., 2006; Guimares et al., 2007) with various degree of success. The advantages and shortcuts of these two approaches will be discussed in section 2.3.

1.2 Objective and scope

Although reactive transport models have achieved various success in explaining coupled subsurface systems, many challenges still remain. Just to name a few:

- For biochemical processes that are involved in groundwater remediation processes, reaction networks need to be set in a flexible way, i.e. users should be able to define various chemical reactions and their corresponding equilibrium/kinetic coefficients.

- The traditional Law of Mass Action (LMA) code is reported to have difficulties in solving certain systems such as redox sensitive problems and chemical environment involving various non-ideal solid solutions, thus limiting the possibility to explore complex mineral-water interactions that contribute to the retardation of radionuclides.

- The chemical processes need to be solved on each grid of the domain, thus requiring large computational resources. The constrains on computational resources keep the model away

1

from solving reactive transport problems in a field/catchment scale.

This PhD work focuses on tackling these challenges. (1) The Biogeochemical Reaction Network Simulator (BRNS), in which the user could define the chemical system, was coupled to OpenGeoSys, verified against the analytical solution, and applied to a groundwater remediation problem. (2) The chemical solver GEMIPM2K, which is based on Gibbs Energy Minimization (GEM) approach, is coupled with mass transport software OpenGeoSys. The coupled code is employed to simulate chemical processes in the near field of a radioactive waste repository, helping identify the main fixation mechanism. (3) A parallel scheme is implemented for both chemical solvers and can be adopted to solve problems with domains of large sizes. The efficiency of the scheme is tested and further developments are discussed.

1.3 Dissertation organisation

This dissertation is organised in the following. Section 2 describes the mathematical background of reactive transport problems and related governing equations. Section 3 documents the technical details regarding the coupling and parallelization of OpenGeoSys-GEM and OpenGeoSys-BRNS. Section 4 introduces the applications of the coupled codes. Publications produced by this work are included at the end.

2 Theory of reactive transport model

2.1 Flow and transport

2.1.1 Equations of ground water flow

Darcy's Law   In the mid-1800s, French engineer Henry Darcy, studied the movement of water through a porous medium. He found out that if h_A and h_B are the hydraulic head [m] on the inlet and outlet of a sand column with length L [m], the flow Q [m^3 s^{-1}] is proportional to the cross-sectional area of the pipe, A [m^2]. When combined with the proportionality constant, K [m s^{-1}], the result is the expression known as Darcy's law:

$$Q = -KA \left(\frac{h_A - h_B}{L} \right) \tag{1}$$

This may also be expressed in a more general term as

$$Q = -KA \left(\frac{dh}{dl} \right) \tag{2}$$

where dh/dl is known as the hydraulic gradient. The quantity dh represents the change in hydraulic head between two points that are very close together, and dl is the small distance between these points. The negative sign indicates that flow is in the direction of decreasing hydraulic head. If the flow rate q [m s^{-1}] is expressed in per unit cross section,

$$q = \frac{Q}{A} = -K \left(\frac{dh}{dl} \right) \tag{3}$$

Representative Elementary Volume (REV)   For the modelling of groundwater flow, it is not possible to catch all the microscopic structure of the porous media. To understand and formulate the dynamics of fluid in the subsurface, the representative elementary volume (REV) is introduced. Parameters are averaged over such a volume that is sufficiently large to describe the porous medium at macroscopic scales (see Fig. 1). Within the REV the detailed structure of the medium is lost and becomes a continuous field. Parameters like porosity, permeability or dispersivity are considered constant over the averaging volume. In the following sections material parameters and governing equations are based on this continuum approach.

Confined Aquifer   The governing equation for flow in confined aquifer is derived from two basic laws of physics, which is the law of mass conservation and the law of energy conservation. The former states that there can be no net change in the mass of a fluid contained in a small volume of an aquifer, and the latter states that the amount of energy is a constant within any closed system. Assuming a very small piece of the confined aquifer, called a controlled volume, the three sides are of the length dx, dy, and dz, respectively. The area of the faces normal to the x-axis is $dydz$; the area of the faces normal to the z-axis is $dxdy$. If the aquifer is homogeneous and isotropic, and the fluid moves in only one direction through the controlled volume, then the actual fluid motion can be subdivided on the basis of the components of flow parallel to the three principle axes. If q is flow per unit cross-sectional area, $\rho_w q_x$ is the portion parallel to the x-axis, where ρ_w is the density of water. The mass flux into the controlled volume is $\rho_w q_x dydz$ along the x-axis. The mass flux out of the controlled volume is $\rho_w q_x dydz + \frac{\partial}{\partial x}(\rho_w q_x)dxdydz$. The net accumulation in the controlled volume due to movement parallel to the x-axis is equal to the inflow less than the outflow, or $-\frac{\partial}{\partial x}(\rho_w q_x)dx\, dydz$. Since there are flow components along
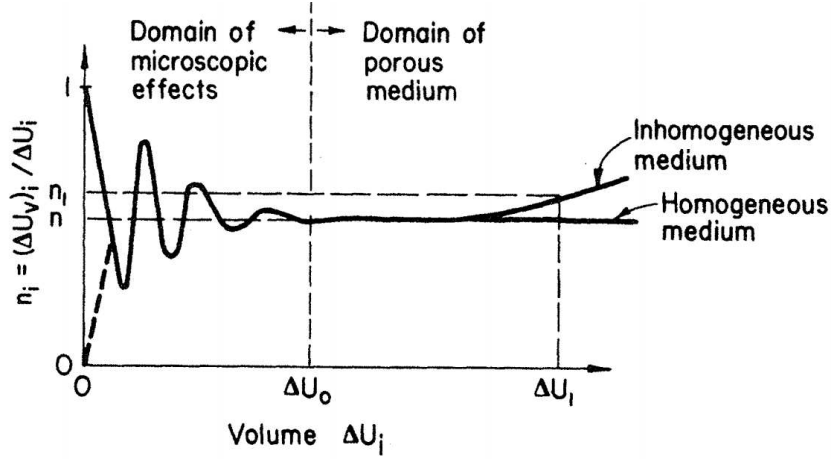
Figure 1: Representative elementary volume concept (Bear, 1972)

all three axes, similar terms can be determined for the other two directions: $-\frac{\partial}{\partial y}(\rho_w q_y)dy \; dxdz$ and $-\frac{\partial}{\partial z}(\rho_w q_z)dz \; dxdy$. Combining these three terms yields the net total accumulation of mass in the controlled volume:

$$-\left(\frac{\partial}{\partial x}\rho_w q_x + \frac{\partial}{\partial y}\rho_w q_y + \frac{\partial}{\partial z}\rho_w q_z\right)dxdydz \tag{4}$$

If the water in the porous media is saturated, then its volume is equal to $ndxdydz$, where n $[-]$ is the porosity. The initial mass of the water is thus $\rho_w ndxdydz$. The volume of solid material is $(1-n)dxdydz$. Any change in the mass of water M [kg], with respect to time t [s] is given by

$$\frac{\partial M}{\partial t} = \frac{\partial}{\partial t}(\rho_w ndxdydz) \tag{5}$$

As the pressure in the controlled volume changes, the fluid density will change, and also the porosity of the aquifer. The compressibility of water, β, is defined as the rate of change in density with regards to pressure, P [Pa]:

$$\beta dP = \frac{d\rho_w}{\rho_w} \tag{6}$$

The aquifer also changes in volume with pressure. Assuming the change is only vertical, the aquifer compressibility, α, is given by

$$\alpha dP = \frac{d(dz)}{dz} \tag{7}$$

As the aquifer compresses or expands, the porosity n will change, while the volume of the solids, V_s will be constant. Likewise, if the only deformation is in the z-direction, $d(dx)$ and $d(dy)$ will be equal to zero:

$$dV_s = 0 = d[(1-n)dxdydz] \tag{8}$$

Differentiation of the above equation yields

$$dzdn = (1-n)d(dz) \tag{9}$$

4

and

$$dn = \frac{(1-n)d(dz)}{dz} \tag{10}$$

The pressure, P, at a point in the aquifer, is equal to $P_0 + \rho_w gh$, where P_0 is atmospheric pressure, and h is the height of a column of water above the point. Therefore, $dP = \rho_w gdh$, and Eq. 6 and Eq. 7 become

$$d\rho_w = \rho_w \beta(\rho_w gdh) \tag{11}$$

and

$$d(dz) = dz\alpha(\rho_w gdh) \tag{12}$$

Eq. 10 can be rearranged if $d(dz)$ is replaced by Eq. 12.

$$dn = (1-n)\alpha\rho_w gdh \tag{13}$$

If dx and dy are constant, the equation for change of mass with time in the control volume, Eq. 5, can be expressed as

$$\frac{\partial M}{\partial t} = \left[\rho_w n \frac{\partial(dz)}{\partial t} + \rho_w dz \frac{\partial n}{\partial t} + ndz \frac{\partial \rho_w}{\partial t} \right] dxdy \tag{14}$$

Substitution of Eq. 11, Eq. 12, and Eq. 13 into Eq. 14 yields

$$\frac{\partial M}{\partial t} = (\alpha\rho_w g + n\beta\rho_w g)\rho_w dxdydz \frac{\partial h}{\partial t} \tag{15}$$

The net accumulation of material expressed as Eq. 14 is equal to Eq. 15, the change of mass with time:

$$\begin{aligned} \left[\frac{\partial(q_x)}{\partial x} + \frac{\partial(q_y)}{\partial y} + \frac{\partial(q_z)}{\partial z} \right] \rho_w dxdydz = \\ (\alpha\rho_w g + n\beta\rho_w g)\rho_w dxdydz \frac{\partial h}{\partial t} \end{aligned} \tag{16}$$

From Darcy's law in Eq. 3,

$$q_x = -K\frac{\partial h}{\partial x} \tag{17}$$

$$q_y = -K\frac{\partial h}{\partial y} \tag{18}$$

and

$$q_z = -K\frac{\partial h}{\partial z} \tag{19}$$

Substituting these into Eq. 16 yields the governing equation of flow in a confined aquifer:

$$K\left(\frac{\partial^2 h}{\partial x^2} + \frac{\partial^2 h}{\partial y^2} + \frac{\partial^2 h}{\partial z^2} \right) = (\alpha\rho_w g + n\beta\rho_w g)\frac{\partial h}{\partial t} \tag{20}$$

which is a general equation for three dimensional flow for an isotropic, homogeneous porous medium. For two-dimensional flow with no vertical components, the storativity, S [−], is define as $S = b(\alpha\rho_w g + n\beta\rho_w g)$, and transmissivity, T [m^2 s^{-1}], is defined as $T = Kb$, where b [m] is the aquifer thickness. Therefore, the general equation for two-dimensional case is

$$\frac{\partial^2 h}{\partial x^2} + \frac{\partial^2 h}{\partial y^2} = \frac{S}{T}\frac{\partial h}{\partial t} \tag{21}$$

Unconfined Aquifer   The general flow equation for two-dimensional unconfined flow is known as the Boussinesq equation:

$$\frac{\partial}{\partial x}\left(h\frac{\partial h}{\partial x}\right) + \frac{\partial}{\partial y}\left(h\frac{\partial h}{\partial y}\right) = \frac{S_y}{K}\frac{\partial h}{\partial t} \tag{22}$$

where h [m] is the hydraulic head, S_y [1/m] is the specific yield, and K is the hydraulic conductivity. If the drawdown in the aquifer is very small compared with the saturated thickness, the variable thickness h, can be replaced with an average thickness b [m], that is assumed to be constant over the aquifer. Then the Boussinesq equation can be linearized by this approximation to the following form

$$\frac{\partial^2 h}{\partial x^2} + \frac{\partial^2 h}{\partial y^2} = \frac{S_y}{K_b}\frac{\partial h}{\partial t} \tag{23}$$

2.1.2 Equations of mass transport

Diffusion   A solute in water will move from an area of greater concentration towards area where it is less concentrated. This process is known as molecular diffusion. Diffusion will occur as long as a concentration gradient exists, even the fluid is not moving. The mass of diffusing is proportional to the concentration gradient, which is expressed as the Fick's first law. In one dimension, Fick's first law is

$$F = -D_d\frac{dC}{dx} \tag{24}$$

where F [kg m^{-2} s^{-1}] is the mass flux of solute per unit area per unit time; D_d [m^2 s^{-1}] is the diffusion coefficient; C [kg m^{-3}] is the solute concentration, and dC/dx is the concentration gradient. If concentrations change with time, Fick's second law is applied. In one dimensional form, it is:

$$\frac{\partial C}{\partial t} = D_d\frac{\partial^2 C}{\partial x^2} \tag{25}$$

In porous media, diffusion cannot proceed as fast as it can in water because the ions must follow longer pathways as they travel around mineral grains. To account for this, an effective diffusion coefficient, D^*, must be used.

$$D^* = \omega D_d \tag{26}$$

where ω is a coefficient that is related to the tortuosity. It is an empirical coefficient that takes into account the effect of the solid phase of the porous medium on the diffusion. In laboratory studies of diffusion of the non-adsorbed ions in the porous geologic materials, ω values between about 0.5 and 0.01 are commonly observed.

Advection   Dissolved solids are carried along with the flowing ground water. This process is called advective transport, or convection. For one dimensional flow normal to a unit cross-sectional area of the porous media, the quantity of water flowing is equal to the average linear velocity v_x times the effective porosity n.

$$v_x = \frac{K}{n}\frac{dh}{dl} \tag{27}$$

where K [m s^{-1}] is the hydraulic conductivity. The one-dimensional mass flux, F_x, due to advection is equal to the quantity of water flowing times the concentration of dissolved solids and is given as follows

$$F_x = v_x nC \tag{28}$$

Hydrodynamic Dispersion The hydrodynamic dispersion coefficient D is represented by the following formulas:

$$D_L = \alpha_L v_i + D^* \tag{29}$$

$$D_T = \alpha_T v_i + D^* \tag{30}$$

where D_L and D_T are the longitudinal and transverse hydrodynamic dispersion coefficient, with α_L and α_T are the longitudinal and transverse dispersivity, respectively.

Advection-Dispersion Equation According to Bear (1972), the derivation of the advection-dispersion equation is based on the conservation of mass of solute flux into and out of a REV of porous media. As the solute will be transported by advection and hydrodynamic dispersion, the solute transport in i direction is given by

$$\text{Advective transport}: \quad v_i nC dA \tag{31}$$

$$\text{Dispersive transport}: \quad nD_i \frac{\partial C}{\partial t} dA \tag{32}$$

where dA is the cross-sectional area of the element and i direction is normal to that cross-sectional face. The total mass of solute per unit cross-sectional area transported in the i direction per unit time, F_i, is the sum of the adjective and dispersive transport and is given by

$$F_i = v_i nC - nD_i \frac{\partial C}{\partial t} \tag{33}$$

The negative sign indicates that the dispersive flux is from areas of greater to areas of lesser concentration. The total amount of solute entering the REV is

$$F_x dz dy + F_y dz dx + F_z dx dy \tag{34}$$

The total amount of solute leaving the REV is

$$\left(F_x + \frac{\partial F_x}{\partial x} dx \right) dz dy + \left(F_y + \frac{\partial F_y}{\partial y} dy \right) dz dx + \left(F_z + \frac{\partial F_z}{\partial z} dz \right) dx dy \tag{35}$$

The difference between the mass of the solute entering the REV and the amount leaving it is

$$-\left(\frac{\partial F_x}{\partial x} + \frac{\partial F_y}{\partial y} + \frac{\partial F_z}{\partial z} \right) dx dy dz \tag{36}$$

The rate of mass change in the REV is therefore

$$n \frac{\partial C}{\partial t} dx dy dz \tag{37}$$

By the law of mass conservation, the rate of mass change in the REV must be equal to the difference in the mass of the solute entering and the mass leaving.

$$\frac{\partial F_x}{\partial x} + \frac{\partial F_y}{\partial y} + \frac{\partial F_z}{\partial z} = -n \frac{\partial C}{\partial t} \tag{38}$$

Substituting Eq. 33 into Eq. 38 and cancelling n yields

$$\begin{aligned} \frac{\partial C}{\partial t} = &\left[\frac{\partial}{\partial x} \left(D_x \frac{\partial C}{\partial x} \right) + \frac{\partial}{\partial y} \left(D_y \frac{\partial C}{\partial y} \right) + \frac{\partial}{\partial z} \left(D_z \frac{\partial C}{\partial z} \right) \right] \\ &- \left[\frac{\partial}{\partial x} (v_x C) + \frac{\partial}{\partial y} (v_y C) + \frac{\partial}{\partial z} (v_z C) \right] \end{aligned} \tag{39}$$

which is the governing equation of three-dimensional mass transport for a conservative solute, i.e. the solute that does not interact with the porous media or undergo sorption or decay processes. If the Laplace operator is applied, the above equation can be rewritten as,

$$\frac{\partial C}{\partial t} = \nabla(D\nabla C) - \nabla(\vec{v}C) \tag{40}$$

where $\vec{v}$ is the velocity vector. If the porous media has a sorption effect on the transported chemical component, following Henry's sorption isotherm,

$$C_s = K_D \cdot C \tag{41}$$

where C_s [kg kg^{-1}] is the concentration of adsorbed species, K_D [m^3 kg^{-1}] is the distribution coefficient. To include this sorption effect, the retardation coefficient R [$-$] is defined as,

$$R = 1 + \frac{\rho_b}{n}K_D = 1 + \frac{1-n}{n}\rho_s K_D \tag{42}$$

with ρ_b the bulk density of the media, n the porosity and ρ_s the solid density of the media. In this case, the governing equation becomes

$$\frac{\partial C}{\partial t} = \nabla(D\nabla C) - \nabla(\frac{\vec{v}}{R}C) - \frac{\rho_b}{R}\frac{\partial C_s}{\partial t} \tag{43}$$

If the transported species is radioactive, then a first-order decay term also needs to be included.

$$\frac{\partial C}{\partial t} = \nabla(D\nabla C) - \nabla(\frac{\vec{v}}{R}C) - \frac{\rho_b}{R}\frac{\partial C_s}{\partial t} - \lambda \cdot C \tag{44}$$

2.2 Geochemical modelling

Chemical Potential The chemical potential μ [J mol^{-1}] for component i is defined as the derivative of its Gibbs free energy G with respect to its mole amount.

$$\mu_i \equiv \frac{\partial G_i}{\partial n_i} \tag{45}$$

Assuming a reaction that includes components B, C, D, and E,

$$bB + cC \iff dD + eE \tag{46}$$

where b, c, d, e and so on are the stoichiometric coefficients. When the reaction reaches equilibrium, that is the minimum point of G, it satisfies

$$d\mu_D + e\mu_E - b\mu_B - c\mu_C = 0 \tag{47}$$

As soon as the chemical potentials in the above equation is found, the equilibrium state of the system is then defined. In reality, chemical components often mix together and form phases, and its potential is not the same as the one in its pure phase. Therefore, the chemical potential for a given component i in a mixed phase is

$$\mu_i = \mu_i^\circ + RT_K \ln X_i \tag{48}$$

Here, R is the ideal gas constant, which is 8.314 J K^{-1} mol^{-1}. T_K is the ambient temperature in Kelvin. X_i [$-$] is the mole fraction of component i in the solution phase. Depending on the type of phases, X_i has different variants. For example, in aqueous phase it is formulated by the activity of dissolved components, while in gas phase, it is represented by fugacity.

Activity For an aqueous species, the activity of a species is defined by the product of molarity m_i, which is the number of moles of the species per kilogramme of solvent, and its activity coefficient γ_i,

$$a_i = \gamma_i m_i \tag{49}$$

It is accounted for the non-ideality of the aqueous solution. In a very dilute solution, the specie's activity approaches unity.

$$\gamma_i \to 1 \quad \text{and} \quad a_i \to m_i \tag{50}$$

In a dilute solution, the activity coefficient γ_i is calculated by the Davies equation (Davies, 1962).

$$log_{10}\gamma_i = -Az_i^2 \left(\frac{\sqrt{I}}{1+\sqrt{I}} - 0.3I \right) \tag{51}$$

where I is the effective molal ionic strength, and z_i is the charge of the component species. The parameter A is 0.5092 at a temperature of 25 °C and a pressure of 1 bar. It is noticed that when ionic strength is high, for example in a deep saline aquifer, other activity calculations such as the Pizter model should be applied, which has already been implemented in the GEMIPM2K code.

Mineral For mineral phases, the molar fraction X $[-]$ for species k is represented by the standard potential μ_k° of this end member in its pure form, together with the activity a_k of this species in the solid solution.

$$\mu_k = \mu_k^\circ + RT_K \ln a_k \tag{52}$$

For practical reasons, most geochemical models consider only minerals of fixed composition in one condensed pure phase. So that its activity is unity,

$$a_k = 1 \tag{53}$$

and its chemical potential and standard potential are the same.

$$\mu_k = \mu_k^\circ \tag{54}$$

The solid solutions can sometimes be assumed to be ideal, so that the activity a_k is equal to the molar fraction of one particular end member. However, this practice leads to errors more severe than just ignoring the solutions altogether. Glynn et al. (1990) points out that there are several conceptual and theoretical problems that increase the difficulty of incorporating solid solution theory into geochemical modelling. Therefore in this work, we consider the non-ideal mixing of end members in the solid solution formation. For an binary solid solution k, the activity coefficient is formed as,

$$\ln\alpha_k = -\sum_{i=1}^{n-1}\sum_{j>i}^{n} q_i q_j \theta_{ij} \tag{55}$$

where $q_i = 1 - \chi_i$ when $i = k$ and $q_i = -\chi_i$ when $i \neq k$. θ_{ij} are the symmetric interaction parameters. Here χ stands for the end member mole fractions. It is the mole amount of end member j divided by the total mole amount of a particular solid phase.

$$\chi_j = \frac{m_j}{\sum m_j \text{ in one solution phase}} \tag{56}$$

Details regarding the symmetric interaction parameters used in this work can be found in Table A4 of [EP2].

Fugacity For a gas species, its chemical potential is given in terms of a standard potential of the pure gas at 1 atm, the temperature of interest, and the gas fugacity f_m, with index m.

$$\mu_m = \mu_m^\circ + RT_K \ln f_m \tag{57}$$

Fugacity is related to partial pressure P_m by a fugacity coefficient x_i.

$$f_m = x_m P_m \tag{58}$$

At low pressure and temperature, ideal gas law can be assumed.

$$x_m \to 1 \qquad \text{and} \qquad f_m \to P_m \tag{59}$$

Equilibrium Constant Assuming the species in Eq. 46 are all aqueous ones, then one can substitute the chemical potential function into Eq. 46. The criterion for equilibrium becomes

$$d\mu_D^\circ + e\mu_E^\circ - b\mu_B^\circ - c\mu_C^\circ = -RT_K \left(d\ln a_D + e\ln a_E - b\ln a_B - c\ln a_C \right) \tag{60}$$

The left side of this equation is the reaction's standard free energy

$$\Delta G^\circ = d\mu_D^\circ + e\mu_E^\circ - b\mu_B^\circ - c\mu_C^\circ \tag{61}$$

Therefore, the equilibrium constant is defined in terms of the standard free energy as

$$\ln K = -\frac{\Delta G^\circ}{RT_K} \tag{62}$$

Eq. 60 can also be written as

$$\ln K = d\ln a_D + e\ln a_E - b\ln a_B - c\ln a_C \tag{63}$$

or, equivalently,

$$K = \frac{a_D^d a_E^e}{a_B^b a_C^c} \tag{64}$$

Based on the above theory, two techniques, the Law of mass action (LMA) and the Gibbs energy minimization (GEM) approaches, can be employed to find the equilibrium of the chemical system.

2.2.1 Law of mass action (LMA) approach

In LMA approach, chemical species are differentiated between base species and secondary species. Secondary species are expressed by the formation reactions of base species. And the base species are those can not be represented by the reactions of other base or secondary species. Depending on the property of the system, we have chosen a basis

$$B = (A_w, A_i, A_k, A_m) \tag{65}$$

Here, A_w is water, A_i are the aqueous species, A_k the minerals, and A_m the gases in the basis. For the secondary species, they are defined as the following reaction

$$A_j \rightleftharpoons v_{wj}A_w + \sum_i v_{ij}A_i + \sum_k v_{kj}A_k + \sum_m v_{mj}A_m \tag{66}$$

v represents the reaction coefficients: $v_w j$ is the number of moles of water in the reaction to form A_j, v_{ij} is the number of moles of the basis species A_i, and so on for the minerals and gases.

Mass Action Equation For each independent reaction above, there is an associated equilibrium constant K_j at the temperature and pressure of interest, and corresponding mass action equation

$$K_j = \frac{a_w^{v_{wj}} \cdot \prod^i (\gamma_i m_i)^{v_{ij}} \cdot \prod^k \gamma_i a_k^{v_{kj}} \cdot \prod^m f_m^{v_{mj}}}{\gamma_j m_j} \tag{67}$$

By eliminating the molalities m_j of the secondary species, the above equation becomes

$$m_j = \frac{1}{K_j \gamma_j} \left(a_w^{v_{wj}} \cdot \gamma_i m_i^{v_{ij}} \cdot \prod^k \gamma_i a_k^{v_{kj}} \cdot \prod^m f_m^{v_{mj}} \right) \tag{68}$$

in term of the molality and activity coefficient of each aqueous species in the basis and the activity or fugacity of each of the other basis entries. This is the final form of mass action equation.

Mass Balance Equation The mass balance equations express the conservation of mass in terms of the components in the basis. The water component, for example, is present in free water molecules of the solvent and also the water required to make up the secondary species. Assuming each mole of species A_j is composed of v_{wj} moles of the water component, the mole number M_w of water component is given

$$M_w = n_w (55.5 + \sum_j v_{wj} m_j) \tag{69}$$

where 1 kg of water is present. For aqueous species,

$$M_i = n_w (m_i + \sum_j v_{ij} m_j) \tag{70}$$

For minerals,

$$M_k = n_k + n_w \sum_j v_{kj} m_j \tag{71}$$

For gas,

$$M_m = n_w \sum_j v_{mj} m_j \tag{72}$$

The final form of the governing equation is given by substituting the mass action equation for each occurrence of m_j in the mass balance equations. The substituted equations are

$$M_w = n_w \left\{ 55.5 + \sum_j \frac{v_{wj}}{K_j \gamma_j} a_w^{v_{wj}} \cdot \prod^i (\gamma_i m_i)^{v_{ij}} \cdot \prod^k (a_k)^{v_{kj}} \cdot \prod^m (f_m)^{v_{mj}} \right\} \tag{73}$$

$$M_i = n_w \left\{ m_i + \sum_j \frac{v_{ij}}{K_j \gamma_j} a_w^{v_{wj}} \cdot \prod^i (\gamma_i m_i)^{v_{ij}} \cdot \prod^k (a_k)^{v_{kj}} \cdot \prod^m (f_m)^{v_{mj}} \right\} \tag{74}$$

$$M_k = n_k + n_w \sum_j \frac{v_{wj}}{K_j \gamma_j} \left\{ a_w^{v_{wj}} \cdot \prod^i (\gamma_i m_i)^{v_{ij}} \cdot \prod^k (a_k)^{v_{kj}} \cdot \prod^m (f_m)^{v_{mj}} \right\} \tag{75}$$

$$M_m = n_w \sum_j \frac{v_{wj}}{K_j \gamma_j} \left\{ a_w^{v_{wj}} \cdot \prod^i (\gamma_i m_i)^{v_{ij}} \cdot \prod^k (a_k)^{v_{kj}} \cdot \prod^m f_m^{v_{mj}} \right\} \tag{76}$$
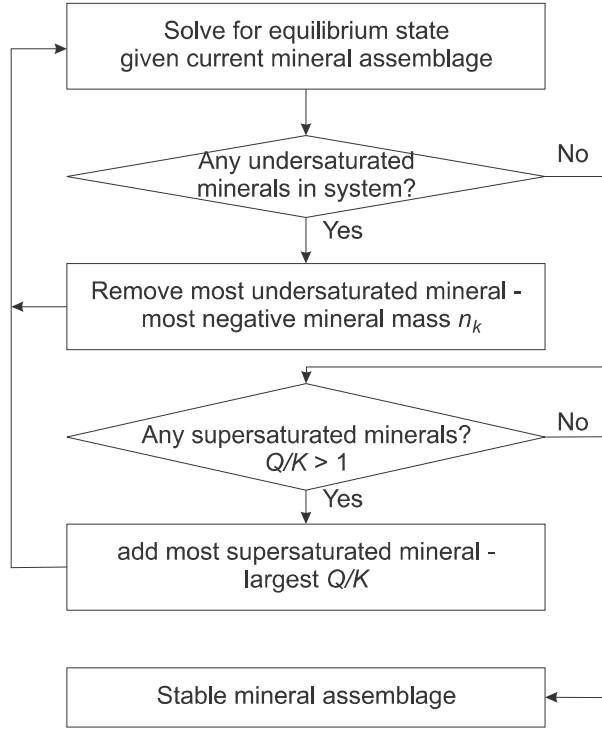
Figure 2: Swap Procedure to find the stable mineral assemblage in a system of known composition

Swap procedure A mineral A_l, which is not in the basis, is formed by the reaction

$$A_l = v_{wl}A_w + \sum_i v_{il}A_w + \sum_k v_{kl}A_k + \sum_m v_{ml}A_m \qquad (77)$$

which has an corresponding equilibrium constant K_l. The saturation state of this reaction is given by the ratio Q_l/K_l, where Q_l is the mineral's activity product

$$Q_l = a_w^{v_{wl}} \cdot \sum_i (\gamma_i m_i)^{v_{il}} \cdot \sum_k (a_k)^{v_{kl}} \cdot \sum_i (f_m)^{v_{ml}} \qquad (78)$$

In order to find the stable mineral assemblage, a so called swap procedure is employed (after Bethke (1996), see Fig. 2). In most cases, there are often more than one mineral that appear to be under- or supersaturated in the chemical system. So that the saturation state for each of these minerals needs to be determined by the swap procedure one after another.

2.2.2 Gibbs energy minimization (GEM) approach

The GEM-Selektor (Kulik et al., 2008) and GEMIPM2K codes use the GEM convex programming approach (Karpov et al., 1997, 2001) which is based on an explicit consideration of independent components (usually chemical elements and charge), dependent components, and phases. In a formal algebraic notation, l_α stands for a set of indices of dependent components included into α-th phase. X_α denotes the mole amount of α-th phase.

$$X_\alpha = \sum_j n_j^{(x)} \qquad j \in l_\alpha \qquad (79)$$

12

where $n_j^{(x)}$ is the mole amount of j-th dependent component (species). If μ_j is a primal approximation of the chemical potential of j-th species and L the set of indexes of all dependent components, then the total Gibbs energy function of the chemical system is

$$G(x) = \sum_j n_j^{(x)} \mu_j \qquad j \in L \tag{80}$$

The equilibrium speciation of the chemical system, or the "primal solution" vector $n^{(x)}$ of elements $n_j^{(x)}$ which are mole amounts of dependent components, can be found by minimising the total Gibbs energy of the system:

$$G(x) \Rightarrow \min \qquad \text{subject to} : \mathrm{An}^{(x)=n^{(b)}}, j \in \mathbb{R} \tag{81}$$

$A = \{a_{ji}\}$, $j \in L$, $i \in N$ is a stoichiometry matrix (a_{ji} is number of moles of i-th independent component in one mole of j-th dependent component); $n^{(b)} = n_i^b$, $\quad i \in N$ is an input vector of the total bulk chemical composition of the system; $n_i^{(b)}$ is total mole amount of i-th independent component in the system; and $\mathbb{R}$ stands for a set of the optional lower-, upper- or two-side kinetic (metastability) constraints to the $n_j^{(x)}$ values. In this GEM setup, concentrations of dependent components are defined separately in their respective phases using $n_j^{(x)}$ and X_α values.

2.3 Coupling of chemistry and mass transport

Existing schemes To couple chemical reactions with mass transport, there are three major approaches existing.

1. Global implicit (GI) scheme. The reaction term is summarised into source and sink terms in the transport equations. These transport equations are solved altogether.

2. Sequential non-iterative (SNI) scheme. The transport equation is solved first, then reaction is solved by chemical solver. The results are used as the output for this time step.

3. Sequential iterative (SI) scheme. The transport equation is first solved, followed by the reaction calculation. It is iterated between transport and reactions, until the concentration on certain locations reaches convergence.

Pros and Cons For Global implicit scheme, it has been favoured for its high accuracy, since transport and chemistry are solved altogether. However, Yeh and Tripathi (1989) rejected its usage due to the large amounts of computer memory needed. For example, a two-dimensional domain discretized with 250×250 grid having 10 chemical components, the Jacobian matrix stored in compressed form as a rectangular matrix of dimension 500 by 62,500 would require about 250 megabytes of memory. For a complex chemical system, the number of chemical components is usually beyond 100. Second problem is the CPU time required. If an unmodified Newton step is carried out, the entire Jacobian matrix must be constructed in each iteration. All these constrains make the GI approach inappropriate for such realistic problems.

On the other side, SNI and SI approaches (also known as operator splitting techniques), require much less memory and therefore can be applied to large-scale problems. The disadvantage of SI approach is that it is subject to operator splitting errors. Valocchi and Malmstead (1992) applied an one-dimensional reactive transport problem with first-order decay. They recommended
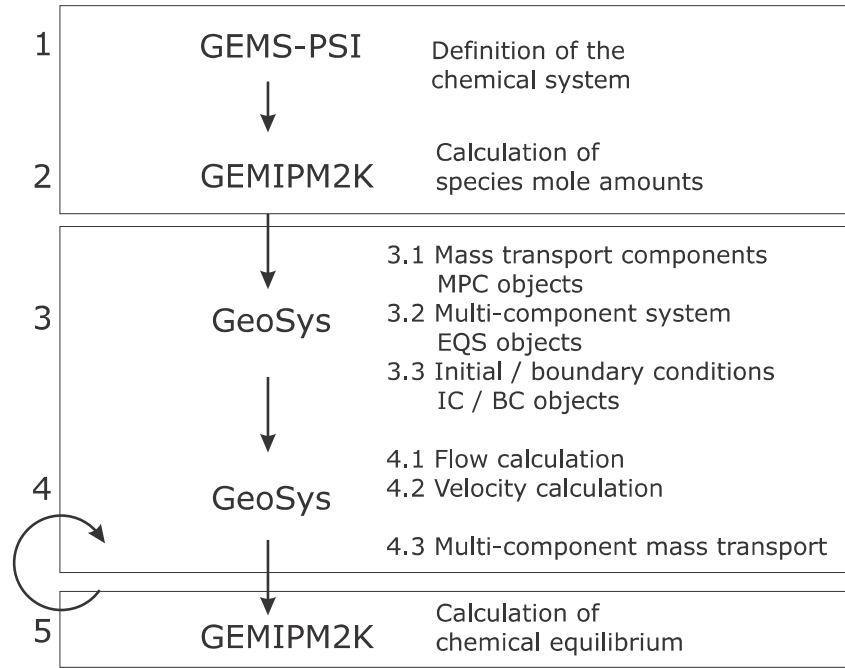
Figure 3: Coupling structure applied for OpenGeoSys-GEM

that the time step Δt has to be chosen so that the product $k\Delta t$ is less than approximately 0.1, in order to keep the final operator splitting error limited less than 1% of the initial concentration.

In this work, the traditional SNI scheme is adopted to couple chemistry with transport, based on the following reasons.

- The chemical solver GEMIPM2K is based on Gibbs Energy Minimization algorithm, which finds the equilibrium based molar amount of chemical components. It can not be directly integrated into mass transport equations, thus the Global Implicit scheme can not be directly applied.

- The SNI schemes requires minimal implementation and modification of the code, and provides an intrinsic parallelization structure for solving the chemistry.

- The accuracy of the SNI scheme is controlled by the time step size. Simulation accuracy is guaranteed by using smaller time steps.

14

3 Implementation of the model

3.1 OpenGeoSys-GEM

GEMIPM2K Before starting a simulation, one needs to set up a chemical environment first, using the GEMIPM2K interface. The user is asked to give the following information, in order to define the system.

- Chemical elements included in the system;

- The ambient temperature and pressure;

- Model of activity coefficients calculation for aqueous phase components;

- Thermodynamic database employed for the calculation;

- Molar amount of chemical components added into the system (so called "the recipe");

In some cases, not all of a specific component is available for reaction. For example, only the outer sphere of the calcite mineral is accessible for dissolution reactions. In this case, one can set the upper and lower constrains for a component, that amount for reaction is restricted.

After these initial constrains are set up, the GEMIPM2K program will calculate the chemical equilibrium of the system, including pH and pe. The accepted results can be exported as data record files. Normally, the boundary conditions, initial conditions, and different material groups are defined as different data records. These records are later converted into OpenGeoSys input files, and used for the reactive transport simulation.

Exchange files When a data record is exported for further usage, several files are automatically generated by GEMIPM2K. Table 3.1 lists their names and the information contained correspondingly. After the exchange files are prepared, a utility program GEMS2GSRF, is employed to convert the information into *.ic (initial conditions), *.bc (boundary conditions), and *.mcp (mass transport components) files, which are supplemented to OpenGeoSys. In addition, a *.gem file needs to be provided (see Fig. 4), in which the record files generated from GEMIPM2K and other specifications are defined, should also be provided. Fig. 4 shows an example of *.gem file, where parameters are given for the reactive transport simulation.

To calculated the porosity of the media during simulation, the mineral amount and mass of water available need to be set up according to the real media. By convention, the volume for the chemical system is calibrated to 1 m^3 , so that the porosity of the media can be updated dynamically after each time step. If a permeability-porosity relationship is provided, the permeability can also be calculated based on porosity values accordingly. For boundary nodes, as they are fixed through out the simulation, the values are expressed in moles per litre of water and the minerals are expressed in moles. For other nodes, aqueous components and minerals are expressed in mole amount per cubic meter volume.

Simulation procedure A reactive transport simulation run by OpenGeoSys-GEM goes through the following procedure:

1. Before the simulation starts, the *.gem file will be first loaded. The data record file specified in it will be used to initialise the chemical system. OpenGeoSys-GEM will go

Table 1: Exported data record files from GEMIPM2K.

File names	Information contained
RecordName-dat.lst	List all the files needed to describe this data record, and flag defining binary or ASCII files.
RecordName-dbr-0-0000.dat	Data bridge file. It contains information of chemical system on one particular node, the last four numbers are node indexes.
RecordName-dch.dat	Data structure file. It describe the number of primary and secondary components, thermodynamics data, constrains on the components etc.
RecordName-ipm.dat	Numerical settings, including the convergence criteria, maximum iteration number, and accuracy for mineral precipitation etc.

```
#GEM_PROPERTIES
$GEM_INIT_FILE
    calcite-init.dat     ; only file name, no path
  $FLAG_NODE_ELEMENT
    0     ; 0-node based; 1-elem based;
  $FLAG_POROSITY_CHANGE
    0     ; 0-not coupled;1=coupled;
  $MIN_POROSITY
    1.e-4
  $MAX_POROSITY
   0.9999
  $FLAG_COUPLING_HYDROLOGY
    0     ; 0-not coupled;1=coupled;
  $PERMEABILITY_POROSITY_MODEL
    0     ; 0-no coupling; 1-Kozeny-Carman; 2-Kozeny-Carman normalised;
  $ITERATIVE_SCHEME
    0     ; 0-not iteration;1=iteration. Not implemented yet.
#STOP
```

Figure 4: Example of *.gem setup file

through each all the nodes in the domain and calculate the local equilibrium on each of them.

2. Porosity values will be calculated for each node based on the volume occupied by the solid phase in its geochemical system. The porosity can change during the simulation, due to corresponding chemical reactions.

3. OpenGeoSys-GEM calculates the flow field of the domain first, then the velocity of the fluid is applied to solve mass transport equations for each chemical species.

4. The solution from mass transport calculation is loaded into the "REACT_GEM" class and feed into GEM chemical solver based on each node. The results of local equilibrium are adopted as the results for this time step.

5. If GEM can not reach equilibrium on some particular nodes, the input amount of chemical components will be scaled 10 times more and this node will be given a second try. If non-convergence still happens, an error message will be reported and the program takes the transport results and goes for the next time step simulation.

3.2 OpenGeoSys-BRNS

BRNS The Biogeochemical Reaction Network Simulator (BRNS) is developed to model complex biochemical processes. Compared to other modelling tools, the main advantage of BRNS is that users can define the reaction networks by themselves and adjust the parameters through a Maple script. Both kinetically controlled and equilibrium reactions, can be specified. To achieve this high degree of flexibility, an automated code generation process is employed, using the Maple symbolic algebra language (Chilakapati, 1995; Regnier et al., 1997). An Automatic Code Generator (ACG) relying on the MACROFORT package (Aguilera et al., 2005; Gómez, 1990) compiles these process descriptions into problem specific Fortran code that complements a numerical engine containing generic routines written in Fortran. The compilation of these routines produces a dynamic linking library (*.dll) file on windows platform or a corresponding solution (*.so) file on Linux machines. In order to maintain high flexibility for further developments in both simulation codes, the interface connecting them is reduced to a minimum. A new object in OpenGeoSys handles all communication between the transport and the reactive code. On the side of BRNS, a new function allows an external caller to make use of the implemented reactive solver, with the original BRNS code staying unchanged.

Simulation procedure Creating a model in OpenGeoSys-BRNS consists of defining two inputs: one describing the model domain including physical parameters, hydrogeological flow, discretization parameters and (bio-)chemical species including diffusion constants for mobile species, and the other specifying the coupled (bio-)chemical reaction processes to be considered in the model. For the first set of input parameters, the standard OpenGeoSys format is used. For the second set, the Maple work sheet format already used in the BRNS model is also applied here. A Windows batch script, accepting the Maple work sheet in Maple Input format (mpl file) via drag and drop, automates the compilation of the problem specific dll library. Fig. 5 summarizes the complete model setup. To be successful, the operation requires that the reactive species appearing in the Maple worksheet file and in the OpenGeoSys input file (mcp file) follow the same order. Furthermore, the units for parameters (reaction rates, transport parameters, etc.) and concentrations must be consistent in both input files. More details regarding the coupling of OpenGeoSys-BRNS can be found in the enclosed publication [EP1].
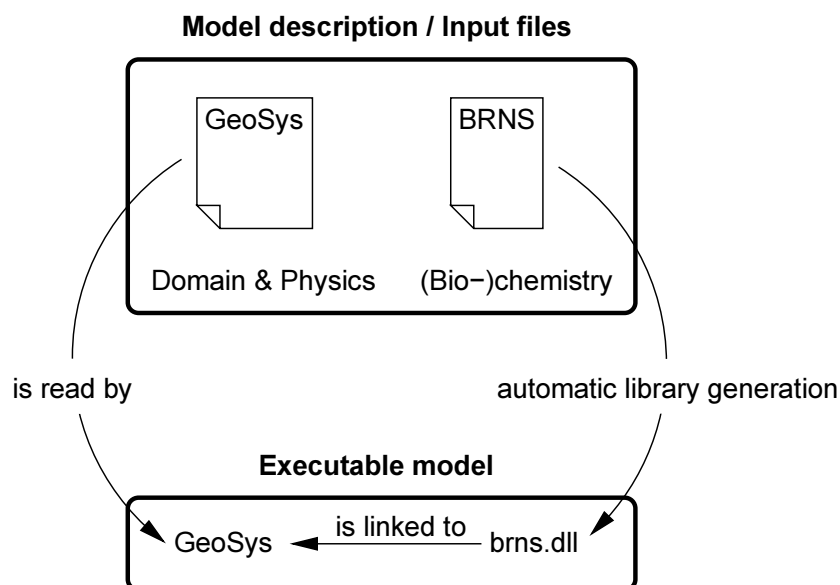
17

Figure 5: Coupling structure between OpenGeoSys and BRNS

3.3 Parallel simulation

3.3.1 Message passing interface (MPI)

Message passing interface (MPI) is the industrial standard for parallel computing on clusters. It is based on the distributed memory structure, meaning each process enjoys its independent memory structure. For the applications tackled in this work, the simulation domain is relatively small, therefore only chemical systems are solved in parallel, as they are naturally independent from node to node.

3.3.2 Implementation of OpenGeoSys-GEM and OpenGeoSys-BRNS

Since MPI structure provides independent memory for each processor, it is not needed to communicate between processors regarding input values of GEM, as they are all the same after mass transport calculation. For the output values (results), a dummy variable structure is designed to receive the data from different processors. Taking 4 processors as an example, Fig. 6 shows the memory structure for dummy variables. When initialised, dummy variables are all set to zero. As each processor is handling the chemical system on different nodes, only those results handled by current processor will be written into dummy variables accordingly. Therefore when the equilibrium calculation on the last node is finished, the "MPI_Allreduce" call will collect all the results to the original variable. It is also important that after each time step, these dummy variables are cleared to zero again for the next usage period. In this way, only the minimal amount of communication is performed, meaning less overhead resources will be occupied.

3.3.3 Speed-up of parallelization

To illustrate the speed-up of the parallel code, we adopt the monod2D example (see section 4.2 for details) and run it on a cluster machine provided by Helmholtz Centre for Environmental Research (UFZ). The cluster is equipped with 256-core AMD Opteron DC CPUs. The operation
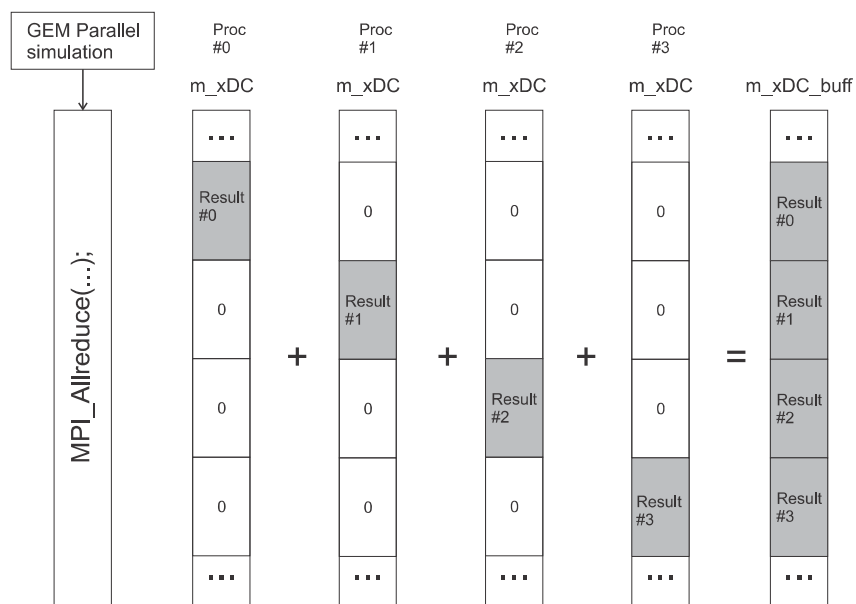
18

Figure 6: Dummy variable applied to collect the simulation result

```
#ifdef USE_MPI_GEMS
  MPI_Bcast(&nNodes, 1, MPI_LONG, 0, MPI_COMM_WORLD);
  // here "myrank" is the index of the CPU Processes,
  // and "size" is the number of CPU Processes
  for ( in = myrank; in < it_num ; in+= mysize )
#else
  for ( in = 0; in < it_num; in++ )
#endif
  {
  ...
  // run GEM on each node.
  ...
  }
```

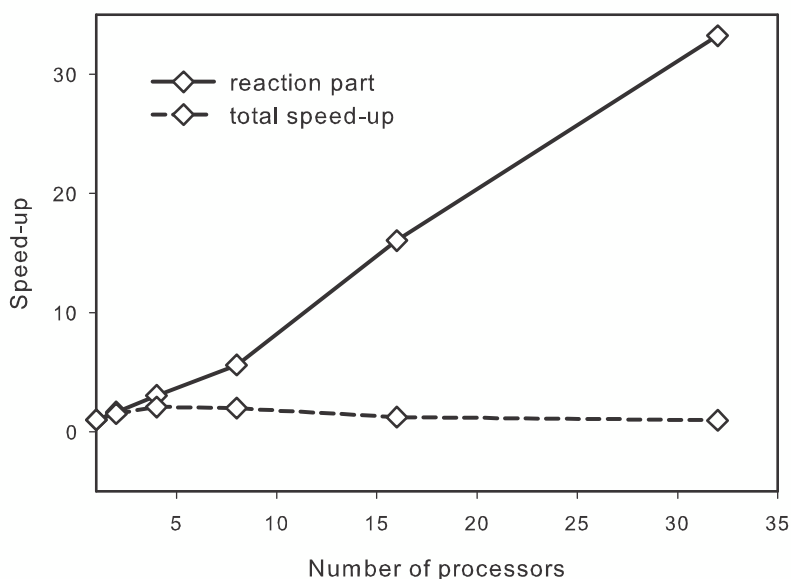Figure 7: Code demonstration to run chemical simulations parallelly.

Figure 8: Speed-up for parallel running Monod2D example.

system is Red Hat Enterprise Linux 4. The task queue is monitored with Sun Grid Engine. Our model source code was compiled with GNU Compiler 3.4.5, together with the MPICH library version 1.2.7.

Simulation was conducted using 1, 2, 4, 8, 16, and 32 cores. The total simulation time, consumed in solving transport equations, and in reaction parts were measured separately. The speed-up for reaction part and for total simulation was plotted in Fig. 8. In this plot, several features can be found for the coupled reactive transport code.

- The total simulation time does not decrease any more after 4 CPU cores.

- The reaction part shows a very good linearity up to 32 cores.

- The speed for solving transport equations actually decreases after 2 CPU cores. The probable reason is that the simulation domain is relatively small (20000 elements) and the time spent on domain decomposition required a lot of inter-core communication and slow down the simulation.

- The time needed to assemble equations also increases with increasing cores. Compared to some realistic chemical systems, which involve around 100 components, the Monod2D exampled tested here only have 5 components. This result reveals that it is usually the transport process, instead of the reactions, that forms the bottle neck of parallel simulation.
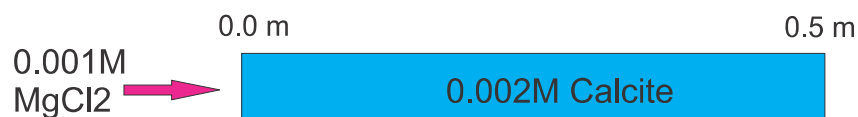
20

0.001M
MgCl2

0.0 m   0.5 m

0.002M Calcite

Figure 9: Model setup of calcite example

4 Applications

4.1 Mineral dissolution and precipitation (Calcite)

This example simulates the dissolution of calcite and precipitation of dolomite in a one dimensional column. It was first proposed by Engesgaard and Kipp (1992) for model verification of the MST1D code and later on used by Prommer (2002) for PHT3D. The ambient temperature is 25 °C and pressure of 1 bar, and was kept as constant. The model domain is a one-dimensional column (see Fig. 9), initially equilibrated with 2.17×10^{-5} mol kg^{-1} calcite. The column is flushed with MgCl$_2$ solution at an aqueous concentration of 1.0×10^{-3} mol L^{-1}, leading to the development of multiple precipitation/dissolution fronts. Dolomite is not present initially, but is formed temporally in the column as a moving zone. The amount of both precipitation and dissolution minerals are so low that porosity and permeability effectively do not change. The parameters for the model setup according to Engesgaard and Kipp (1992) are listed in Table 1. The Nagra/PSI Chemical Thermodynamic Data Base (Hummel et al., 2002) has been used in both LMA and GEM chemical solvers. These logK values are slightly different from those in Engesgaard and Kipp (1992). As the Nagra/PSI database provide the same chemical thermodynamic input data for both LMA and GEM methods, consistent simulations can be conducted for comparison of the different geochemical approaches.

To verify the code coupling, simulation results of OpenGeoSys-PHREEQC and OpenGeoSys-ChemApp were compared. PHREEQC is a geochemical speciation code based on the Law of Mass Action (LMA) approach (Parkhurst and Appelo, 1999). ChemApp is a commercial software which is also based on Gibb Energy Minimization method. Fig. 10 shows the concentration profiles for Cl, Mg, Ca, calcite and dolomite obtained by the two alternative chemical solvers respectively. The agreement of the simulations results using different methods for geochemical reactions confirms the correct implementation of code coupling in OpenGeoSys-GEM.

4.2 Mixing controlled bioremediation (Monod2D)

The Monod2D example is a two dimensional scenario that represents bio-remediation processes in groundwater systems. The model domain is a rectangle with 0.2 m width and 5 m length (Fig. 11). Chemical component A and B , representing carbon source and electron acceptor, are introduced into the domain at the left boundary, and undergo the reaction $A + B \longrightarrow C$. This reaction is facilitated by the microorganisms existing in the domain. Let C_A, C_B, C_C, and C_{bio} be the concentrations of component A, B, C, and microorganisms, their values are influenced by two processes. On the one side, the growth of the microorganisms is controlled by the double Monod kinetics, which consume both component A and B and produce component C. On the other side, the microorganism undergoes the first order decaying process, which consumes the mass of its own. The mathematical expression regarding the change of each component is
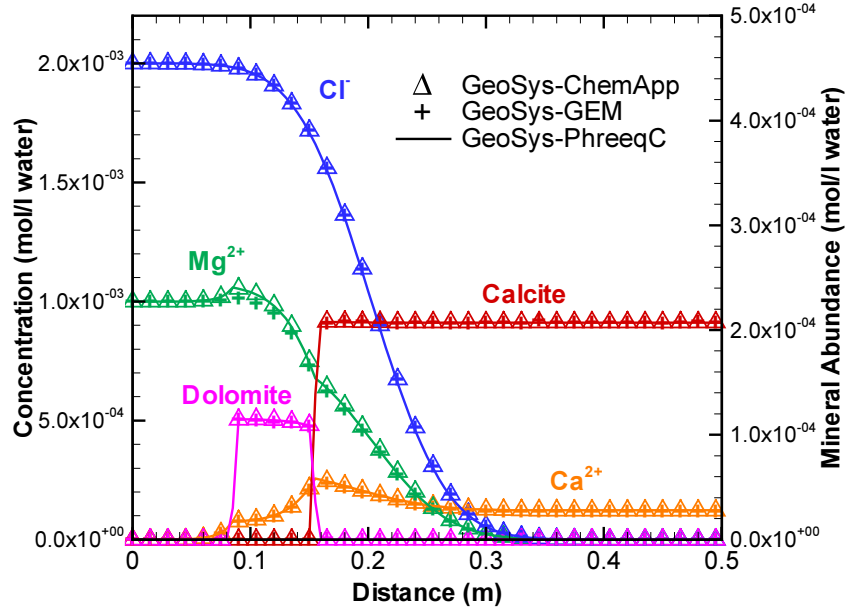
Figure 10: Simulation result of calcite example using OpenGeoSys-GEMS, OpenGeoSys-PhreeqC, and OpenGeoSys-ChemApp

expressed as follows.

$$\frac{\partial C_C}{\partial t} = \frac{C_A}{K_A + C_A} \cdot \frac{C_B}{K_B + C_B} \cdot k \tag{82}$$

$$\frac{\partial C_A}{\partial t} = -\frac{C_A}{K_A + C_A} \cdot \frac{C_B}{K_B + C_B} \cdot k = -\frac{\partial C_C}{\partial t} \tag{83}$$

$$\frac{\partial C_B}{\partial t} = -\frac{C_A}{K_A + C_A} \cdot \frac{C_B}{K_B + C_B} \cdot k = -\frac{\partial C_C}{\partial t}. \tag{84}$$

where K_A and K_B are the double Monod coefficients, μ_{max} are the maximum growth rate, and Y is the specific yield. The values of these parameters can be found in Cirpka and Valocchi (2007).

For this model, Cirpka and Valocchi (2007) presented an analytical solution for the steady state condition. The original solution was adopted to verify the coupling of OpenGeoSys-BRNS. The newly developed numerical model has been run for a long time, in order to approximate the steady state condition. The numerical solution was found to have small discrepancies to the analytical one at places close to the domain boundary. To further investigate this difference, reactive transport code TBC (Schäfer et al., 1998) was adopted to simulate the scenario using the same model setup. An error in the analytical solution was found and a comment on the original paper was produced [EP2]. Based on our argument, author of the analytical solution refined their methods and produced an correction (Cirpka and Valocchi, 2009). The updated analytical solution fits the numerical results of both TBC and OpenGeoSys-BRNS very well (see Fig. 12).
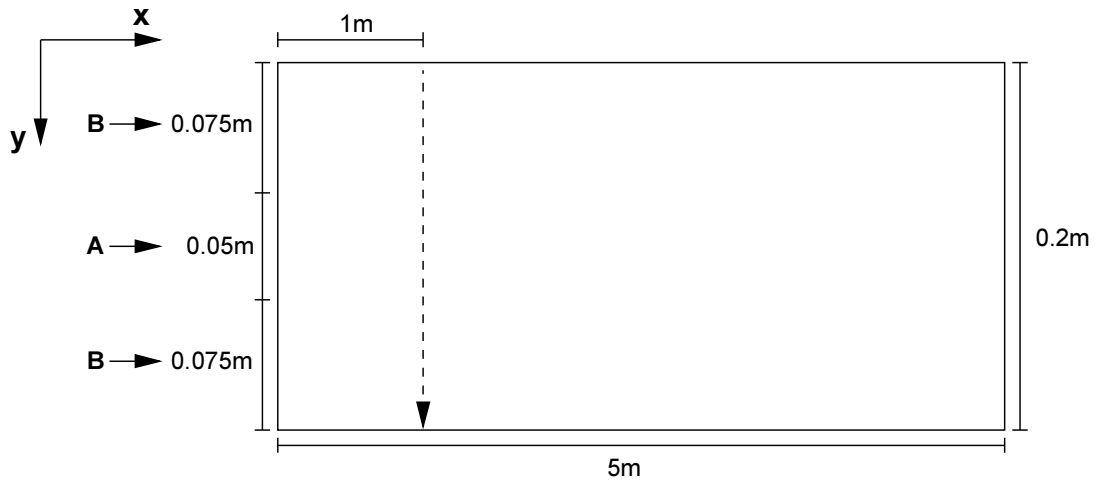
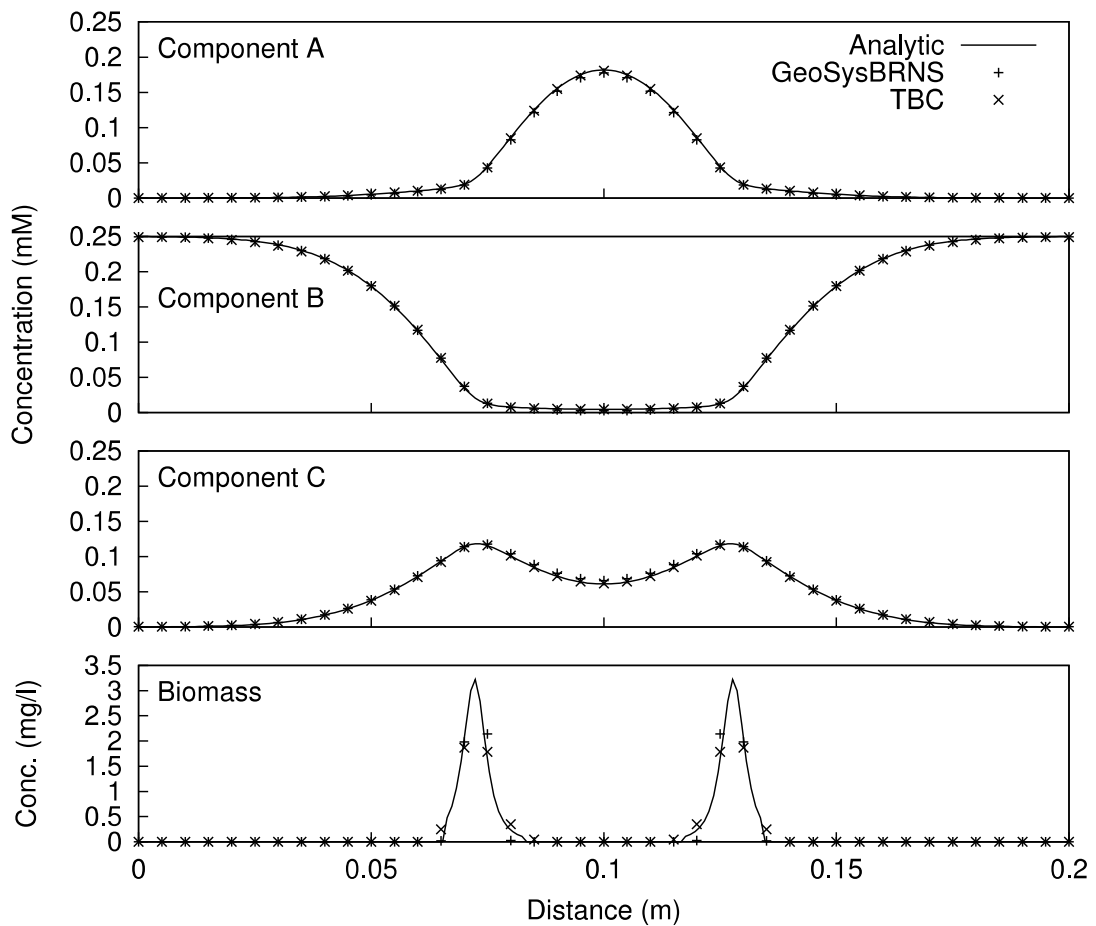Figure 11: Domain of Monod2D example

Figure 12: Comparison of OpenGeoSys-BRNS results, TBC results, and analytical solution for the double-Monod kinetics with biomass scenario. Profiles are recorded at day 300 along a vertical transect located one meter down stream of the in flow boundary.

4.3 Radium retardation in a radioactive waste repository

Solid Solution Theory The co-precipitation of radium with barium sulfates was first investigated by Doerner and Hoskins (1925). They found that in presence of a large excess of barium over radium, radium ions will be removed from the aqueous phase although the solubility product of radium sulfate is not exceeded. Langmuir and Riese (1985) derived the thermodynamic data of radium solid solution in sulfate and carbonate minerals. Zhu (2004) also provided fundamental data of binary mixing properties of radium for the barite isostructural family. Martin et al. (2003) evaluated experimentally the mobility of radium, and reported that dissolution of a $(Ba, Ra)SO_4$ solid solution controls the aqueous concentration of radium and barium in pore water released from nuclear waste repositories. In this context, for a better understanding of the retardation process on radionuclides in the near field of a nuclear waste repository, it is necessary to include the formation of Radium solid solutions in the model.

Retardation of Ra by solid solutions To demonstrate the retardation of radium by solid solution formations, a one dimensional column is set up in the model to represent the tunnel connecting an intermediate level waste repository. The simulation was set up in a way that at the beginning, radium cations (Ra^{2+}) and sulfate anions (SO_4^{2-}) diffuse into the tunnel from the opposite ends. Due to the presence of excess carbonate in the pore water of the bentonite-sand mixture, Ra^{2+} is first captured in Ba-Sr carbonate solid solutions. However, when sulfate anions enter the system, the carbonates are expected to be replaced with much less soluble Ba-Sr sulfates (barite and celestite). In turn, as the dissolved aqueous sulfates arrive at these areas, Ra^{2+} and radium in carbonates will be converted into sulfates, and the Ra^{2+} aqueous concentration will strongly decrease. In this way, most of the mobile radium will be immobilised in sulfate solid solutions. Upon further supply of sulfate ions, the dissolved concentrations of Ba, Sr and Ra are expected to continue decreasing, because of the so-called "common-anion" effect. For instance, if maximum dissolved concentration of sulfate is controlled by the presence of gypsum ($CaSO_4 \cdot 2H_2O$) which is much more soluble than celestite or barite, the dissolved Ba or Ra will be about two orders of magnitude less than that without extra gypsum. Details of the model setup can be found in [EP3].

The numerical reactive transport simulation results confirm this scenario. Fig. 13 depicts the aqueous radium and sulfate concentration at around 100 years. At places where Ra^{2+} meets SO_4^{2-}, Ra^{2+} concentration was immediately lowered and can not diffuse further. Fig. 14 compared the calculated Ra profile to the analytical solutions generated using a traditional K_D concept. The following set of Ra distribution coefficients $K_D = 0.0, 3.0 \times 10^{-4}, 2 \times 10^{-3}$ and 0.1 m^3/kg from the Nagra Technical Report (Nagra, 2002) was used for comparison. These values stand for no retardation, pessimistic, reference and optimistic estimation of the Ra sorption in compacted bentonite, respectively. As can be found, none of the K_D concept can reproduce the radium profile in this dynamic reaction system.

To test the model sensitivity on sulfate content, the amounts of barium, strontium and sulfate were varied and the simulation results were compared. In the system of interest, the limiting dissolved concentration of sulfate is expected to be set by the solubility of gypsum ($CaSO_4 \cdot 2H_2O$). Hence, we prepared five chemical setups of the backfill material containing 0.1%, 0.25%, 0.5%, 0.75% and 1% mass of gypsum, respectively. They were used as initial conditions in the reactive transport model. The sulfate-rich left boundary was removed, to let only Ra^{2+} diffusing from right to left. Therefore the shape of the radium front in Fig. 15 is different compared to Fig.
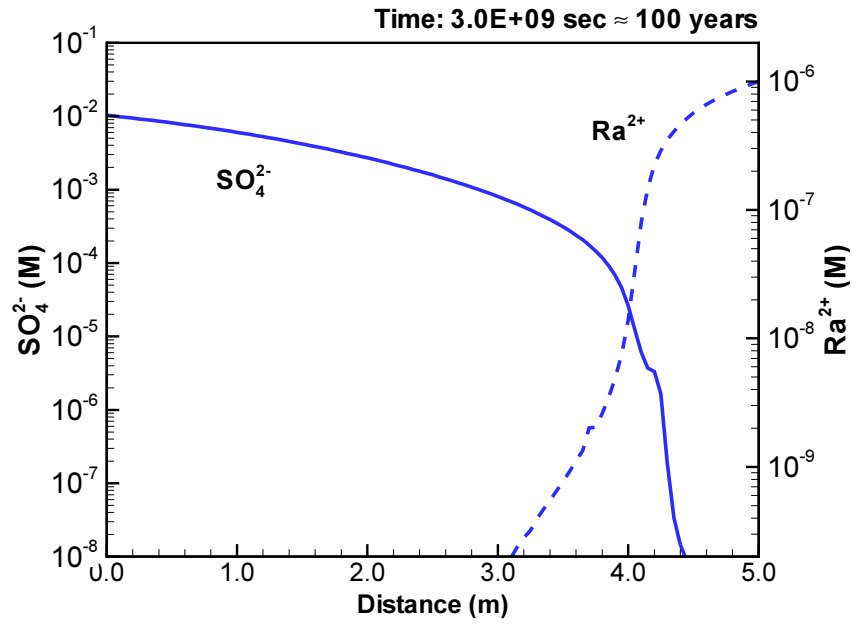
Figure 13: Temporal evolution of sulfate and radium aqueous concentration profiles at about 100 years; solid lines are SO_4^{2-} and dashed lines are Ra^{2+} results.
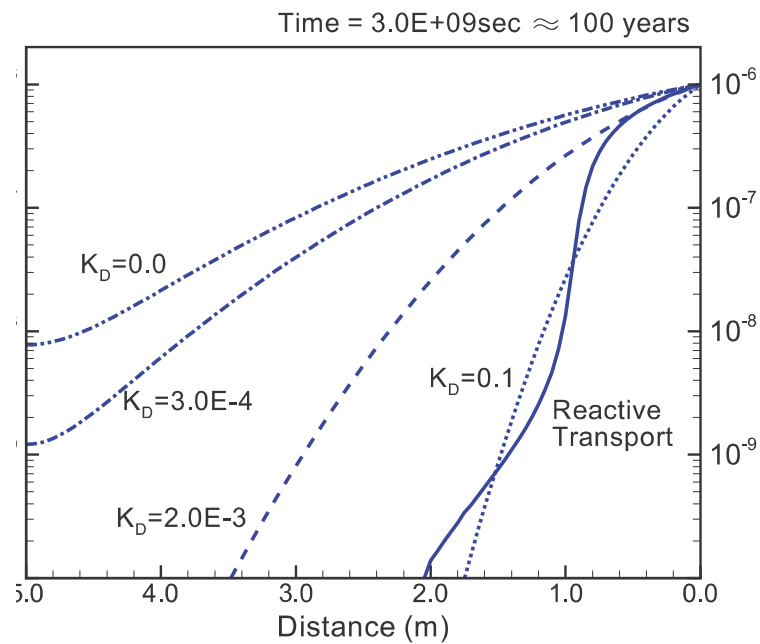

Figure 14: Comparison of the retardation behavior using solid solution and the traditional K_D concept. Solid lines are concentration profiles of Ra^{2+} using the solid solution approach, dashed, double-dotted lines, dashed-dotted lines, dashed lines and dotted lines are profiles calculated for K_D values of 0.0, 3×10^{-4}, 2×10^{-3}, and $0.1 m^3/kg$ respectively.
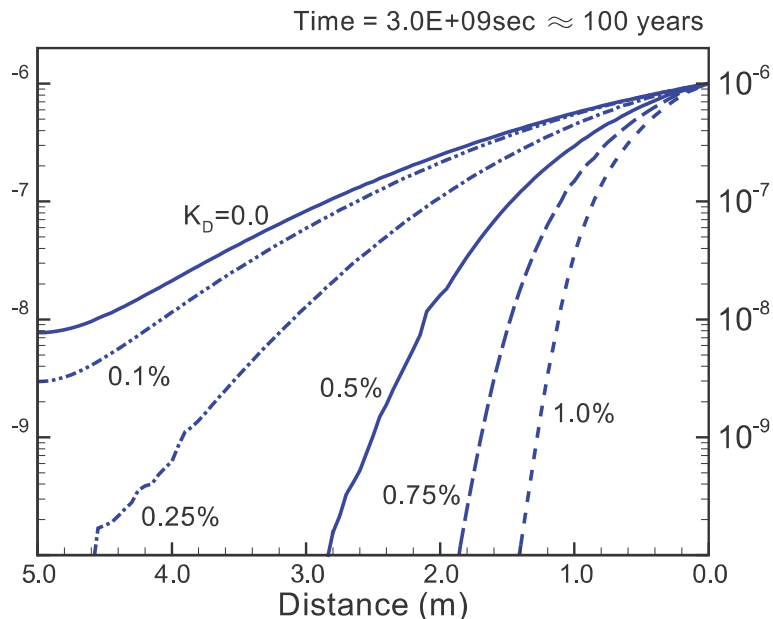
Figure 15: Sensitivity of retardation effects regarding the available amount of SO_4^{2+}. From right to left, the curves are Ra^{2+} concentration profiles calculated for 1%, 0.75%, 0.5%, 0.25% and 0.1% of gypsum initially existing in the solid phase of the buffer material, compared to the amount of calcite, respectively. The left most solid line is the reference profile calculated for a K_D value of zero.

13. It is found that the amount of sulfate heavily influences the formation of solid solutions. With 0.1% of gypsum added, the calculated Ra^{2+} profile is close to the reference curve that has no retardation effect. The more sulfate is available, the more strongly Ra^{2+} is retarded. Therefore, the availability of sulfate seems to be the most important factor for the retardation of radium.

Compare to ion-exchange effects For the bentonite, the ion-exchange process has long been considered as the major mechanism that contributes to the retardation of radio nuclide. In this context, it is necessary to model ion-exchange and solid solution effect together and investigate their combined influences on the retardation of radium. To achieve this, a new chemical component Na-Montmorillonite ($NaMgAl_5(Si_4O_{10})_3(OH)_6$, known as Mont in this work) was setup using GEMIPM2K. Its Gibbs formation energy (G°)was first taken from a thermodynamic database (SAIC, 2004) and then calibrated according to cation concentrations obtained in a dissolution experiments. Fernandez (2004) conducted the experiment on the cation exchange capacity of the Spanish FEBEX bentonite and reported the corresponding selectivity coefficients, following the Gaines and Thomas convention. To incorporate their measurement results, these coefficients were first converted to Vanselow coefficients and then to Gapon coefficients (see [EP4] for details), so that they can be used as equilibrium constants for cation exchange reactions. Based on these information, GEMIPM2K program calculates the G° values for all the other cation occupied end members, including K-, Mg-, Ca-, Sr, Ba- and Ra-Montmorillonites.
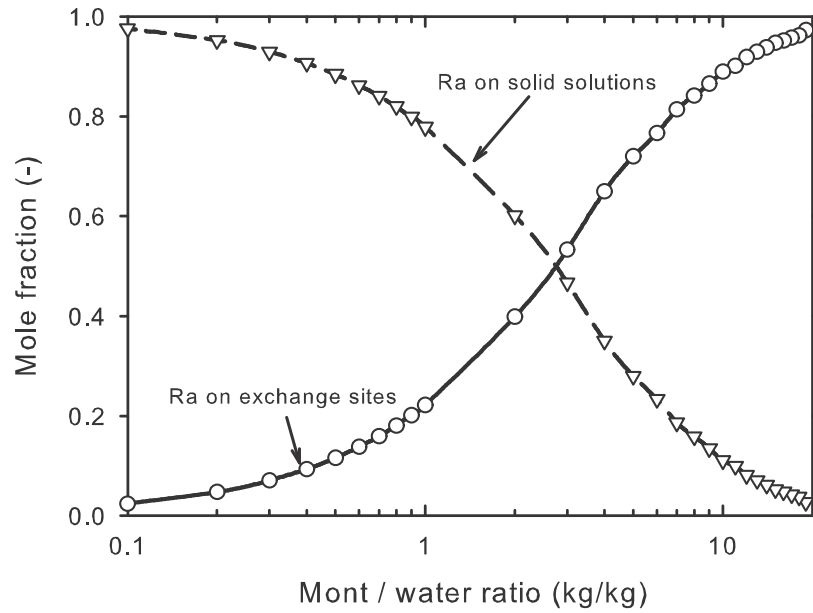
Figure 16: Influence of Mont/water ratio on the radium distribution among cation exchange sites and solid solution formations.

Details regarding the equilibrium exchange coefficients and model details can be found in the enclosed publication [EP4].

The introduction of ion-exchange process and the simulation of reactive transport in the idealised bentonite column reveals some new understandings. First, the Mont/water ratio in the geochemical system is varied from 0.1 to 19, and the distribution of Ra in cation exchange sites and solid solution formations is depicted in Fig. 16. At a Mont/water ratio of 19, bentonite is in a compacted form, which is used to seal the high level waste canister. Cation exchange sites in the Mont phase attract most of the Ba and Sr in the system so that, while carbonate and sulfate are abundant in the aqueous phase, insufficient Ba and Sr restrains the formation of Ra sulfate solid solutions. Sufficient Ba and Sr remain for sulfate formation only when the Mont/water ratio is lowered to approximately unity. Despite the fact that the limited clay content lowers the total amount of Ra bound in the Mont phase, the sulfate solid solutions compensate for this and provide a secondary fixation mechanism.

When the ratio is about 0.1, only a minor proportion of Ra is retained in the montmorillonite, and the incorporation in sulfate solid solution becomes the major retardation mechanism for the transport of radium. Fig. 17 shows the concentration profile for aqueous Ra^{2+} after 1000 years. The shape and extension of the profiles are similar at three different Mont/water ratios of 0.1, 1.0, and 10 kg/kg. The aqueous radium concentrations is lowered by $2 \sim 3$ orders of magnitude, as soon as it diffuses into the column. Both sulfate and Mont solid solutions provide the capacity to fix radium.
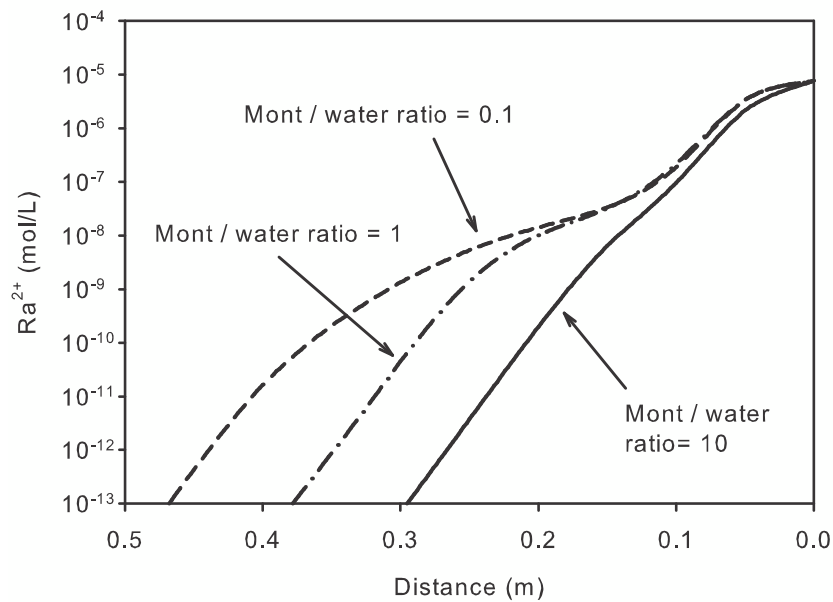
27

Figure 17: Aqueous phase radium profile after 1000 years, with clay content adjusted by Mont/water ratio of 10, 1.0 and 0.1 kg/kg.

5 Summary and outlook

In this work, an interface that connects mass transport and chemical reaction simulators was developed utilising the operator splitting technique. Two different chemical simulators, the Gibbs Energy Minimization Selektor (GEM), and the Bioreactive Reaction Network Simulator (BRNS), were coupled with the finite element tool OpenGeoSys. Both coupling has been verified against analytical solutions and results from other reactive transport codes. The coupled code OpenGeoSys-GEM, is applied to compare different retardation mechanisms in the near field of radio active waste repositories.

One drawback of this coupled structure is that the time step of the simulation needs to be manually adjusted to ensure the accuracy of the final result. In some cases, the reaction only happens when the front of one component meets the other, which makes the small time step on the beginning stage of the simulation not necessary. Possible solution is an adaptive time step scheme or a sequential iterative scheme. The former scheme decides the time size in the next step based on the error of the last result, and the latter iterates between transport and reaction to ensure the accuracy of the final result. Both of them are on-going works.

This work also explored the parallelization feature of the operator splitting scheme. The test with Monod2D example shows that the reaction part has a linear speed-up with regard to the increasing CPU cores. However, the transport part requires many communications. In sequential simulations, the chemical reaction consumes the majority of simulation time. In parallel ones, transport becomes the most time-consuming part. In order to achieve the shortest simulation time, a possible solution for the user is to only choose the parallelization for the reaction part.

28

With the coupled codes, reactive transport in a saturated porous media can be modelled. There will be several focuses in the future development. First, multi-phase flow processes will be integrated into the current code. This gives the opportunity to simulate chemical reactions in an unsaturated porous media, for applications such as CO_2 sequestration. Second, the sequential iterative scheme should be introduced to minimise the numerical error caused by operator splitting. Such feature is critical when chemical reactions change the flow field in cases like clogging. Last but not least, a global implicit scheme that solves reaction and transport together will be considered. The monolithic structure may fully exploit the potential of parallelization on a multi-processor high-performance computing platform.

References

Aguilera, D., Jourabchi, P., Spiteri, C., Regnier, P., 2005. A knowledge-based reactive transport approach for the simulation of biogeochemical dynamics in earth systems. Geochemistry, Geophysics, Geosystems 6, Q07012.

Bear, J., 1972. Dynamics of Fluids in Porous Media. Dover Publications, New York.

Bethke, C. M., 1996. Geochemical Reaction Modeling. Oxford University Press.

Chilakapati, A., 1995. Raft: A simulator for reactive flow and transport of groundwater contaminants, Internal Report 10636. Tech. rep., Pacific Northwest Laboratory, Richland, Washington.

Cirpka, O. A., Valocchi, A. J., 2007. Two-dimensional concentration distribution for mixing-controlled bioreactive transport in steady state. Advances in Water Resources 30, 1668–1679.

Cirpka, O. A., Valocchi, A. J., 2009. Reply to comments on "two-dimensional concentration distribution for mixing-controlled bioreactive transport in steady state" by H. Shao et al. Advances in Water Resources 32 (2), 298 − 301.

Clauser, C. E., 2003. Numerical Simulation of Reactive Flow in Hot Aquifers (SHEMAT and Processing SHEMAT). Springer, Berlin.

Cleverley, J., Hornby, P., Poulet, T., 2006. Reactive transport modelling in hydrothermal systems using the gibbs minimization approach. Geochimica et Cosmochimica Acta 70, A106.

Davies, C. W., 1962. Ion Association. Butterworths, Washington DC.

Doerner, H., Hoskins, W., 1925. Co-precipitation of radium and barium sulfates. Journal of American Chemical Society 47, 662 − 675.

Engesgaard, P., Kipp, K., 1992. A geochemical transport model for redox controlled movement of mineral fronts in groundwater flow systems - a case of nitrate removal by oxidation of pyrite. Water Resources Research 28(10), 2829–2843.

Fernandez, A. M., Baeyens, B., Bradbury, M., Rivas, P., 2004. Analysis of the porewater chemical composition of a spanish compacted bentonite used in an engineered barrier. Physics and Chemistry of the Earth 29, 105 − 118.

Glynn, P. D., Reardon, E. J., Plummer, L. N., Busenberg, E., 1990. Reaction paths and equilibrium end-points in solid-solution aqueous-solution systems. Geochimica et Cosmochimica Acta 54, 267–282.

Gómez, C., 1990. Macrofort: A fortran code generator in maple, rapport technique 119. Tech. rep., Institut National de Recherche en Informatique et en Automatique, Le Chesnay, France.

Guimares, L., Gens, A., Olivella, S., 2007. Coupled thermo-hydro-mechanical and chemical analysis of expansive clay subjected to heating and hydration. Transport in Porous Media 66, 341–372.

Karpov, I., Chudnenko, K., Kulik, D., 1997. Modeling chemical mass transfer in geochemical processes: thermodynamic relations, conditions of equilibria, and numerical algorithms. American Journal of Science 297, 767–806.

Karpov, I., Chudnenko, K., Kulik, D., Avchenko, O., Bychinski, V., 2001. Minimization of gibbs free energy in geochemical systems by convex programming. Geochemistry International 39, 1108–1119.

Kolditz, O., Bauer, S., 2004. A process-orientated approach to compute multi-field problems in porous media. International Journal of Hydroinformatics 6, 225–244.

Kulik, D., Dmytrieva, S., Chudnenko, K., Thoenen, T., Wagner, T., 2008. Gem-selektor (gems-psi) - research package for thermodynamic modeling of aquatic (geo)chemical systems by gibbs energy minimization. Paul Scherrer Institut, http://gems.web.psi.ch/.

Lagneau, V., Lagneau, A., Catalette, H., 2005. Reactive transport modeling of co2 sequestration in deep saline aquifers. Oil & Gas Science and Technology - Revue de l'IFP 60, 231–247.

Langmuir, D., Riese, A., 1985. The thermodynamic properties of radium. Geochimica et Cosmochimica Acta 49, 1593–1601.

Martin, A., Crusius, J., McNee, J. J., Yanful, E., 2003. The mobility of radium-226 and trace metals in pre-oxidized subaqueous uranium mill tailings. Applied Geochemistry 18, 1095–1110.

Mayer, K., Frind, E., Blowes, D., 2002. Multicomponent reactive transport modeling in variably saturated porous media using a generalized formulation for kinetically controlled reactions. Water Resources Research 38(9), 1174.

Nagra, 2002. Models, codes and data for safety assessment. Technical Report 02-06, National Cooperative for the Disposal of Radioactive Waste, Wettingen, Switzerland, iSSN 1015-2636.

Prommer, H., 2002. A reactive multicomponent transport model for saturated porous media, user's manual version 1.0. Tech. rep., Contaminated Land Assessment and Remediation Research Centre, The University of Edinburgh, UK.

Pruess, K., Garcia, J., Kovscek, T., Oldenburg, C., Rutqvist, J., Steefel, C., Xu, T., 2004. Code intercomparison builds confidence in numerical simulation models for geological disposal of co2. Applied Geochemistry 29, 1431–1444.

Regnier, P., Wollast, R., Steefel, C. I., 1997. Long-term fluxes of reactive species in micro-tidal estuaries: Estimates from a fully transient, multi-component reaction-transport model. Marine Chemistry 58, 127–145.

SAIC, B., 2004. Qualification of Thermodynamic Data for Geochemical Modeling of Mineral-Water Interactions in Dilute Systems. U.S. Department of Energy, Office of Scientific & Technical Information, Springfield, VA, page 6-42.

Schäfer, D., Schäfer, W., Kinzelbach, W., 1998. Simulation of reactive processes related to biodegradation in aquifers 1. structure of the three-dimensional reactive transport model. Journal of Contaminant Hydrology 31(1-2), 167–186.

Steefel, C. I., DePaolo, D. J., Lichtner, P. C., 2005. Reactive transport modeling: An essential tool and a new research approach for the earth sciences. Earth and Planetary Science Letters 240, 539–558.

Valocchi, A., Malmstead, M., 1992. Accuracy of operator splitting for advection-dispersion-reaction problems. Water Resources Research 28, 1471–1476.

Van der Lee, J., Windt, L. D., Lagneau, V., Goblet, P., 2003. Module-oriented modeling of reactive transport with hytec. Computers & Geosciences 29, 265–275.

Xie, M., Bauer, S., Kolditz, O., Nowak, T., Shao, H., 2006. Numerical simulation of reactive processes in an experiment with partially saturated bentonite. Journal of Contaminant Hydrology 83, 122–147.

Xu, T., Apps, J., Pruess, K., 2004. Numerical simulation of CO_2 trapping in deep aquifers. Applied Geochemistry 19, 917–936.

Xu, T., Pruess, K., 2001. Modeling multiphase non-isothermal fluid flow and reactive geochemical transport in variably saturated fractured rocks: 1. methodology. American Journal of Science 301, 16–33.

Yeh, G.-T., Tripathi, V., 1989. A critical evaluation of recent developments in hydrogeochemical transport models of reactive multichemical components. Water Resources Research 25, 93–108.

Zhu, C., 2004. Coprecipitation in the barite isostructural family: 1. binary mixing properties. Geochimica et Cosmochimica Acta 68 (16), 3327–3337.

Enclosed Publications

[EP1] Florian Centler, **Haibing Shao**, Cecilia De Bias, Chan-Hee Park, Pierre Regnier, Olaf Kolditz and Martin Thullner (2009): GeoSysBRNS - A Flexible Multidimensional Reactive Transport Model for Simulating Biogeochemical Subsurface Processes, *Computers & Geosciences*, in print.

[EP2] **Haibing Shao**, Florian Centler, Cecilia De Biase, Martin Thullner and Olaf Kolditz (2009): Comments on "Two-dimensional concentration distribution for mixing-controlled bioreactive transport in steady-state flow" by O.A. Cirpka and A.J. Valocchi, *Advances in Water Resources* 32(2), 293-297.

[EP3] **Haibing Shao**, Svitlana V. Dmytrieva, Olaf Kolditz, Dmitrii A. Kulik, Wilfried Pfingsten and Georg Kosakowski (2009): Modeling reactive transport in non-ideal aqueous solid solution system, *Applied Geochemistry* 24(7), 1287-1300.

[EP4] **Haibing Shao**, Dmitrii A. Kulik, Urs Berner, Georg Kosakowski and Olaf Kolditz (2009): Modeling the competition between solid solution formation and cation exchange on the retardation of aqueous radium in an idealized bentonite column, *Geochemical Journal* 43(6), e37-e42.

Enclosed Publication

[EP1]   Florian. Centler,   **Haibing Shao**, Cecilia De Bias, Chan-Hee Park, Pierre
        Regnier, Olaf Kolditz and Martin Thullner (2009): GeoSysBRNS - A Flexible
        Multidimensional Reactive Transport Model for Simulating Biogeochemical
        Subsurface Processes, *Computers & Geosciences*, in print.

GeoSysBRNS—A flexible multidimensional reactive transport model for simulating biogeochemical subsurface processes

Florian Centler [a,*], Haibing Shao [b], Cecilia De Biase [a], Chan-Hee Park [b], Pierre Regnier [c,d], Olaf Kolditz [b], Martin Thullner [a]

[a] UFZ – Helmholtz Centre for Environmental Research, Department of Environmental Microbiology, Permoserstraße 15, D-04318 Leipzig, Germany
[b] UFZ – Helmholtz Centre for Environmental Research, Department of Environmental Informatics, Permoserstraße 15, D-04318 Leipzig, Germany
[c] Utrecht University, Department of Earth Sciences–Geochemistry, PO Box 80021, 3508TA Utrecht, The Netherlands
[d] Université Libre de Bruxelles, Department of Earth and Environmental Sciences, CP 160/02, 50 Av. F. D. Roosevelt, B-1050 Brussels, Belgium

ARTICLE INFO

ABSTRACT

The description of reactive transport processes in subsurface environments requires a sound understanding of both the biogeochemical complexity of the system and the spatially resolved transport of reactive species. However, most existing reactive transport models, for example in the field of contaminant hydrology, are specialized either in the simulation of the reactive or of the flow and transport processes. In this paper, we present and test the coupling of two highly flexible codes for the simulation of reactive transport processes in the subsurface: the Biogeochemical Reaction Network Simulator (BRNS), which contains a solver for kinetically and thermodynamically constrained biogeochemical reactions, and GeoSys/RockFlow, a multidimensional finite element subsurface flow and transport simulator. The new model, named GeoSysBRNS, maintains the full flexibility of the original models. The coupling is handled using an operator splitting scheme, which allows the reactive solver to be compiled into a problem specific library that is accessed by the transport simulator at runtime. The accuracy of the code coupling within GeoSysBRNS is demonstrated using two benchmark problems from the literature: a laboratory experiment on organic carbon degradation in a sand column via multiple microbial degradation pathways, and a dispersive mixing controlled bioreactive transport problem in aquifers, assuming three different reaction kinetics.

© 2009 Elsevier Ltd. All rights reserved.

1. Introduction

The fate of reactive species in subsurface environments, for example in soils, aquifers, or aquatic sediments, depends on a multitude of hydrological, geochemical, and microbiological processes. These processes are not only highly interlinked, but also act in parallel, making the identification and quantification of the key processes controlling the systems dynamics difficult. As high resolution field measurements are seldom available, and laboratory results usually cannot be transferred to the field scale easily, simulation tools that can integrate this coupled interplay have proven essential to improve our qualitative and quantitative understanding of subsurface systems. This knowledge is of paramount value in the context of bioremediation of contami-

nated field sites and, more generally, to help unravel the cycling of reactive species in the environment.

To address the complex interplay of processes and their impact on the fate of bioreactive species in the subsurface, many numerical modeling approaches have been presented in the literature (Murphy and Ginn, 2000; Barry et al., 2002; Brun and Engesgaard, 2002; Thullner et al., 2007; Berner, 1980; Van Cappellen and Gaillard, 1996; Boudreau, 1997; Meysman et al., 2003; Jourabchi et al., 2005; Bauer et al., 2006). For soil and groundwater environments, the description of reactive processes often needs to be combined with an accurate simulation of flow and transport in multiple dimensions. In recent years, many simulation models that implement such a coupling have been introduced (e.g., Schäfer et al., 1998a; Prommer et al., 2003; Mayer et al., 2002; Clement et al., 1998; Pfingsten, 1996). Although the flexibility of these reactive transport models has increased over the years, current models are still limited with respect to the type of reactive processes that can be implemented. Usually, chemical rate laws describing the reactive processes to be included in the model have to follow a predefined form (e.g., Monod-type terms or power law degradation terms).

* Corresponding author. Tel.: +49 341 235 1336; fax: +49 341 235 1351.
E-mail addresses: florian.centler@ufz.de (F. Centler),
haibing.shao@ufz.de (H. Shao), cecilia.debiase@ufz.de (C. De Biase),
chanhee.park@ufz.de (C.-H. Park), p.regnier@geo.uu.nl (P. Regnier),
olaf.kolditz@ufz.de (O. Kolditz), martin.thullner@ufz.de (M. Thullner).

Furthermore, microbially mediated processes are often attributed to a single generic biomass species, concealing the fact that bacterial communities consisting of many species providing different biochemical transformation pathways are usually involved. As more and more details on biotic and abiotic reactive processes in the subsurface are uncovered, a flexible simulation framework is desirable that allows for the inclusion of arbitrary reaction dynamics (Zhang et al., 2007). Providing such flexibility without the need to make changes at the source code level of the simulator has been the main motivation for the development of the Biogeochemical Reaction Network Simulator (BRNS, Regnier et al., 2002; Aguilera et al., 2005). This code can simultaneously consider an arbitrary number of kinetically and thermodynamically constrained reactions coupled to transport and has been successfully applied to subsurface problems ranging from marine sediments to groundwater aquifers (Thullner et al., 2005; Jourabchi et al., 2005). The BRNS simulator is, however, restricted to one-dimensional systems. This limits its application range, especially in the field of contaminant hydrology. The present study aims at overcoming this restriction by coupling the reaction network component embedded in the BRNS to GeoSys/RockFlow, a finite element simulator for flow, transport, and deformation processes in fractured-porous media (Kolditz and Bauer, 2004; Wang and Kolditz, 2007).

This article is organized as follows. After a short introduction of both codes and the employed coupling technique (Section 2), the coupled model is tested for two exemplary applications (Section 3), followed by a discussion and outlook on the applicability of the new model (Section 4).

2. Technical implementation

2.1. GeoSys/RockFlow

The scientific open source software GeoSys/RockFlow is a numerical simulator for the analysis of thermo-hydraulic-mechanically (THM) coupled processes in porous media. It has been originally developed in the 1980s at the University of Hannover. Currently, the 4th version of GeoSys is written in C++ following the object-oriented programming paradigm (Kolditz and Bauer, 2004; Wang and Kolditz, 2007), which enables both developers and users to easily reorganize the code for particular applications in geotechnics (Park et al., 2008; Rutqvist et al., 2008) and hydrology (Bauer et al., 2006; Kolditz et al., 2008). GeoSys is based on the finite element method (FEM), which handles one-, two-, and three-dimensional model domains. Space is discretized by regular and irregular meshes using line, triangle, quad, tetrahedron, and hexahedron elements, facilitating complex model domain geometries. GeoSys is capable of modeling saturated, unsaturated, and multiphase flow, as well as density dependent flows, heat and mass transport, and mechanical deformation. It is also available in a parallelized version, based on the message passing interface (MPI), allowing for large scale simulations on high-performance-computing (HPC) clusters.

2.2. BRNS

The biogeochemical reaction network simulator (BRNS) has been developed to simulate one-dimensional flow, solute transport, and coupled biogeochemical processes (Aguilera et al., 2005, and references therein). One key aspect of its design concerns the high flexibility with which alternative biogeochemical process descriptions can be included and combined within the model. Kinetically controlled and equilibrium reactions, and mixtures of both can be specified. The equations describing the transformations of the chemical and biotic species can be of arbitrary form. To achieve this high degree of flexibility, an automated code generation process is employed, using the MAPLE symbolic algebra language (Chilakapati, 1995; Regnier et al., 1997). An Automatic Code Generator (ACG) relying on the MACROFORT package (Gómez, 1990; Aguilera et al., 2005) compiles these process descriptions into problem specific Fortran code that complements a numerical engine containing generic routines written in Fortran. By using full operator splitting, the transport and reactive calculations are fully separated in the original stand-alone version of BRNS. Within the employed sequential non-iterative approach (SNIA), first the transport step, and then the reactive step is solved in each time step of the simulation loop. While the transport is solved using a fully implicit finite difference approximation, the biochemical step is solved by using the iterative Newton–Raphson method.

2.3. Coupling structure

The reactive solver of BRNS is coupled to GeoSys following the sequential non-iterative approach already used in BRNS. In each time step of the simulation loop, first the transport calculations are performed in GeoSys, followed by the reactive step. Within this reactive step, the species concentrations of a specific node of the domain and the time step size are passed to the reactive solver implemented in BRNS. Next, the concentration changes are computed according to the defined chemical kinetic and equilibrium reactions, and the updated concentrations are then passed back to GeoSys. This chemical computation step is consecutively performed for all nodes of the simulation domain. Note that the implemented coupling procedure can also be used to bi-directionally pass additional information between the transport and reactive part of the simulator. Hence, reactive processes having effects on the transport (e.g., changes in porosity) can easily be implemented in future versions of GeoSysBRNS.

In order to maintain high flexibility for further developments in both simulation codes, the interface connecting them is reduced to a minimum. A new object in GeoSys handles all communication between the transport and the reactive code. On the side of BRNS, a new function allows an external caller to make use of the implemented reactive solver, with the original BRNS code staying unchanged. The chemical solver and the problem specific description of reactive processes to be included in the model are compiled into a library, which is linked to the GeoSys simulator at runtime (Fig. 1). This modular approach has several advantages. Model development benefits as both codes can be further developed completely independently. By compiling the chemical part into a dynamic link library on the Windows platform (dll file) and a shared object file on the Unix platform (so file), this flexibility is paired with fast data exchange and low computational overhead of the coupling.

2.4. Running a coupled simulation

Creating a model in GeoSysBRNS consists of defining two inputs: one describing the model domain including physical parameters, hydrogeological flow, discretization parameters and (bio-)chemical species including diffusion constants for mobile species, and the other specifying the coupled (bio-)chemical reaction processes to be considered in the model. For the first set of input parameters, the standard GeoSys format is used. For the second set, the Maple worksheet format already used in the BRNS model is also applied here. A Windows batch script, accepting the Maple worksheet in Maple Input format (mpl file) via drag and

Model description / Input files
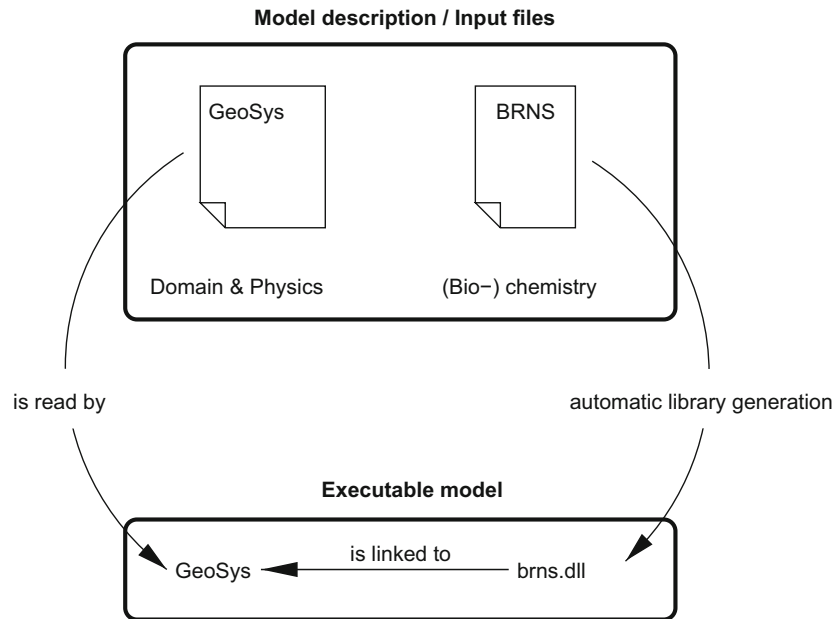
Fig. 1. Setup of GeoSysBRNS. Model description is divided into two parts: model domain definition, physical parameters, hydrogeological flow, and discretization parameters in GeoSys format, and description of coupled (bio-)chemical reaction processes in BRNS format which is compiled into a problem specific library that is accessed by GeoSys at runtime.

drop, automates the compilation of the problem specific dll library. Fig. 1 summarizes the complete model setup. To be successful, the operation requires that the reactive species appearing in the Maple worksheet file and in the GeoSys input file (mcp file) follow the same order. Furthermore, the units for parameters (reaction rates, transport parameters, etc.) and concentrations must be consistent in both input files.

3. Applications

To test the coupled code, we present two applications. First, GeoSysBRNS simulation results are compared with those obtained with the stand-alone version of BRNS (Thullner et al., 2005) in the case of a one-dimensional sand column experiment dealing with organic carbon degradation. Second, an aquifer scenario in two dimensions is run with GeoSysBRNS assuming three different reaction kinetics. Results of the simulations are compared to analytical solutions or outputs from the reactive transport models TBC (Schäfer et al., 1998a) and MIN3P (Mayer et al., 2002).

3.1. One-dimensional sand column experiment

Column experiments are often used to study the degradation of organic contaminants in the saturated groundwater zone. An experimental study by von Gunten and Zobrist (1993) has been used to validate the reactive transport models TBC (Schäfer et al., 1998b) and BRNS (Thullner et al., 2005). Both models could reproduce the experimental data set. We compare GeoSysBRNS simulation runs with the BRNS results published in Thullner et al. (2005) to validate the coupled model.

3.1.1. Model setup

In the example referred to as "Scenario 1" in Thullner et al. (2005), a sand column of 29 centimeters length is constantly flushed with water containing lactate as electron donor, and oxygen, nitrate, and sulfate as terminal electron acceptors (TEAs). Manganese and iron oxyhydroxides are bound to the sand matrix
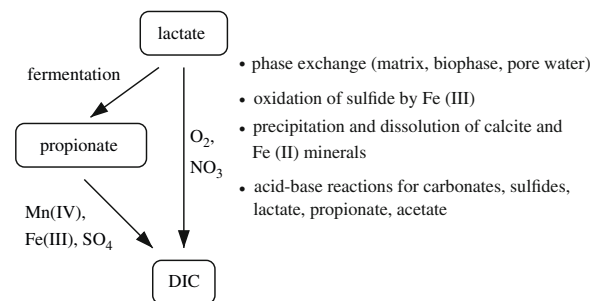
Fig. 2. Modeling organic carbon degradation in sand column experiment. Microbial degradation pathways with corresponding TAEs (left) and coupled abiotic processes considered (right).

in solid phases and act as two additional TEAs. Five distinct microbial groups, which catalyze the reduction of each TEA to sustain their growth, are considered in the model. The experimental results suggest that lactate is concomitantly mineralized into dissolved inorganic carbon (DIC) and fermented to acetate and propionate, with the latter being further oxidized into DIC. In addition to these microbial degradation pathways, reactive species concentrations are influenced by a set of abiotic reactions (Fig. 2). The complete reaction network of the model consists of 21 mobile and 18 immobile reactive species. The dynamics of the system is determined by 24 kinetically controlled chemical reactions and nine equilibrium reactions describing acid base dissociations.

3.1.2. Results

We simulate the experiment with GeoSysBRNS using two spatial resolutions and three different temporal resolutions per spatial setting, ensuring Courant numbers less than 1.0 in all cases. As in previous studies (Thullner et al., 2005; Schäfer et al., 1998b), we choose 48 days as the target time for comparing the results of the present model to those obtained with the BRNS model using the same set of spatio-temporal resolution settings. At this target time, the system is still in the transient phase.

The simulation results of GeoSysBRNS and BRNS agree very well for all 39 reactive species at the highest spatial and temporal resolution (see selected species in Figs. 3 and 4). Decreasing the spatial resolution leads to slightly different results, with the present model generally staying closer to the high resolution result than BRNS (Figs. 3 and 4).

When the time step size is increased, the numerical results of both models diverge from the high resolution result (Fig. 5). While increasing the time step from 4 to 43.2 s does not lead to significant changes for both models and both spatial resolutions, a noticeable deviation is observed when the time step size is further increased to 108 s for the high, and to 216 s for the low spatial resolution. For these larger time step sizes, the results of GeoSysBRNS are again generally closer to the high resolution result than the BRNS solutions. The observed differences can be attributed to the different numerical schemes used by BRNS (finite differences) and GeoSysBRNS (finite elements).

3.2. Two-dimensional aquifer scenario

The natural attenuation process in contaminated groundwaters is usually limited by the coexistence of electron donor (organic carbon) and acceptor substrates. Recently, Cirpka and Valocchi (2007) presented a two-dimensional analytical solution for the steady state case where the spatial overlap of the reactants is dominated by transversal mixing. This example serves here as a two-dimensional benchmark to validate the present model. The dynamics of the redox reaction was assumed to be controlled by three different mechanisms: instantaneous (thermodynamical) equilibrium, double-Monod kinetics, and double-Monod kinetics with biomass. In the equilibrium case, GeoSysBRNS simulation results are compared to an analytical solution provided by Cirpka and Valocchi (2007). Simulations with double-Monod kinetics are compared to numerical results obtained with TBC (Schäfer et al., 1998a), a reactive transport
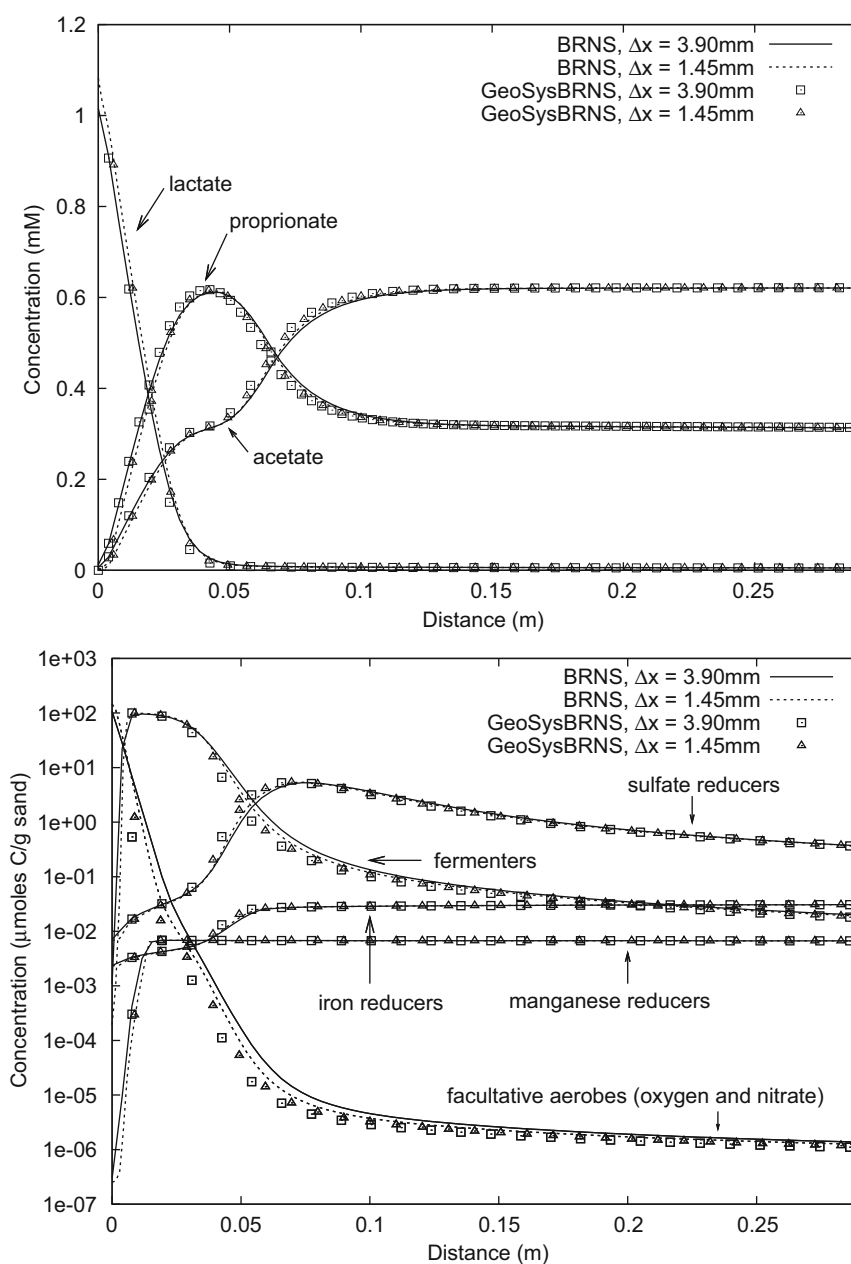
Fig. 3. Comparison of simulation results obtained with BRNS (lines) and GeoSysBRNS (symbols): organic species (top) and all five bacterial groups (bottom) at day 48 using highest temporal resolution ($\Delta t = 4$ s) and two spatial resolutions.
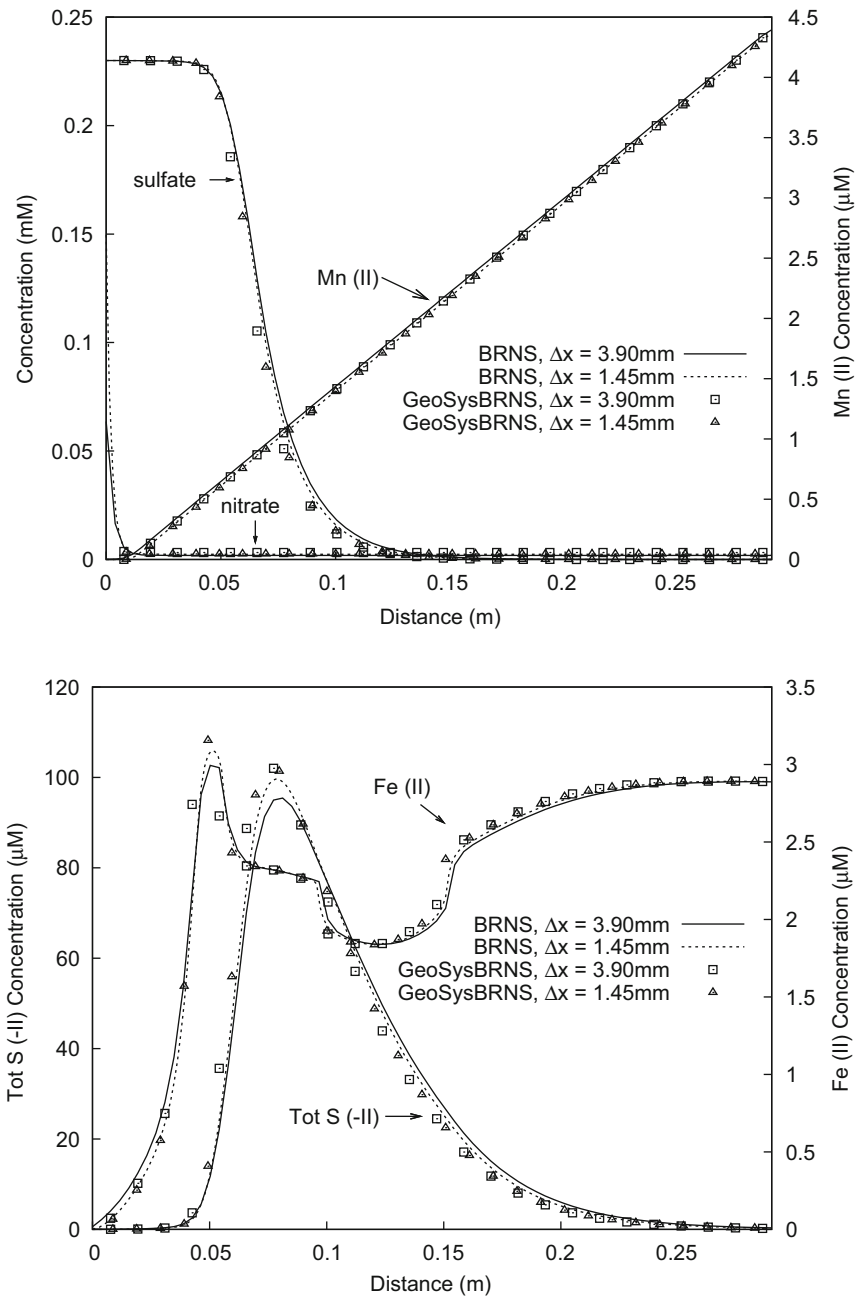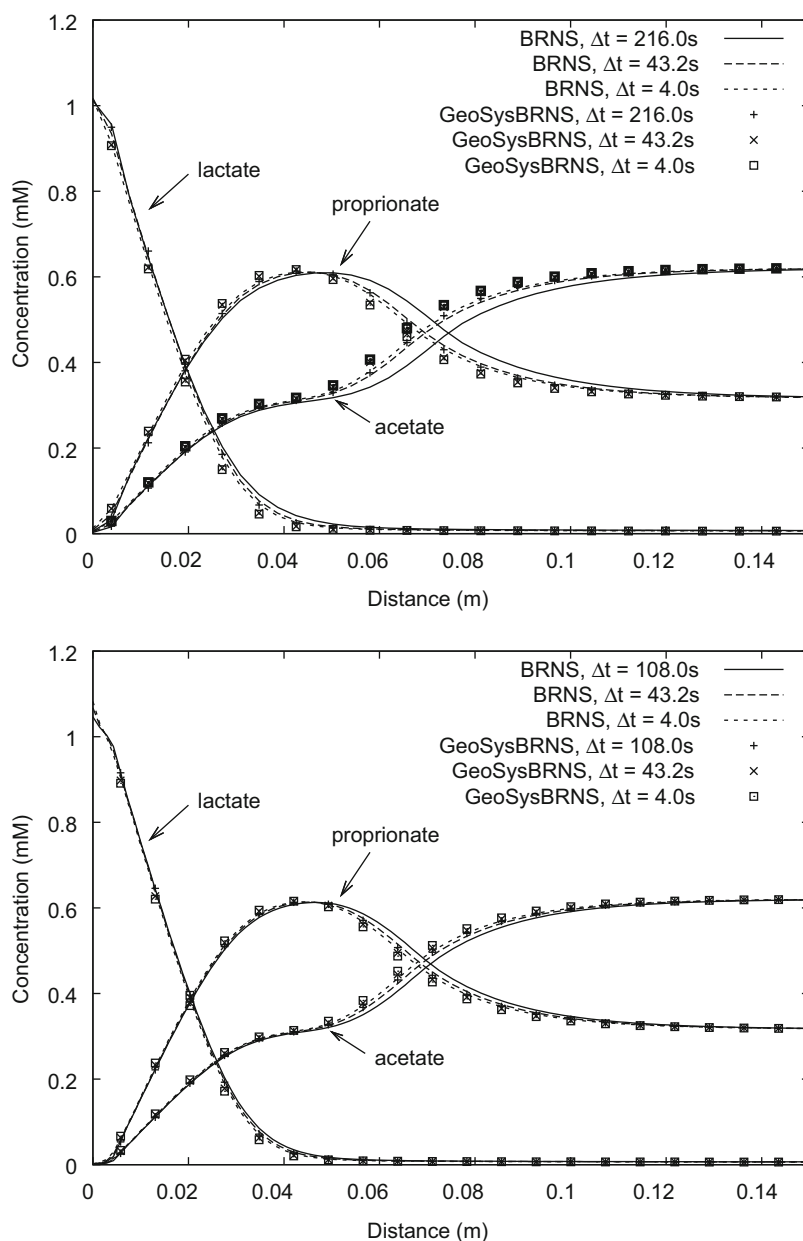
Fig. 4. Comparison of simulation results obtained with BRNS (lines) and GeoSysBRNS (symbols): inorganic species at day 48 using highest temporal resolution ($\Delta t = 4$ s) and two spatial resolutions.

code following an operator splitting approach, and MIN3P (Mayer et al., 2002), a simulation code that employs a global implicit solution method. When double-Monod kinetics with biomass is considered, GeoSysBRNS simulation results are compared to TBC runs and to an analytic solution provided by Cirpka and Valocchi (2007) in its revised form (Cirpka and Valocchi, 2009; Shao et al., 2009).

3.2.1. Model setup

The model domain spans 5 m in x-direction and 20 cm in y-direction (see Fig. 6). Groundwater flows along the positive x-direction at a transport velocity of 1 m/d. The porosity is 0.5 and the transversal dispersion coefficient is 2.5 cm^2/d. While the

analytical solution neglects any longitudinal dispersion, a numerical simulation always contains some numerical dispersion. For our simulations, we choose a longitudinal dispersion coefficient of 250 cm^2/d. Smaller values did not change the steady state simulation results. Two chemical compounds A and B are continuously entering the model domain with inflowing water at the left boundary during the entire simulation time, acting as carbon source or electron acceptor, respectively, in the biodegradation reaction of the form $A + B \rightarrow C$. The carbon source A is entering the domain at a concentration of 3.3×10^{-4} M along a 5 cm section in the center of the inflow boundary, and the electron acceptor B is entering the domain at a concentration of 2.5×10^{-4} M along the remaining parts of the inflow boundary. To test the accuracy of the flow and

Fig. 5. Comparison of simulation results obtained with BRNS (lines) and GeoSysBRNS (symbols) at day 48 using two spatial resolutions (top: $\Delta x = 3.9$ mm, bottom: $\Delta x = 1.45$ mm) and different time step sizes for lactate, proprionate, and acetate.
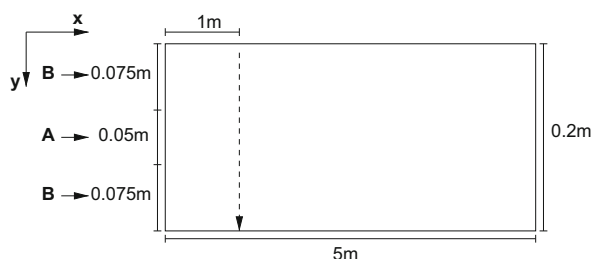
Fig. 6. Simulation domain. Groundwater flows along positive x-direction, with components A and B being injected at indicated segments of left boundary. Numerical simulation results are compared using concentration profiles along a transect at a distance of 1 m from inflow boundary, as indicated by dashed arrow.

transport modules in the model, a conservative tracer enters the domain at a concentration of 1.0 M along the same central section as A. Components A, B, and the reaction product C are mobile while biomass is considered immobile. The initial biomass concentration in the whole domain is set to 1.0×10^{-6} g/l.

All numerical simulations are performed using a discretization of $\Delta x = 2.5$ cm, $\Delta y = 5$ mm, and $\Delta t = 2$ min. Concentration profiles are compared at steady state along a vertical transect through the domain located 1 m downstream of the inflow boundary (cf. dashed arrow in Fig. 6).

We consider three different mechanisms controlling the redox reaction dynamics:

Equilibrium kinetics: Following Cirpka and Valocchi (2007), microbial degradation is described here by the instantaneous reaction $A + B \leftrightarrow C$. This reaction is assumed to be in thermodynamic equilibrium. Instead of requiring $C_A C_B = 0$ M^2 as in the analytical derivation, we demand $C_A C_B = 10^{-10}$ M^2 as a more realistic setting.

Double-Monod kinetics: When bacterial growth is assumed to follow double-Monod kinetics, the rate of change of reactant (A, B) and product (C) concentrations can be described by three
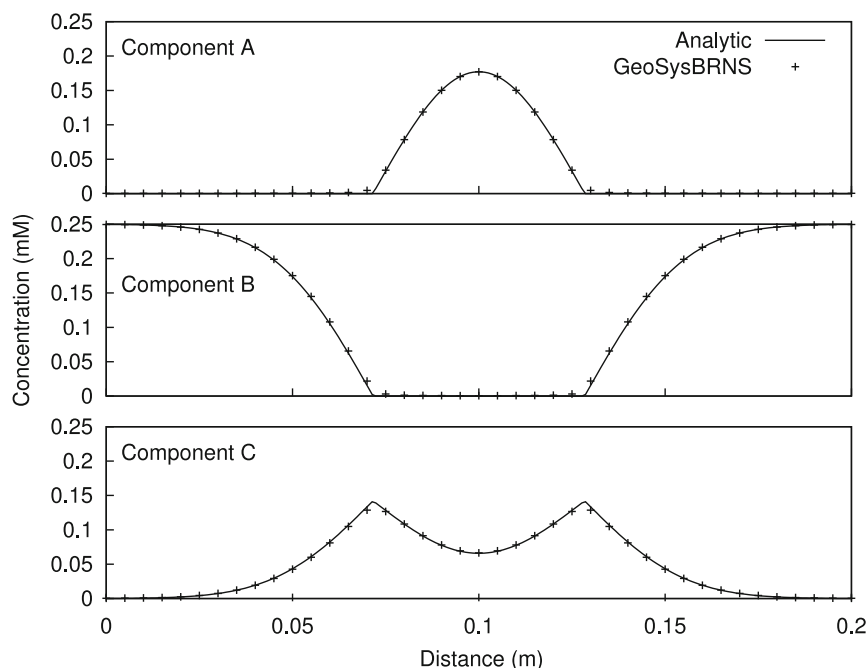
Fig. 7. Comparison of GeoSysBRNS results to analytical solution for equilibrium scenario. Profiles are recorded at day 20 along a vertical transect located 1 m downstream of inflow boundary.

differential equations:

$$\frac{\partial C_C}{\partial t} = \frac{C_A}{K_A + C_A}\frac{C_B}{K_B + C_B}k \tag{1}$$

$$\frac{\partial C_A}{\partial t} = -\frac{C_A}{K_A + C_A}\frac{C_B}{K_B + C_B}k = -\frac{\partial C_C}{\partial t} \tag{2}$$

$$\frac{\partial C_B}{\partial t} = -\frac{C_A}{K_A + C_A}\frac{C_B}{K_B + C_B}k = -\frac{\partial C_C}{\partial t} \tag{3}$$

We choose for the parameters: $K_A = 8.33 \times 10^{-5}$ M, $K_B = 3.13 \times 10^{-5}$ M, and $k = 5.0 \times 10^{-9}$ M/s.

Double-Monod kinetics with biomass: In this scenario, biomass (bio) is now explicitly represented in the model. The reaction rate does no longer depend only on the reactants following double-Monod kinetics, but also linearly on the biomass concentration C_{bio}. Biomass decays with constant first order rate parameter d. The system now contains four differential equations:

$$\frac{\partial C_{bio}}{\partial t} = \frac{C_A}{K_A + C_A}\frac{C_B}{K_B + C_B}\mu_{\max}C_{bio} - dC_{bio} \tag{4}$$

$$\frac{\partial C_A}{\partial t} = -\frac{1}{Y}\frac{C_A}{K_A + C_A}\frac{C_B}{K_B + C_B}\mu_{\max}C_{bio} \tag{5}$$

$$\frac{\partial C_B}{\partial t} = -\frac{1}{Y}\frac{C_A}{K_A + C_A}\frac{C_B}{K_B + C_B}\mu_{\max}C_{bio} \tag{6}$$

$$\frac{\partial C_C}{\partial t} = \frac{1}{Y}\frac{C_A}{K_A + C_A}\frac{C_B}{K_B + C_B}\mu_{\max}C_{bio} \tag{7}$$

We choose the same parameter values as Cirpka and Valocchi (2007): maximum growth rate $\mu_{\max} = 1.0\,\mathrm{d}^{-1}$, $d = 0.1\,\mathrm{d}^{-1}$, $Y = 1.0\,\mathrm{g/mol}$. The remaining parameters are set to the same values as in the double-Monod scenario without biomass.

3.2.2. Results

For all used codes, the simulated conservative tracer profiles agree very well with the analytical solution, confirming that flow and transport is simulated correctly (results not shown).

The equilibrium scenario was simulated for 20 days. Steady state has been reached during this simulation time. The numerical GeoSysBRNS results are in good agreement with the analytical solution provided by Cirpka and Valocchi (2007) (Fig. 7). However, a small deviation can be observed where the concentrations of components *A* and *B* change from zero to non-zero values. While the analytical solution assumes that both components are mutually exclusive present at any location in the domain, the numerical simulation has been set up with a less strict constraint as a more realistic scenario, leading to the observed deviation.

Simulating the double-Monod scenario for 20 days provides the steady state concentration distribution within the simulation domain. As an analytic solution was not available for this scenario, we compare the GeoSysBRNS result to simulation runs with TBC and MIN3P. All three codes agree very well (Fig. 8), despite using different methodologies: while GeoSysBRNS and TBC follow an operator splitting scheme, MIN3P employs a global implicit solution method.

The double-Monod scenario with biomass is simulated for 300 days. While the solute species concentration profiles are identical after 150 and 300 days of simulation, the biomass concentration still shows subtle changes within this time interval, indicating that the system converges very slowly to the steady state. The numerical simulation results of GeoSysBRNS are nevertheless in good agreement with the analytical solution provided by Cirpka and Valocchi (2009) in its revised form (Shao et al., 2009) (Fig. 9). A simulation run with TBC produces similar results as GeoSysBRNS and is slightly closer to the analytical solution in the middle of the domain (Fig. 9).

The presented results for the two-dimensional aquifer scenario indicate that the coupling of transport and reactive part in GeoSysBRNS is also working correctly for multidimensional simulation domains. Simulated concentration profiles match closely with analytical solutions (where available) and with established numerical codes using the same spatio-temporal discretization parameter settings.
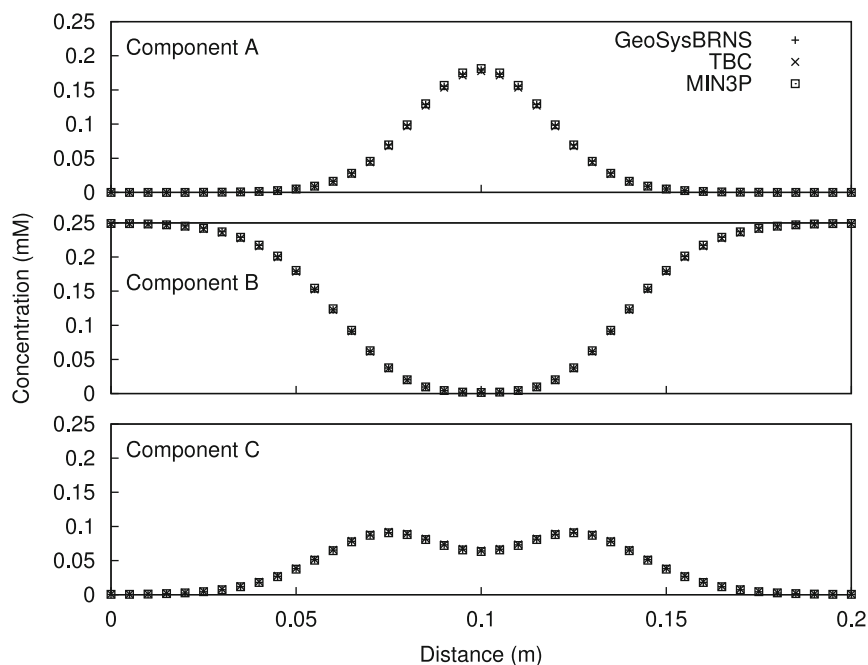
Fig. 8. Comparison of GeoSysBRNS results to TBC and MIN3P results for double-Monod kinetics scenario. Profiles are recorded at day 20 along a vertical transect located 1 m downstream of inflow boundary.
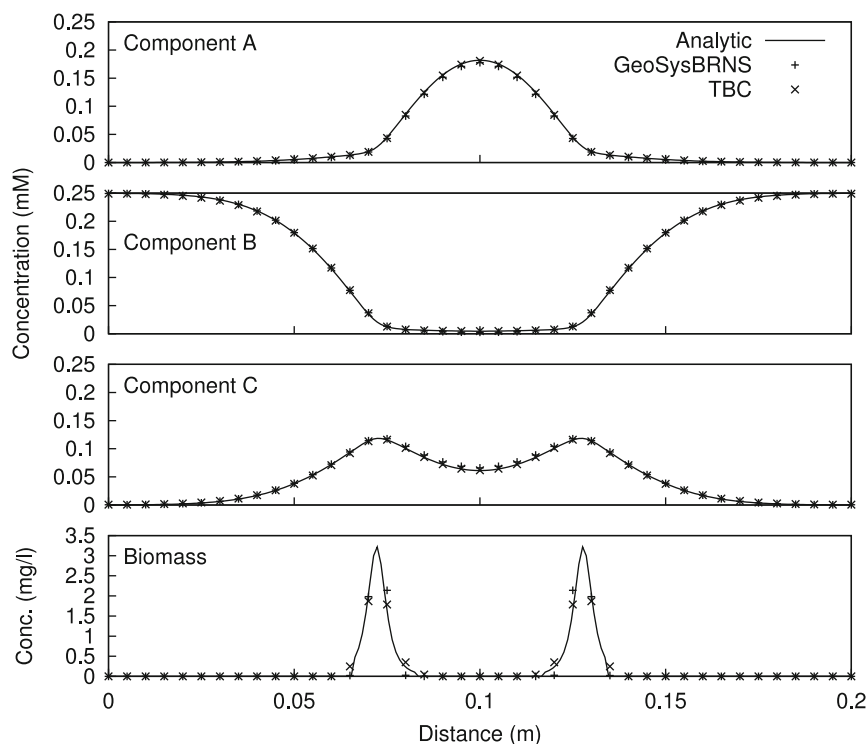
Fig. 9. Comparison of GeoSysBRNS results, TBC results, and analytical solution for double-Monod kinetics with biomass scenario. Profiles are recorded at day 300 along a vertical transect located 1 m downstream of inflow boundary.

4. Discussion and outlook

We have presented the reactive transport simulation code GeoSysBRNS which is suitable for modeling reactive transport problems involving complex (bio-)chemical process networks. The new model couples the chemical reaction network simulator of the BRNS to the flow and transport simulator GeoSys/RockFlow. While existing simulation codes are usually limited in the

formulation of the rate laws describing reactive processes, the multidimensional GeoSysBRNS model has been developed using techniques which preserve the versatility and adaptability of both codes it is based on. Soil systems, for example, are more and more recognized as self-organizing entities featuring many biochemical and biophysical interactions and non-linear feedback loops between processes (Young and Crawford, 2004). The flexibility in the formulation and combination of reactive processes

provided by GeoSysBRNS is a prerequisite to accommodate such complexity in multidimensional reactive transport simulations. By using an operator splitting scheme for the coupling, both codes can easily be maintained and further improved independently. The simulation results presented here demonstrate that the coupling is implemented correctly. A good agreement is achieved with analytical solutions (where available) and with numerical simulation results obtained by established simulation codes.

Multidimensional reactive-transport simulations are generally computationally demanding. The computational effort for transport and chemical solver varies with the considered transport and reaction network. For example, the chemical solver consumed approximately 44 percent of the total runtime in the one-dimensional sand column experiment, but only 4 percent in the two-dimensional aquifer example. GeoSysBRNS has not yet been optimized for speed and was approximately three to four times slower than the comparison codes in the presented two-dimensional examples. In order to reduce simulation time, GeoSysBRNS will be optimized for execution speed and a parallel version will be implemented. Calls to the chemical solver can readily be distributed to separate processors. Furthermore, the parallel support for GeoSys using MPI can easily be extended to the coupled model, allowing for the utilization of today's high-performance-computing clusters.

References

Aguilera, D., Jourabchi, P., Spiteri, C., Regnier, P., 2005. A knowledge-based reactive transport approach for the simulation of biogeochemical dynamics in earth systems. Geochemistry, Geophysics, Geosystems 6 (Q07012), 1–18 10.1029/2004GC000899.

Barry, D.A., Prommer, H., Miller, C.T., Engesgaard, P., Brun, A., Zhen, C., 2002. Modelling the fate of oxidisable organic contaminants in groundwater. Advances in Water Resources 25, 945–983.

Bauer, S., Beyer, C., Kolditz, O., 2006. Assessing measurement uncertainty of first-order degradation rates in heterogeneous aquifers. Water Resources Research 42 (W01420), 1–14 10.1029/2004WR003878.

Berner, R.A., 1980. Early Diagenesis: A Theoretical Approach. Princeton University Press, Princeton, NJ 241pp.

Boudreau, B.P., 1997. Diagenetic Models and Their Implementation. Springer, Berlin, Germany 414pp.

Brun, A., Engesgaard, P., 2002. Modelling of transport and biogeochemical processes in pollution plumes: literature review and model development. Journal of Hydrology 256, 211–227.

Chilakapati, A., 1995. Raft: a simulator for reactive flow and transport of groundwater contaminants. Internal Report 10636, Pacific Northwest Laboratory, Richland, WA, 137pp.

Cirpka, O.A., Valocchi, A.J., 2007. Two-dimensional concentration distribution for mixing-controlled bioreactive transport in steady state. Advances in Water Resources 30, 1668–1679.

Cirpka, O.A., Valocchi, A.J., 2009. Reply to comments on "Two-dimensional concentration distribution for mixing-controlled bioreactive transport in steady state" by H. Shao et al. Advances in Water Resources 32 (2), 298–301.

Clement, T.P., Sun, Y., Hooker, B.S., Petersen, J.N., 1998. Modeling multispecies reactive transport in ground water. Ground Water Monitoring and Remediation 18, 79–92.

Gómez, C., 1990. Macrofort: a fortran code generator in maple. Rapport Technique 119, Institut National de Recherche en Informatique et en Automatique, Le Chesnay, France, 14pp.

Jourabchi, P., Van Cappellen, P., Regnier, P., 2005. Quantitative interpretation of pH distributions in aquatic sediments: a reactive transport modeling approach. American Journal of Science 305, 919–956.

Kolditz, O., Bauer, S., 2004. A process-orientated approach to compute multi-field problems in porous media. Journal of Hydroinformatics 6, 225–244.

Kolditz, O., Delfs, J.-O., Bürger, C., Beinhorn, M., Park, C.-H., 2008. Numerical analysis of coupled hydrosystems based on an object-oriented compartment approach. Journal of Hydroinformatics 10 (3), 227–244.

Mayer, K.U., Frind, E.O., Blowes, D.W., 2002. Multicomponent reactive transport modeling in variably saturated porous media using a generalized formulation for kinetically controlled reactions. Water Resources Research 38, 1174 10.1029/2001WR000862.

Meysman, J.R., Middelburg, J.J., Herman, P.M.J., Heip, C.H.R., 2003. Reactive transport in surface sediments. I. Model complexity and software quality. Computers & Geosciences 29, 291–300.

Murphy, E.M., Ginn, T.R., 2000. Modeling microbial processes in porous media. Hydrogeology Journal 8, 142–158.

Park, C.-H., Beyer, C., Bauer, S., Kolditz, O., 2008. Using global node-based velocity in random walk particle tracking in variably saturated porous media: application to contaminant leaching from road constructions. Environmental Geology 55, 1755–1766.

Pfingsten, W., 1996. Efficient modeling of reactive transport phenomena by a multispecies random walk coupled to chemical equilibrium. Nuclear Technology 116 (2), 208–221.

Prommer, H., Barry, D.A., Zheng, C., 2003. Modflow/mt3dms-based reactive multicomponent transport modeling. Ground Water 41, 247–257.

Regnier, P., O'Kane, J., Steefel, C., Vanderborght, J., 2002. Modeling complex multi-component reactive-transport systems: towards a simulation environment based on the concept of a knowledge base. Applied Mathematical Modelling 26, 913–927.

Regnier, P., Wollast, R., Steefel, C.I., 1997. Long-term fluxes of reactive species in microtidal estuaries: estimates from a fully transient, multicomponent reaction-transport model. Marine Chemistry 58, 127–145.

Rutqvist, J., Barr, D., Birkholzer, J.T., Chijimatsu, M., Kolditz, O., Liu, Q., Oda, Y., Wang, W., Zhang, C., 2008. International simulation study on coupled thermal, hydrological, and mechanical (thm) processes near geological nuclear waste repositories. Journal of Nuclear Technology 163 (1), 101–109.

Schäfer, D., Schäfer, W., Kinzelbach, W., 1998a. Simulation of reactive processes related to biodegradation in aquifers: 1. Structure of the three-dimensional reactive transport model. Journal of Contaminant Hydrology 31, 167–186.

Schäfer, D., Schäfer, W., Kinzelbach, W., 1998b. Simulation of reactive processes related to biodegradation in aquifers. 2. Model application to a column study on organic carbon degradation. Journal of Contaminant Hydrology 31, 187–209.

Shao, H., Centler, F., De Biase, C., Thullner, M., Kolditz, O., 2009. Comments on "Two-dimensional concentration distribution for mixing-controlled bioreactive transport in steady state" by O. A. Cirpka, A. J. Valocchi. Advances in Water Resources 32 (2), 293–297.

Thullner, M., Regnier, P., Van Cappellen, P., 2007. Modeling microbially induced carbon degradation in redox-stratified subsurface environments: concepts and open questions. Geomicrobiology Journal 24, 139–155.

Thullner, M., Van Cappellen, P., Regnier, P., 2005. Modeling the impact of microbial activity on redox dynamics in porous media. Geochimica et Cosmochimica Acta 69 (21), 5005–5019.

Van Cappellen, P., Gaillard, J.-F., 1996. Biogeochemical dynamics in aquatic sediments. Reviews in Mineralogy 34, 335–376.

von Gunten, U., Zobrist, J., 1993. Biogeochemical changes in groundwater-infiltration systems: column studies. Geochimica et Cosmochimica Acta 57, 3895–3906.

Wang, W., Kolditz, O., 2007. Object-oriented finite element analysis of thermo-hydro-mechanical (THM) problems in porous media. Journal of Numerical Methods in Engineering 69 (1), 162–201.

Young, I.M., Crawford, J.W., 2004. Interactions and self-organization in the soil–microbe complex. Science 304, 1634–1637.

Zhang, F., Yeh, G.-T., Parker, J.C., Brooks, S.C., Pace, M.N., Kim, Y.-J., Jardine, P.M., Watson, D.B., 2007. A reaction-based paradigm to model reactive chemical transport in groundwater with general kinetic and equilibrium reactions. Journal of Contaminant Hydrology 92, 10–32.

Enclosed Publication

[EP2] **Haibing Shao**, Florian Centler, Cecilia De Biase, Martin Thullner and Olaf Kolditz (2009): Comments on "Two-dimensional concentration distribution for mixing-controlled bioreactive transport in steady-state flow" by O.A. Cirpka and A.J. Valocchi, *Advances in Water Resources* 32(2), 293-297.

Comments on "Two-dimensional concentration distribution for mixing-controlled bioreactive transport in steady-state" by O.A. Cirpka and A.J. Valocchi

Haibing Shao [a,c,*], Florian Centler [b], Cecilia De Biase [b], Martin Thullner [b], Olaf Kolditz [a,c]

[a] Department of Environmental Informatics, UFZ, Helmholtz Centre for Environmental Research – UFZ, Permoserstrasse 15, 04318 Leipzig, Germany
[b] Department of Environmental Microbiology, UFZ, Helmholtz Centre for Environmental Research – UFZ, Permoserstrasse 15, 04318 Leipzig, Germany
[c] Applied Environmental System Analysis, Dresden University of Technology, Helmholtzstrasse 10, 01069 Dresden, Germany

ARTICLE INFO

ABSTRACT

In this comment we present a re-analysis of the analytical solution presented by Cirpka and Valocchi for steady-state concentrations of dissolved bioreactive compounds and bacterial biomass in porous media. We discuss the validity range of the analytical solution. In particular, the criterion used to determine the sustainability of biomass is revisited. This re-analysis shows that the ω criterion used by Cirpka and Valocchi is only a necessary but not a sufficient criterion to determine the bioreactive zones. As a consequence, the analytical solution does not provide the exact distribution of compounds throughout the domain, but can serve as upper or lower boundaries for species concentrations at a given location. These conclusions are supported by the simulation results obtained from an established reactive transport model.

© 2008 Elsevier Ltd. All rights reserved.

1. Introduction

Recently, Cirpka and Valocchi presented an analytical framework to calculate steady-state concentrations of bioreactive dissolved compounds and the associated concentration of bacterial biomass in porous media [4]. To demonstrate the influence of transversal dispersion on the degradation of groundwater contaminants, they employed an example in which a spatially separated inflow, with electron donor and acceptor dissolved in it, flushes through a two-dimensional domain at a uniform velocity. This framework has been used in a followup study to investigate reactive transport in randomly heterogeneous porous media [3], and by other researchers for the interpretation of their experimental data [1].

Regarding the reaction kinetics, three different scenarios are considered by [4]: (1) an instantaneous reaction, (2) double-Monod kinetics with first-order biomass decay and (3) double-Monod kinetics with concentration-dependent biomass decay.

For the second scenario, we re-examine the analytical solution (Section 2) presented by [4]. In particular, we investigate the ω criterion used by [4] to separate bioreactive zones from zones not supporting any microbial activity. Our analytical re-analysis is accompanied by numerical reactive transport simulations (Section 3). The limitations of the analytical approach in [4] is discussed in this work.

2. Analytical solution – revisited

In [4], the generic compounds A, B, and C undergo a microbially induced chemical reaction, with f_a, f_b and f_c as stoichiometric coefficients:

$$f_a A + f_b B \overset{bio}{\rightarrow} f_c C. \tag{1}$$

The rate of the reaction is assumed to be given by double-Monod expressions, which results in the following steady-state expressions for the three compounds A, B, C, and the biomass of the bacteria that is catalyzing the reaction:

$$v\frac{\partial c_A}{\partial x} - D_t \frac{\partial^2 c_A}{\partial y^2} = -\frac{c_A}{K_A + c_A}\frac{c_B}{K_B + c_B}\frac{\mu_{max}}{Y}f_a c_{bio}, \tag{2}$$

$$v\frac{\partial c_B}{\partial x} - D_t \frac{\partial^2 c_B}{\partial y^2} = -\frac{c_A}{K_A + c_A}\frac{c_B}{K_B + c_B}\frac{\mu_{max}}{Y}f_b c_{bio}, \tag{3}$$

$$v\frac{\partial c_C}{\partial x} - D_t \frac{\partial^2 c_C}{\partial y^2} = \frac{c_A}{K_A + c_A}\frac{c_B}{K_B + c_B}\frac{\mu_{max}}{Y}f_c c_{bio}, \tag{4}$$

$$\frac{\partial c_{bio}}{\partial t} = \frac{c_A}{K_A + c_A}\frac{c_B}{K_B + c_B}\mu_{max} c_{bio} - k_{dec} c_{bio} = 0, \tag{5}$$

where v is the uniform groundwater flow velocity along the x-direction; c_A, c_B, c_C are mass concentrations of components A, B, and C respectively; c_{bio} is the biomass concentration of the bacteria catalyzing the biodegradation of compounds A and B; D_t is the transverse dispersion coefficient; K_A and K_B are Monod coefficients of

* Corresponding author. Address: Department of Environmental Informatics, Helmholtz Centre for Environmental Research – UFZ, Permoserstrasse 15, 04318 Leipzig, Germany. Tel.: +49 341 235 1884.
E-mail address: haibing.shao@ufz.de (H. Shao).

respective compounds in the biomass growth term; μ_{max} is the maximum specific growth rate; k_{dec} is the rate coefficient of biomass decay; and Y is the yield coefficient.

Furthermore, a set of total concentrations c_A^{tot} and c_B^{tot} is given by:

$$c_A^{tot} = c_A + \frac{f_a}{f_c} c_C, \tag{6}$$

$$c_B^{tot} = c_B + \frac{f_b}{f_c} c_C. \tag{7}$$

This approach was applied to a generic two-dimensional setup where component A is introduced in the center part of the left boundary ($x = 0m$) with concentration c_A^{in} and an injection width of w, and meanwhile component B is introduced with c_B^{amb} in all remaining parts of the left boundary (see Fig. 1). The mixing ratio of the injected solute with the ambient water $X(x,y)$ is described by [4] in analogy to the steady-state distribution of a conservative tracer:

$$X(x,y) = \frac{1}{2}\left(\text{erf}\left(\frac{y+w/2}{2\sqrt{xD_t/v}}\right) - \text{erf}\left(\frac{y-w/2}{2\sqrt{xD_t/v}}\right) \right). \tag{8}$$

Under the condition that seepage velocity v is uniform and parallel to the x-direction, and that the transverse dispersion coefficient D_t is identical for all compounds, c_A^{tot} and c_B^{tot} are conservative with respect to the reaction (1). Therefore, they can be linearly scaled with X and $1 - X$.

$$c_A^{tot}(x,y) = X(x,y)c_A^{in}, \tag{9}$$

$$c_B^{tot}(x,y) = (1 - X(x,y))c_B^{amb}. \tag{10}$$

To obtain an analytical solution for this steady-state problem, Cirpka and Valocchi introduced the following dimensionless criterion ω:

$$\omega = \frac{c_A^{tot}}{K_A + c_A^{tot}} \frac{c_B^{tot}}{K_B + c_B^{tot}} \frac{\mu_{max}}{k_{dec}}. \tag{11}$$

In [4], at all locations where $\omega > 1$ is satisfied, a non-trivial solution of the biomass balance Eq. (5) was obtained by substituting Eqs. (6) and (7) into Eq. (5), which is divided by c_{bio}, and yields the following form:

$$\left(c_A^{tot} - \frac{f_a}{f_c}c_C\right)\left(c_B^{tot} - \frac{f_b}{f_c}c_C\right) = \frac{k_{dec}}{\mu_{max}}\left(K_A + c_A^{tot} - \frac{f_a}{f_c}c_C\right)\left(K_B + c_B^{tot} - \frac{f_b}{f_c}c_C\right). \tag{12}$$

As c_C is the only unknown variable in Eq. (12), a rearrangement yields the quadratic expression:

$$\underbrace{\frac{f_a f_b}{f_c^2}\left(1 - \frac{k_{dec}}{\mu_{max}}\right)}_{p_2}c_C^2$$

$$+ \underbrace{\left(\frac{k_{dec}}{\mu_{max}}(K_A + c_A^{tot})\frac{f_b}{f_c} + \frac{k_{dec}}{\mu_{max}}(K_B + c_B^{tot})\frac{f_a}{f_c} - c_A^{tot}\frac{f_b}{f_c} - c_B^{tot}\frac{f_a}{f_c}\right)}_{p_1}c_C$$

$$+ \underbrace{c_A^{tot}c_B^{tot} - \frac{k_{dec}}{\mu_{max}}(K_A + c_A^{tot})(K_B + c_B^{tot})}_{p_0} = 0. \tag{13}$$

One of the two solutions of (13) is:

$$c_C = \frac{-p_1 - \sqrt{p_1^2 - 4p_0 p_2}}{2p_2}. \tag{14}$$

The other one with a positive sign before the square root is physically not meaningful, thus being neglected. By substituting (14) back into Eqs. (6) and (7), the corresponding c_A and c_B values can be obtained for all locations where $\omega > 1$.

Biomass concentration can be finally determined from following relationship for different ω values:

$$c_{bio} = \begin{cases} \left(v\frac{\partial c_C}{\partial x} - D_t\frac{\partial^2 c_C}{\partial y^2}\right)\frac{(K_A + c_A)(K_B + c_B)}{c_A c_B \mu_{max}f_c}Y & \text{if } \omega > 1 \\ 0 & \text{if } \omega < 1. \end{cases} \tag{15}$$

It was claimed in [4] that biomass can only be present in regions where $\omega > 1$. This condition, however, while necessary, is not sufficient for the presence of biomass in steady-state. It rather indicates regions, in which the growth of biomass would be possible if no upstream consumption of the compounds takes place. We here introduce a much stricter criterion ω^* to exactly define regions with non-trivial steady-state concentrations of biomass c_{bio}.

Inspecting Eq. (5) reveals that for a positive c_{bio}, the following equation must be fulfilled in steady-state:

$$\omega^* := \frac{c_A}{K_A + c_A} \frac{c_B}{K_B + c_B} \frac{\mu_{max}}{k_{dec}} = 1. \tag{16}$$

We argue that the derivation of the steady-state concentrations for the mobile compounds and biomass presented in [4] is only valid in regions with $\omega^* = 1$. In regions with $\omega > 1$ but $\omega^* < 1$, biomass can not sustain in steady-state, resulting in $c_{bio} = 0$. As a consequence, the concentrations of dissolved compounds presented by Cirpka and Valocchi are only valid in regions where $\omega^* = 1$.

However, for regions with $\omega > 1$ but $\omega^* < 1$, Cirpka and Valocchi's derivation can still be used to define upper and lower boundaries for the steady-state concentrations. Instead of starting
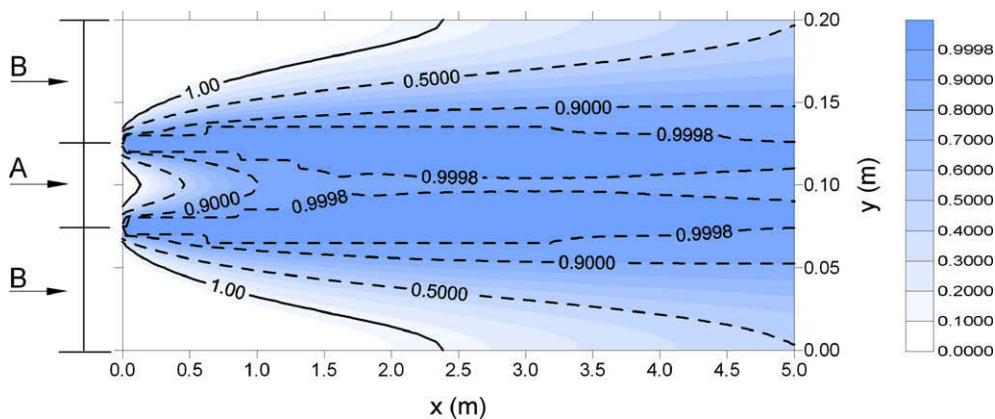

Fig. 1. ω^* values in the domain, calculated from TBC simulation results. The contours in dashed lines are for ω^* values. The solid lines mark the boundary where $\omega = 1$.

Table 1
Model parameters.

w	5	cm	μ_{max}	1	1/d
v	100	cm/d	k_{dec}	0.1	1/d
D_t	2.5	cm^2/d	Y	1	mg/mmol
f_a	1	–	K_A	8.33×10^{-2}	mmol/l
f_b	1	–	K_B	3.13×10^{-2}	mmol/l
f_c	1	–	c_A^{in}	0.33	mmol/l
c_B^{amb}	0.25	mmol/l			

with Eq. (5), we start the derivation with the corresponding inequality which holds true for regions where $\omega > 1$ and $\omega^* < 1$:

$$\frac{\partial c_{bio}}{\partial t} = \frac{c_A}{K_A + c_A} \frac{c_B}{K_B + c_B} \mu_{max} c_{bio} - k_{dec} c_{bio} < 0. \tag{5'}$$

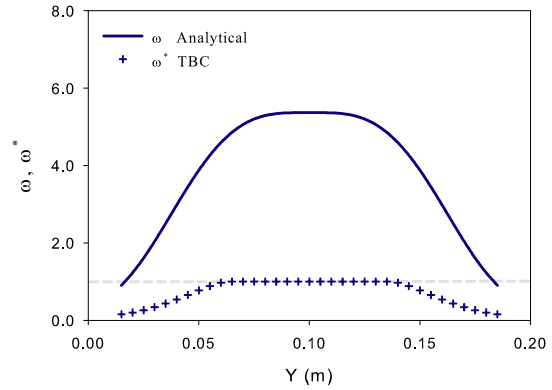Following the same transformations as in [4] leads to

$$\frac{-p_1 - \sqrt{p_1^2 - 4p_0 p_2}}{2p_2} < c_C < \frac{-p_1 + \sqrt{p_1^2 - 4p_0 p_2}}{2p_2}. \tag{17}$$

The term on the right-hand side again leads to unreasonable values. Thus, only considering the left-hand side of the inequation results in a lower bound for c_C, and upper bounds for c_A and c_B:
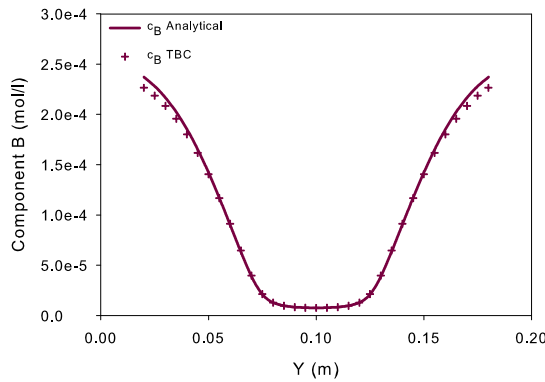
$$c_C > \frac{-p_1 - \sqrt{p_1^2 - 4p_0 p_2}}{2p_2}, \tag{18}$$

(a) Concentration of Component A

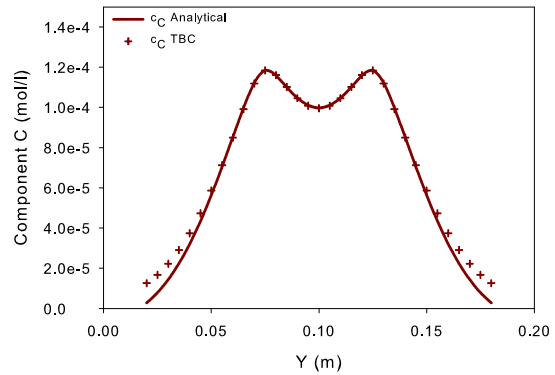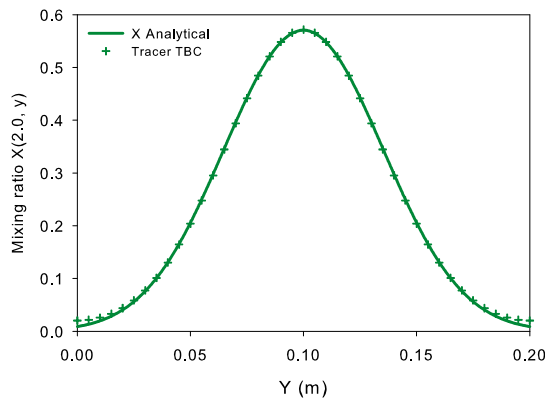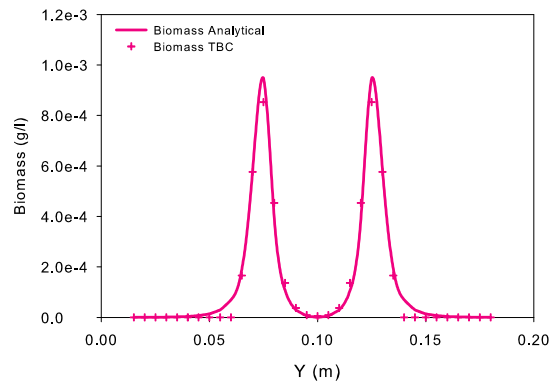(b) Values of ω and ω^*
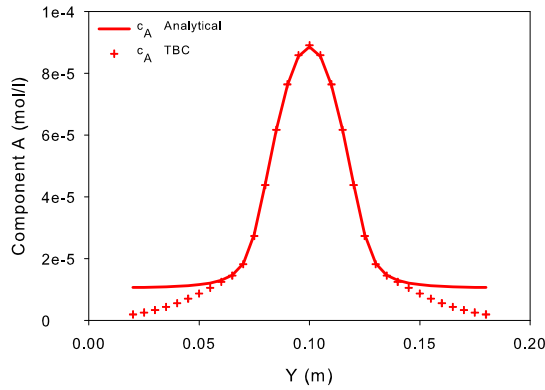
(c) Concentration of Component B

(d) Concentration of Component C

(e) Mixing Ratio X

(f) Concentration of Biomass

Fig. 2. Comparison of c_A, c_B, c_C, c_{bio}, ω, and ω^* at cross-section at $x = 2m$, with $f_a = f_b = f_c = 1$. Solid lines are profiles generated by Cirpka and Velocchi's method; symbols are TBC results.

$$c_A < c_A^{tot} - \frac{f_a(-p_1 - \sqrt{p_1^2 - 4p_0 p_2})}{2f_c p_2}, \qquad (19)$$

$$c_B < c_B^{tot} - \frac{f_b(-p_1 - \sqrt{p_1^2 - 4p_0 p_2})}{2f_c p_2}. \qquad (20)$$

These results are confirmed by numerical simulations presented in the following section.

3. Numerical results

In order to examine both criterions, ω and ω^*, we employ the well established reactive transport code TBC [5]. Using the same parameters and domain setup as in [4] (listed also in Table 1), the spatial distribution of the bioreactive dissolved species c_A, c_B, c_C, and biomass c_{bio}, are simulated. Transient simulations have been run until reaching steady-state. To confirm the results, the same simulations have been performed using a self-developed reactive transport code GeoSysBRNS [2], and it yields the same concentration distributions (not shown) as with TBC.

As numerical models can not completely avoid longitudinal dispersion effects, we have run the simulations using different longitudinal dispersivities (up to the value of 2.5 cm. However, if given sufficiently long simulation time, i.e. when the numerical simulations approach steady-state, the solutions do not depend on this parameter. The presented results are obtained using a spatial discretization of 2.5 cm in x-direction and 5 mm in y-direction. The temporal discretization is 2 min. A further refinement of the spatial and temporal discretization provides nearly identical results (not shown).

Fig. 1 shows the calculated ω and ω^* criterions using total concentrations (as proposed by [4]) and actual concentrations (as suggested in this work). Results show that the locations where ω^* is approaching 1 are confined to a much smaller subregion than the area defined by $\omega > 1$. This confirms that ω^* is a stricter criterion than ω.

To compare numerical and analytical results for stoichiometric ratios of $f_a = f_b = f_c = 1$, concentration profiles are shown for a vertical cross-section at $x = 2m$ (Fig. 2). For conservative species, both approaches show a very good agreement, except for miner differences at the vicinity of the domain boundary (Fig. 2e). These discrepancies are due to the infinite boundary assumption in the analytical solution and a Neumann boundary condition in the numerical model. Still, the good agreement confirms a sufficient accuracy of the numerical approximation.

For the reactive species, results are only shown for part of the cross-section where the analytical solution is claimed to be valid by [4] (regions where $\omega > 1$) (Fig. 2a, c, d, and f). In the center region of the cross-section, where ω^* is close to 1 (Fig. 2b), there is a good agreement between numerical and analytical results. However, outside this region, where $\omega^* < 1$ (i.e. biomass is not sustainable), an increasing deviation between the numerical simulation results and analytical approach by [4] can be observed: the analytically derived biomass distribution slightly extends into regions with $\omega^* < 1$, and more obvious discrepancies are found for the dissolved species. In particular for component A, concentration remains at a non-negligible plateau value whereas the numerical results continuously decrease towards 0 with distance from the reactive region (Note that in this part the numerical and analytical results for the conservative tracer are nearly identical.). At all locations, the statements in Eq. (20) are confirmed that the results of [4] can be used to define an upper concentration limit for components A and B and a lower limit for component C. The results shown here confirm the mathematical analysis of the ω criterion in Section 2.

As shown by Eqs. (11) and (16), the discrepancy between ω and ω^* is influenced by the stoichiometric ratio f_a, f_b, and f_c. To test this influence, we re-investigated the above example, assuming $f_a = 6$, $f_b = 1$, and $f_c = 6$. With this setup, the concentration of component A (Fig. 3a) shows a much bigger discrepancy between analytical and numerical results.

4. Summary and conclusion

Cirpka and Valocchi presented an analytical framework to calculate steady-state concentrations of bioreactive dissolved compounds and bacterial biomass in porous media [4]. They introduced an ω criterion based on total concentrations in order to distinguish between regions where biomass can be sustained or not. By mathematical analysis and numerical simulations we showed that this ω criterion is necessary but not sufficient. Thus at certain regions, the analytical solution is overestimating the concentration of the reactants and underestimating concentration of the biodegradation product. We here proposed a modified and stricter ω^* criterion that is based on actual concentrations. The validity of this modified criterion is proved by numerical analysis using the reactive transport code TBC.

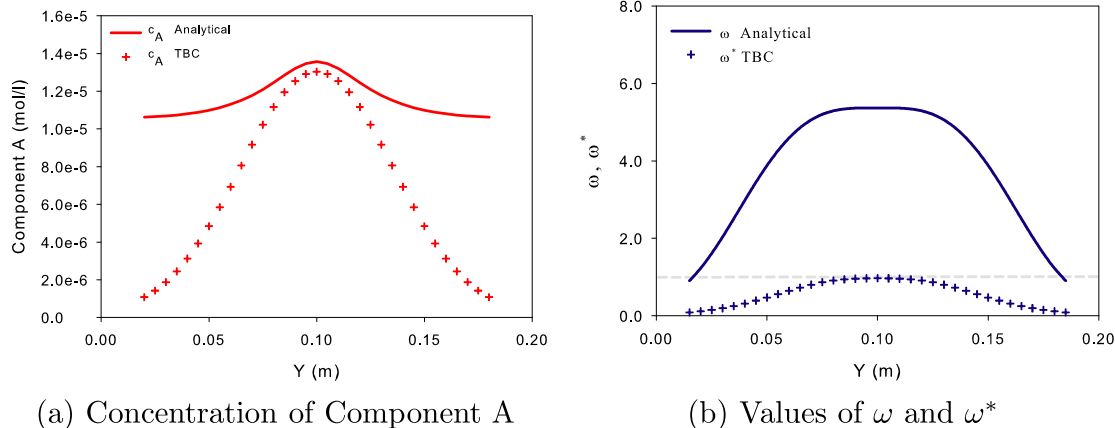(a) Concentration of Component A

(b) Values of ω and ω^*

Fig. 3. Comparison of c_A, ω, and ω^* at cross-section $x = 2m$, with $f_a = f_c = 6$, and $f_b = 1$. Solid lines are profiles generated by Cirpka and Velocchi's method; symbols are TBC results.

Acknowledgements

References

[1] Bauer RD, Maloszewski P, Zhang Y, Meckenstock RU, Griebler C. Mixing-controlled biodegradation in a toluene plume – results from two-dimensional laboratory experiments. J Contam Hydrol 2008;96(1–4):150–68.

[2] Centler F, Shao H. Developing GeoSysBRNS – a flexible reactive transport model for simulating biogeochemical subsurface processes. Technical report, Department of Environmental Microbiology, Department of Environmental Informatics, Helmholtz Centre for Environmental Research – UFZ, 2008.

[3] Cirpka OA, Schwede RL, Luo J, Dentz M. Concentration statistics for mixing-controlled reactive transport in random heterogeneous media. J Contam Hydrol 2008;98(1–2):61–74.

[4] Cirpka OA, Valocchi AJ. Two-dimensional concentration distribution for mixing-controlled bioreactive transport in steady state. Adv Water Res 2007;30:1668–79.

[5] Schäfer D, Schäfer W, Kinzelbach W. Simulation of reactive processes related to biodegradation in aquifers 1, structure of the three-dimensional reactive transport model. J Contam Hydrol 1998;31(1–2):167–86.

Enclosed Publication

[EP3] **Haibing Shao**, Svitlana V. Dmytrieva, Olaf Kolditz, Dmitrii A. Kulik, Wilfried Pfingsten and Georg Kosakowski (2009): Modeling reactive transport in non-ideal aqueous solid solution system, *Applied Geochemistry* 24(7), 1287-1300.

Modeling reactive transport in non-ideal aqueous–solid solution system

Haibing Shao [a,d,*], Svitlana V. Dmytrieva [b,c], Olaf Kolditz [a,d], Dmitrii A. Kulik [c],
Wilfried Pfingsten [c], Georg Kosakowski [c]

[a] UFZ-Helmholtz Centre for Environmental Research, Department Environmental Informatics, Permoserstraße 15, 04318 Leipzig, Germany
[b] SSC Technocentre, Nauky Prosp. 46, 03650 Kyiv, Ukraine
[c] Laboratory for Waste Management, Paul Scherrer Institute, 5232 Villigen PSI, Switzerland
[d] Applied Environmental System Analysis, TU Dresden, Helmholtzstraße 10, 01069 Dresden, Germany

ARTICLE INFO

ABSTRACT

The numerical simulation of reactive mass transport processes in complex geochemical environments is an important tool for the performance assessment of future waste repositories. A new combination of the multi-component mass transport code GeoSys/RockFlow and the Gibbs Energy Minimization (GEM) equilibrium solver GEM-Selektor is used to calculate the accurate equilibrium of multiple non-ideal solid solutions which are important for the immobilization of radionuclides such as Ra. The coupled code is verified by a widely used benchmark of dissolution–precipitation in a calcite–dolomite system. A more complex application shown in this paper is the transport of Ra in the near-field of a nuclear waste repository. Depending on the initial inventories of Sr, Ba and sulfate, non-ideal sulfate and carbonate solid solutions can fix mobile Ra cations. Due to the complex geochemical interactions, the reactive transport simulations can describe the migration of Ra in a much more realistic way than using the traditional linear K_D approach only.

1. Introduction

Reactive transport models have been widely used for many geotechnical applications, e.g. in predicting the performance of radioactive or chemo-toxic waste repositories (Glynn, 2003; Soler, 2003; Spycher et al., 2003; Xie et al., 2006), investigating pathways of CO_2 sequestration in the deep geological environment (Xu et al., 2004; Pruess et al., 2004; Lagneau et al., 2005), and evaluating remediation strategies of contaminated sites (Schäfer et al., 1998; Mayer et al., 2002a; Steefel et al., 2005; MacQuarrie and Mayer, 2005). On one side, most processes that govern the performance of a nuclear waste repository are directly related to geochemistry, i.e. the solubility and sorption behavior of radionuclides, degradation of tunnel backfill materials, and corrosion of waste canisters (Pfingsten, 2002; Van Loon and Jakob, 2005; Pfingsten et al., 2006; Kulik, 2006a; Soler and Mäder, 2007). On the other side, the temporal and spatial evolution of the geochemical environment is heavily influenced by transport processes. Therefore, accounting for detailed geochemical reactions with mass transport is crucial for an enhanced understanding of the investigated geotechnical systems.

One such example is the transport of Ra out of a nuclear waste repository. Radium emerges mainly as a product of the U decay chain, which is expected to take place in both high and intermediate level waste packages (Nagra, 2002). Normally, for the transport of Ra in the near-field of a waste repository, it is assumed that it behaves similarly to other alkaline earth metals like Sr. Its transport in clay materials like bentonite is retarded mainly by cation-exchange and to a lesser degree by surface complexation mechanisms (Glynn, 2003; Bradbury and Baeyens, 2004). The non-linear sorption isotherm is then translated into a linear isotherm, which is finally used for the performance assessment (Nagra, 2002). A process not considered so far in this approach is the incorporation of Ra into solid solution with Ba and Sr sulfates and carbonates.

The co-precipitation of Ra with Ba sulfates was investigated by Germann (1921) and Doerner and Hoskins (1925). They found that in the presence of a large excess of Ba over Ra, SO_4^{2-} ions will precipitate Ra even though the solubility product of Ra sulfate is not exceeded. Langmuir and Riese (1985) derived the thermodynamic data of Ra solid solution in sulfate and carbonate minerals, based on published distribution coefficients. Martin and Akber (1999) studied the sorption/desorption of radionuclides and secondary mineral formation in groundwater systems close to U mine tailings. Their data indicated that Ra was almost completely immobilized by the formation of a barite solid solution. Later on, Martin et al. (2003) evaluated experimentally the mobility of Ra, and reported that dissolution of a $(Ba, Ra)SO_4$ solid solution controls the aqueous concentration of Ra and Ba in pore water released from nuclear waste repositories. Following a thermodynamic approach, Berner and Curti established a simple ideal solid solution

* Corresponding author. Address: UFZ-Helmholtz Centre for Environmental Research, Department Environmental Informatics, Permoserstraße 15, 04318 Leipzig, Germany. Tel.: +49 341 235 1884; fax: +49 341 235 1939.
    E-mail address: haibing.shao@ufz.de (H. Shao).

model and predicted a Ra solubility of 8.6×10^{-12} mol L^{-1} in the near-field of a repository for high-level radioactive waste planned in Switzerland (Nagra, 2002). This concentration is 3 orders of magnitude lower, compared to the scenario in which only pure a Ra sulfate phase is considered. Zhu (2004a) provided fundamental data of binary mixing properties of multiple metals including Ra for the barite isostructural family. A reactive transport simulation is also done to demonstrate the solubility of Ra influenced by (Ba, Ra)SO$_4$ coprecipitation (Zhu, 2004b) in groundwater aquifers. Recently, Grandia et al. (2008) calculated that the solubility of Ra(II) in a similar repository environment should be in the range of 10^{-11} mol L^{-1} with the presence of (Ba, Ra)SO$_4$ co-precipitation and it will be 3 orders of magnitude higher if only a pure RaSO$_4$ solid phase is considered. Although solid solution and co-precipitation models have already been used for the calculation of Ra solubility in the vicinity of a nuclear waste repository, to the authors' knowledge, the effect of transport processes on the migration and co-precipitation of Ra with sulfate minerals has not been explicitly investigated as yet.

To simulate these process interactions, various models that couple chemistry with mass transport have been developed in the past. Based on the methodology used for simulation of chemical processes, they can be divided into two groups, Law of Mass Action (LMA) concept and Gibbs Energy Minimization (GEM) approach. Generally, they are complementary with advantages and disadvantages on both sides. The majority of coupled codes use the LMA approach (Bethke, 1996; Yeh and Tripathi, 1998). Some known codes that use this approach are TBC (Schäfer et al., 1998), Min3P (Mayer et al., 2002b), TOUGHREACT (Xu and Pruess, 2001), PHT3D (Prommer, 2002), HYTEC (Van der Lee et al., 2003), SHEMAT (Clauser, 2003; Kühn and Gessner, 2006), CRUNCH (Steefel et al., 2005), and GeoSys/RockFlow (Kolditz and Bauer, 2004; Xie et al., 2006). Only recently, the integration of GEM chemical solvers in coupled codes has been attempted (Cleverley et al., 2006; Guimarães et al., 2007) with various degree of success.

The GEM convex programming approach (Karpov et al., 1997, 2001; Kulik et al., 2004) is computationally more expensive than LMA and requires more thermodynamic data. However, the GEM method has certain advantages to describe complex geochemical environments, like aqueous–solid solution equilibria that include two or more multi-component phases. Unequivocal selection of stable phases is performed in GEM using the dual solution of the chemical speciation problem (chemical potentials of elements in equilibrium state). With help of the GEM concept, also problems like surface complexation can be solved without site mole balances (Kulik, 2006a). The redox state (pe) and activities (pH, fugacities of gases) are intrinsically computed from the GEM dual solution and standard chemical potentials.

In the following, the basic approach of multi-species reactive transport modeling is briefly summarized. A description is given of how aqueous–solid solution systems are calculated with the GEM method. Then, the coupling of the multi-species mass transport code GeoSys and GEMIPM2K (the standalone GEM numerical kernel of GEM-Selektor-PSI code) is presented. The coupling scheme is verified by comparing the results of calcite/dolomite benchmark test to those from Engesgaard and Kipp (1992) and others. Finally, the coupled code GeoSys-GEM is applied to a chemical system containing Ra–Ba–Sr carbonate and SO$_4$ solid solutions to demonstrate their potential retardation effects on radionuclide transport in the near-field of a nuclear waste repository.

2. Basic approach

In this study, the mass transport and chemical reactions are solved separately in a sequential non-iterative approach (SNIA).

The reactive mass transport is represented as (Bear and Bachmat, 1990):

$$\begin{cases} \frac{\partial C_i}{\partial t} = -\nabla(vC_i) + \nabla(D_i \nabla C_i) + Q_i \\ \frac{\partial C_i}{\partial t} = \Gamma_i(C_1 \ldots C_m) \end{cases}, \quad i = 1, 2, \ldots, m$$

where C_i denotes the molar concentration of the ith species of a m multi-species system; v is the pore water velocity of groundwater flow; D_i is the diffusion–dispersion coefficient of component i; Q_i is the source/sink term and $\Gamma_i(C_i \ldots C_m)$ is the source/sink term of species i due to equilibrium chemical reactions with other species. In this study, the GEMIPM2K code was adopted to solve the reaction term $\Gamma_i(C_i \ldots C_m)$ in an "operator-splitting" fashion.

The GEM-Selektor (Kulik et al., 2004, 2008) and GEMIPM2K codes use the GEM convex programming approach (Karpov et al., 1997, 2001) which is based on an explicit consideration of independent components (usually chemical elements and charge), dependent components, and phases. In a formal algebraic notation, l_α stands for a set of indices of dependent components included into αth phase. X_α denotes the mole amount of αth phase

$$X_\alpha = \sum_j n_j^{(x)} \quad j \in l_\alpha,$$

where $n_j^{(x)}$ is the mole amount of jth dependent component (species). If μ_j is a primal approximation of the chemical potential of jth species and L the set of indexes of all dependent components, then the total Gibbs energy function of the chemical system is

$$G(x) = \sum_j n_j^{(x)} \mu_j \quad j \in L$$

The equilibrium speciation of the chemical system, or the "primal solution" vector $n^{(x)}$ of elements $\{n_j^{(x)}\}$ which are mole amounts of dependent components, can be found by minimizing the total Gibbs energy of the system:

$$G(x) \Rightarrow \min \qquad \text{subject to} : An^{(x)} = n^{(b)}, \quad j \in \Re$$

$A = \{a_{ji}\}, j \in L, i \in N$ is a stoichiometry matrix (a_{ji} is number of moles of ith independent component in one mole of jth dependent component); $n^{(b)} = \{n_i^{(b)}\}, i \in N$ is an input vector of the total bulk chemical composition of the system; $n_i^{(b)}$ is total mole amount of ith independent component in the system; and $\Re$ stands for a set of the optional lower-, upper- or two-side kinetic (metastability) constraints to the $n_j^{(x)}$ values. In this GEM setup, concentrations of dependent components are defined separately in their respective phases using $n_j^{(x)}$ and X_α values. To express activities of dependent components (which go into primal chemical potentials μ_j) through their concentrations, the activity coefficients γ_i must be calculated between GEM iterations. In this work, in the aqueous electrolyte phase, the activity coefficients were computed using the Davies equation (Davies, 1962):

$$\log_{10} \gamma_j = -A_{DH} Z_j^2 \left(\frac{I_m^{0.5}}{1 + I_m^{0.5}} - 0.3 I_m \right)$$

where I_m is the effective molal ionic strength, and Z_j is the charge of the component species. The parameter A_{DH} is 0.5092 at a temperature of 25 °C and a pressure of 1 bar. Calculation of activity coefficients of the solid solution end members is described below.

3. Calculation of non-ideal solid solutions

In the application example on Ra transport in the vicinity of a nuclear waste repository, two ternary non-ideal solid solutions (Ba–Ra–Sr carbonate and sulfate) have been considered together with an aqueous solution and several pure solid phases.
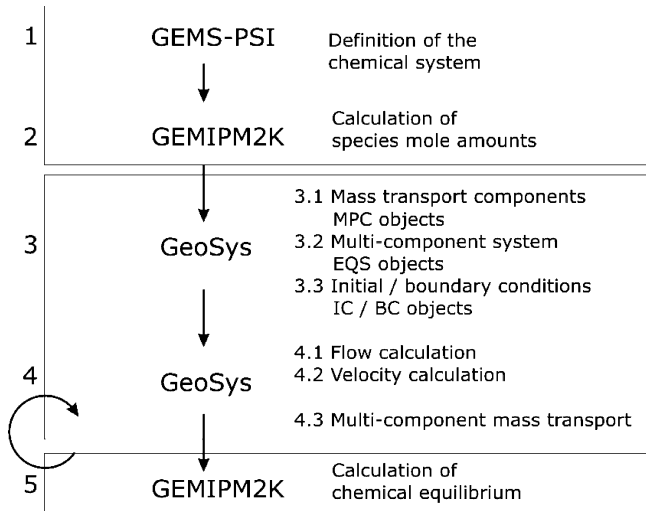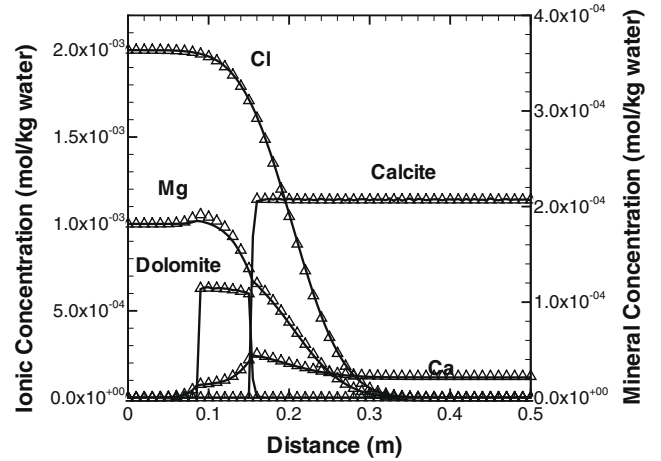
Fig. 1. Code coupling scheme for GeoSys-GEM.

Fig. 2a. Concentration profiles at t = 21000 sec for Cl, Mg, Ca, calcite and dolomite; solid lines are GeoSys-GEM and symbols (triangles) are GeoSys-PHREEQC results.
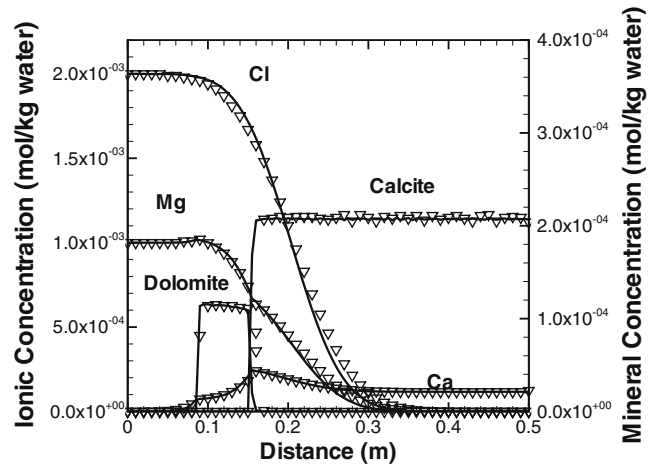

Fig. 2b. Concentration profiles at t = 21000 sec for Cl, Mg, Ca, calcite and dolomite; solid lines are GeoSys-GEM and symbols (nabla) are MCOTAC-GEM results.

A regular mixing model was used for carbonate and sulfate solid solutions (Glynn, 2000) because the available experimental data do not justify fitting them with more than one interaction parameter per binary sub-system. The excess molar Gibbs energy of mixing for a regular multi-component solid solution with n end members is expressed in general as (Powell and Holland, 1993):

$$G_{EX} = \sum_{i=1}^{n-1} \sum_{j>i}^{n} \chi_i \chi_j W_{ij}$$

where χ stands for the end-member mole fractions, e.g. $\chi_j = n_j^{(x)}/X_a$. The coefficients $W_{ij} = W_{ji}$ are symmetric binary interaction parameters (in J mol^{-1}); they are often expressed also in dimensionless form as $\alpha_{ij} = W_{ij}/RT$, where R is the ideal gas constant and T is the temperature. The activity coefficient for each end-member k is then calculated as:

$$\ln f_k = -\sum_{i=1}^{n-1} \sum_{j>i}^{n} q_i q_j \alpha_{ij}$$

where $q_i = 1 - \chi_i$ when $i = k$ and $q_i = -\chi_i$ when $i \neq k$. In a binary system, positive values of $\alpha_{ij} > 2$ result in the appearance of a (symmetric) miscibility gap inside of which two phases of different composition coexist with a single composition of the aqueous phase. The width of the miscibility gap decreases with increasing temperature up to "critical" T_c. Above this temperature, the miscibility gap disappears. At ambient temperatures, the values of α_{ij} range from nearly zero (ideal mixing) to maximum 13–14 in various ionic binary mixtures, i.e. from complete miscibility to $\chi_1 \leqslant n \times 10^{-6}$. If experimental compositions of the two phases co-existing within the symmetric miscibility gap are known, then the

value of the interaction parameter α can be estimated (Glynn, 2000); $\chi_A < 0.5$ is the mole fraction of end-member A in one of the phases:

$$\alpha = \frac{\ln \chi_A - \ln(1 - \chi_A)}{2\chi_A - 1}$$

Similar, but more complex relations hold for the miscibility gaps in ternary or higher-order multi-component systems. More details can be found in Kulik (2006b) and Bruno et al. (2007). The values of α for

Table 1
Model setup of the calcite–dolomite benchmark.

Parameters	Symbol	Value	Unit
Column length	L	0.5	m
Effective porosity	Θ	0.32	–
Column bulk density	ρ_b	1.8×10^3	kg/m^3
Longitudinal dispersion length	α_L	0.0067	m
Pore velocity	v	9.375×10^{-6}	m/s
Flow rate	Q	3×10^{-6}	m^3/s
Initial calcite concentration	$C_{CaCO_3, \text{ soil}}$	2.17×10^{-5}	mol/kg soil
Initial aqueous calcium carbonate concentration	$C_{CaCO_3, \text{ aq}}$	1.22×10^{-4}	M(mol/dm^{3}water)
Inflow MgCl$_2$ aqueous concentration	C_{MgCl_2}	1.0×10^{-3}	M

carbonate and sulfate solid solutions used in the present aqueous–solid solution model are given in Appendix, Table A4.

4. Software implementation

For coupling the mass transport with multi-species chemical equilibration processes, three major approaches exist. (1) In the *global implicit approach*, the chemical reaction equations are integrated with mass transport equations and solved simultaneously (Mayer et al., 2002b). (2) The *sequential non-iterative approach* (SNIA) solves the transport and reaction governing equations separately in a sequential manner without iteration between them (Pfingsten, 1994; Schäfer et al., 1998; Yabusaki et al., 1998; Xie et al., 2007). (3) The *sequential iterative approach* (SIA) back-couples between these two parts and solves for the converged results (Yeh and Tripathi, 1998; Van der Lee et al., 2003). The coupling of GeoSys and GEM is based on a sequential non-iterative approach (SNIA). In this operator-splitting scheme, transport and reaction equations are solved in a sequential manner. Since the source codes of both GeoSys and GEMIPM2K are written in C/C++ and accessible from the developers (open source concept), the code coupling has been conducted at source level in an object-oriented (OO) style.

The technical coupling scheme is illustrated in Fig. 1. The chemical system is defined in the pre-processing step (Fig. 1, step 1) where selection of species to be involved in the chemical reactions is done. At a second step (Fig. 1, step 2), mole amounts of all possible chemical species are calculated at given thermodynamic conditions (temperature and pressure) of interest. Each chemical species is represented by a component property (CP) object derived from the "Component Property" class. The number of CP instances is automatically created from the definition of the chemical system obtained from the GEMIPM2K code and thermodynamic data base (Fig. 1, step 3.1). For the multi-component mass transport problem, each CP instance requires the formation of the corresponding equation system (EQS) object (Fig. 1, step 3.2). The equilibrium concentrations of the multi-component species which are initially calculated by GEMIPM2K (Fig. 1, step 2) are used to define the initial and boundary conditions. All nodal concentration values are initialized with equilibrated chemical concentrations. The initial conditions (IC) object is then used to initialize the solution vectors of the equation systems (EQS).

GeoSys is based on the finite element method for solving partial differential equations (Wang and Kolditz, 2007). During the numerical simulation, first the flow problem is solved (Fig. 1, step 4.1), based on which the groundwater velocities are calculated (Fig. 1, step 4.2). Then, the concentrations of all chemical species are determined by solving the multiple mass-conservation equations (Fig. 1, step 4.3). Afterwards, the speciation vector (re-scaled to mole amount $n_j^{(x)}$) is passed to GEMIPM2K for the calculation of new chemical equilibrium states at all grid nodes (Fig. 1, step 5). The equilibrated concentrations are retrieved for the next time step of the mass transport calculation (Fig. 1, step 4.3). These intervening transport and equilibration loops keep going until the time interval for the reactive transport simulation is complete (Fig. 1, steps 4.3 and 5).

5. Code verification: mineral dissolution–precipitation

For verification of the coupling scheme in the reactive transport model, a hypothetical example is considered regarding instanta-
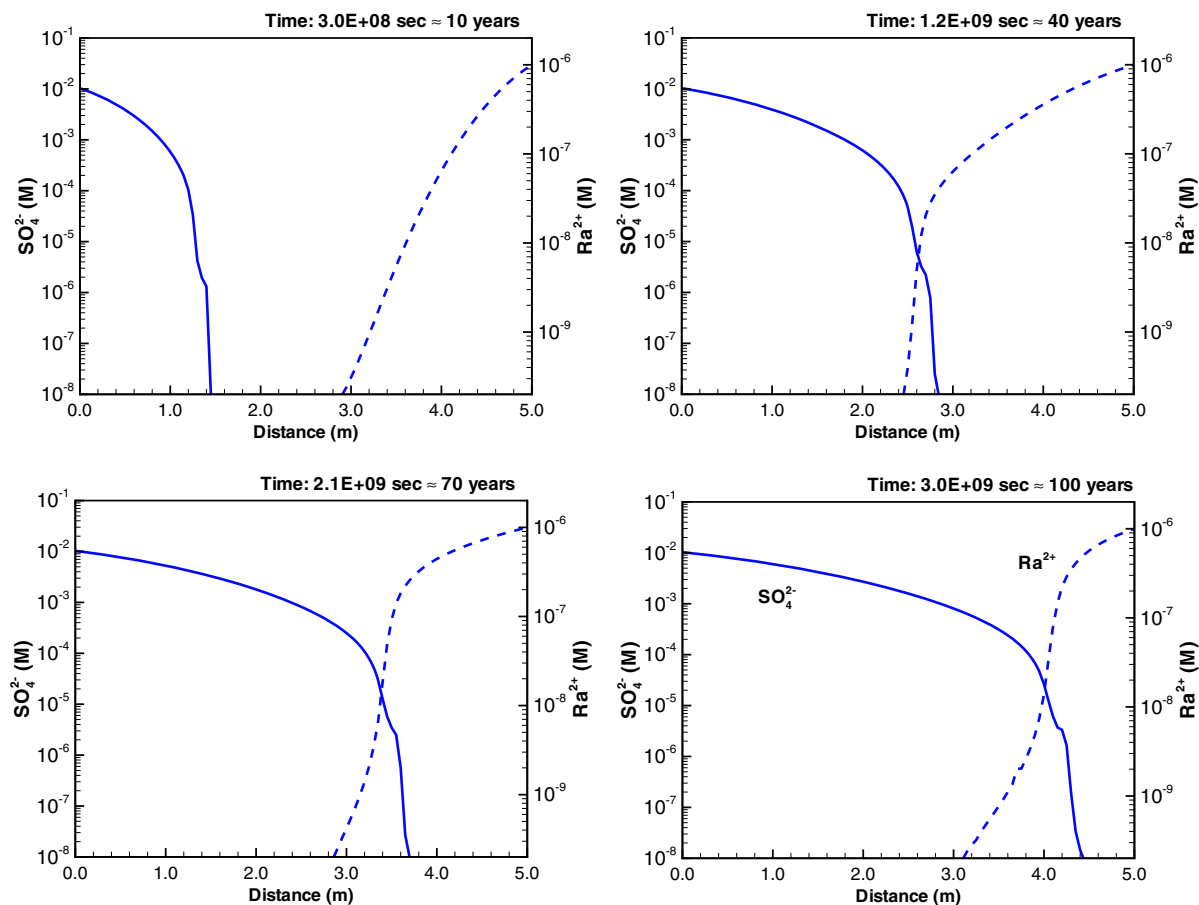

Fig. 3. Temporal evolution of SO_4^{2-} and Ra aqueous concentration profiles at about 10, 40, 70 and 100 a; solid lines are SO_4^{2-} and dashed lines are Ra^{2+} results.

neous mineral dissolution and precipitation as a benchmark test. This test case includes one-dimensional mass transport, calcite dissolution and dolomite precipitation processes. It was first proposed by Engesgaard and Kipp (1992) for model verification of the MST1D code and later used by Prommer (2002) for PHT3D. The ambient temperature of 25 °C and pressure of 1 bar are set constant during the whole simulation. The model domain is a one-dimensional column, initially equilibrated with 2.17×10^{-5} mol/kg calcite. The column is flushed with $MgCl_2$ solution at an aqueous concentration of 1.0×10^{-3} mol/l, leading to the development of multiple precipitation/dissolution fronts. Dolomite is not present initially, but is formed temporally in the column as a moving zone. The amount of both precipitation and dissolution minerals are so low that porosity and permeability effectively do not change. The parameters for the model setup according to Engesgaard and Kipp (1992) are listed in Table 1. The Nagra/PSI Chemical Thermodynamic Data Base (Hummel et al., 2002) has been used in both LMA and GEM chemical solvers (see Appendix). These log K values are slightly different from those in Engesgaard and Kipp (1992). As the Nagra/PSI database provides the same chemical thermodynamic input data for both LMA and GEM methods, consistent simulations can be conducted for comparison of the different geochemical approaches.

To verify the code coupling, simulation results of GeoSys-LMA (using PHREEQC) and GeoSys-GEM were compared. PHREEQC is a geochemical speciation code based on the Law of Mass Action (LMA) approach (Parkhurst and Appelo, 1999). It differentiates between master species, whose concentrations directly enter into mass-conservation equations, and secondary species, whose con-centrations are found through the LMA expressions using master species activities and equilibrium constants of formation reactions. During the calculation, the total balance quantities of the master species are given as system mass balance constraints. This allows the solution of the mass-conservation equations iteratively together with the LMA expressions using a Newton–Raphson or a similar numerical algorithm.

Fig. 2a shows the concentration profiles for Cl, Mg, Ca, calcite and dolomite obtained by the two alternative chemical solvers. Acting as a conservative tracer which is not involved in any chemical reaction, the Cl concentration remains the same for both simulations. Since the same geochemical database is used, the results are almost identical. Additionally, the benchmark test was calculated with the reactive transport code MCOTAC-GEM, which uses a method of multispecies random walk (Pfingsten, 1994) for mass transport and GEMIPM2K as a chemical solver. A comparison of the numerical results is shown in Fig. 2b. There are small differences regarding the solute and mineral concentrations which are caused by the different numerical methods for solving the mass transport equations (finite elements vs. random walk). The agreement of the simulation results using different methods for mass transport and geochemical reactions confirm the correct implementation of code coupling in GeoSys-GEM.

6. Application: aqueous–solid solution system containing radium

For the performance assessment of nuclear waste repositories, the traditional linear K_D concept is the standard method to account
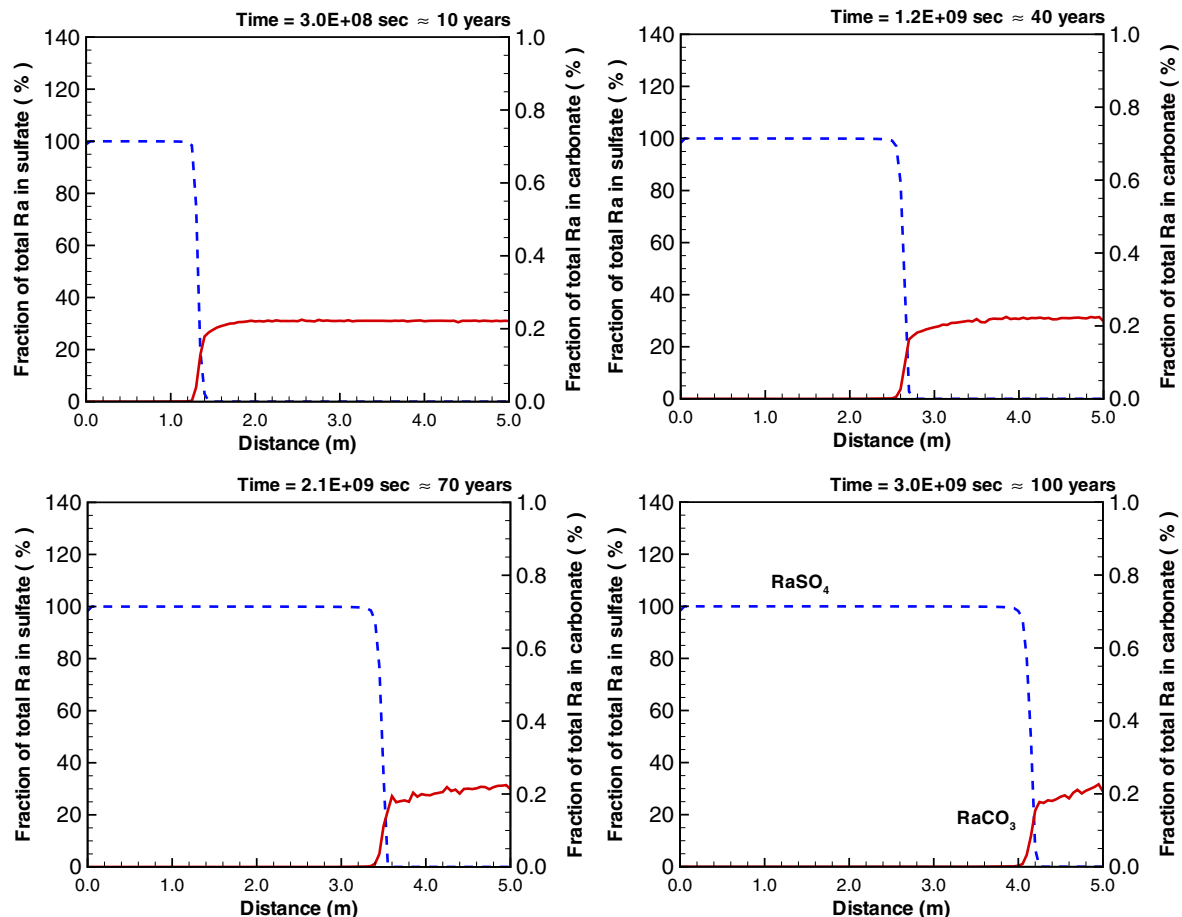

Fig. 4a. Fraction of total Ra fixed in sulfate and carbonate solid solution end members. Dashed lines are percentage of Ra fixed in sulfate phase, and solid lines are those fixed in carbonate phase.

for the retardation of radionuclides due to chemical interactions with the near- and far-field materials. Parameter value uncertainties and conceptual uncertainties due to process simplifications are often covered in terms of distribution functions for material parameters that are bound by optimistic and pessimistic values. In this application example, a mechanistic model is used for the retardation of Ra in bentonite or bentonite–sand mixtures and an attempt is made to compare the simulation results with the results obtained with the linear K_D concept.

In order to demonstrate the influence of solid solution formation on the transport of mobile Ra cations, a strongly simplified one-dimensional scenario of a tunnel connecting to an intermediate level radioactive waste repository is considered. Spatial and temporal discretization is set to 0.05 m and 139 days. According to the engineering design, bentonite will be mixed with sand and used as back-filling material in the tunnel. Due to the low permeability of this material (up to 5.0×10^{-11} m/s) and low hydraulic gradient, the transport of radionuclides in the tunnel will be dominated by diffusion. The effective diffusion coefficients estimated by Nagra for Ra is 2.0×10^{-10} m²/s. Considering an initial porosity of 0.3 for the bentonite, and to keep charge balance in mass transport, the apparent diffusion coefficients for all mobile chemical components is set to 5.0×10^{-10} m²/s. The temperature was assumed to be 25 °C and pressure 1 bar. A boundary condition of constant Ra concentration representing the source leakage of the radionuclides out of the repository at the right end of the tunnel backfill was used. The source term, i.e. aqueous concentration of Ra²⁺, was fixed at 1.0×10^{-6} mol/L. Such a concentration of Ra is

possible in the cementitious backfill material of caverns for intermediate level waste (Gaucher and Blanc, 2006). In bentonite such a concentration is much too high, as solubility limits are expected to be much lower (Nagra, 2002). At the left end, a constant concentration for dissolved SO_4^{2-} was set, which could emerge e.g. as a product of pyrite oxidation during the tunnel excavation period. As the time span of analysis (around 100 a) is much shorter than the half-life of ²²⁶Ra (1700 a), radioactive decay is not considered in this model. However, it is assumed that re-crystallization or co-precipitation rates of carbonate and sulfate solid solutions are fast enough to approach chemical equilibrium within the mass transport time step.

Bentonite usually contains some sorbed Sr and Ba together with significant amounts of CaCO₃, re-crystallization of which may lead to the formation of carbonate solid solutions between RaCO₃, BaCO₃, SrCO₃, and CaCO₃ end members. Because it is generally assumed that sorption of Ba, Sr and Ra on clay minerals is weak (e.g. Bradbury and Baeyens, 2003), aqueous speciation of these metals was considered, as well as their carbonate and sulfate mineral forms, but no sorption on clay component. Ingression of SO_4^{2-}, e.g. from wall rock, may result in re-partitioning of Ba, Ra and Sr into sulfate solid solutions. Consequently, in the geochemical model setup both carbonate and sulfate non-ideal solid solutions of Ba, Sr and Ra are considered (see Appendix) together with calcite CaCO₃. The ternary carbonate and sulfate solid solution phases are each included twice because of the possible miscibility gaps which would result e.g. in Sr and Ba dominated sulfate phases co-existing in the particular equilibrium state. Lead–Ca carbonates
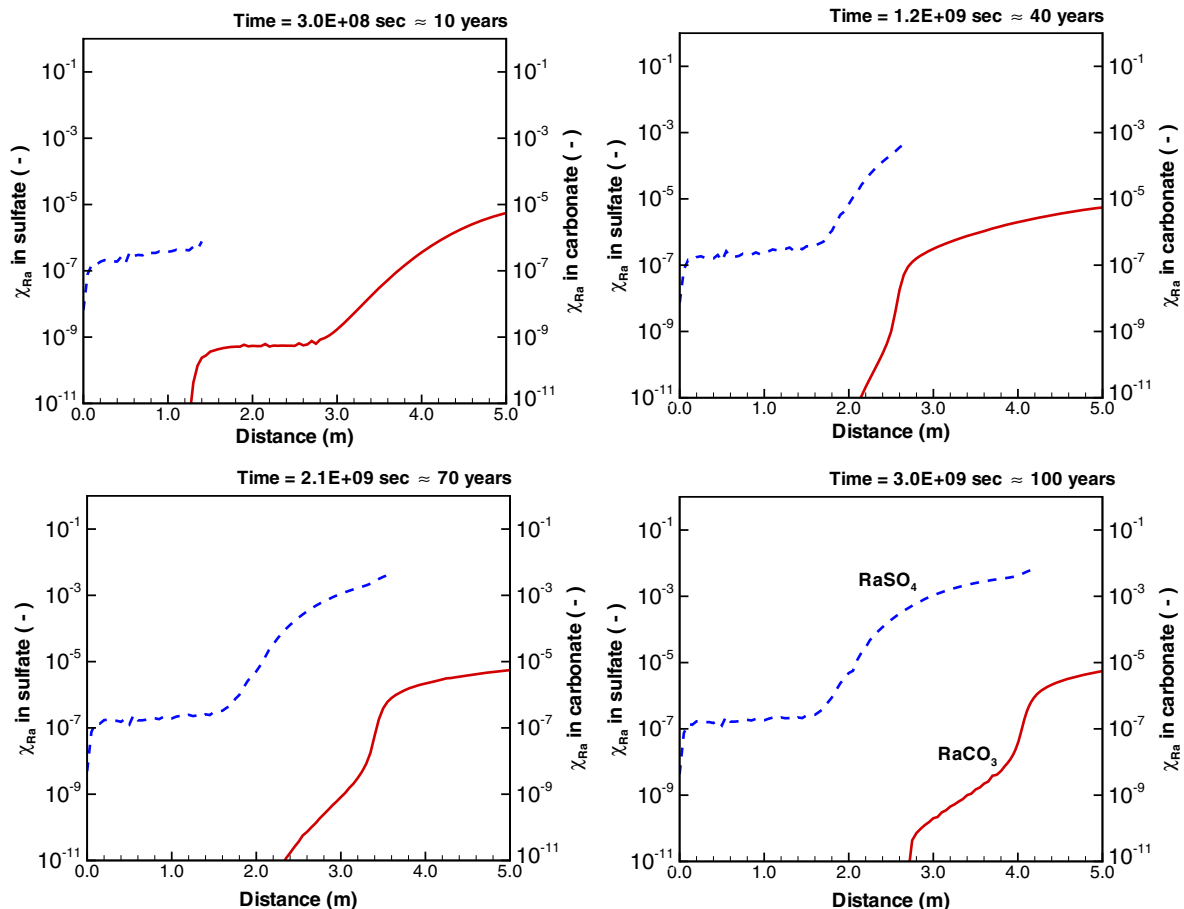
Fig. 4b. Temporal evolution of mole fractions of Ra end members χRa in sulfate and carbonate solid solutions. Dashed lines are for χRa in sulfate and solid lines for χRa in carbonate phases. When the SO_4^{2-} front enters into the carbonate region, the (Ba, Sr, Ra)CO3 phase is dissolved and (Ba, Sr, Ra)SO₄ phase precipitates.

were also added for completeness. However, in all the simulations their concentrations are found to be more or less constant and do not interfere with the Ba–Sr–Ra ones, therefore they were not further investigated.

It should be noted that although this chemical system contains five non-ideal solid solutions (four ternary Ba–Sr–Ra carbonates and sulfates, plus one binary Ca–Pb carbonate) together with many pure solid phases, it is still a simplification compared with the natural bentonite system. For instance, the Ba, Sr, and Ra end members in calcite were ignored for two reasons: (1) Ba–Sr–Ra carbonates belong to the aragonite group which has a different structure compared with the calcite group carbonates (e.g. calcite and cerussite $PbCO_3$). (2) Large cations such as Sr, Ba and Ca are difficult to incorporate into the calcite structure, which results in large uncertainties in determining the properties of respective pure end members with a calcite structure. In any case, their miscibility with calcite is expected to be quite limited, as the interaction parameters α are larger than 3. For similar reasons, the Ba, Sr and Ra end members of gypsum were omitted. However, it is believed that even the simplified chemical system will realistically reproduce the main trends in partitioning of Ra, Ba and Sr between aqueous, carbonate and sulfate phases.

The simulation was set up in a way that at the beginning, Ra^{2+} cations and SO_4^{2-} anions diffuse into the tunnel from the opposite ends. Due to the presence of excess carbonate in the pore water of the bentonite–sand mixture, Ra^{2+} is first captured in Ba–Sr carbonate solid solutions. However, when SO_4^{2-} enter the system, the

carbonates are expected to be replaced with much less soluble Ba–Sr sulfates (barite and celestite). In turn, as the dissolved aqueous sulfates arrive at these areas, Ra in the aqueous phase and in carbonate solid solutions will be converted into sulfate solid solutions, and the Ra^{2+} aqueous concentration will strongly decrease. In this way, most of the mobile Ra will be immobilized in sulfate solid solutions. Upon further supply of SO_4^{2-}, the dissolved concentrations of Ba, Sr and Ra are expected to continue to decrease, because of the so-called "common-anion" effect. For instance, if maximum dissolved concentration of SO_4^{2-} is controlled by the presence of gypsum ($CaSO_4 \cdot 2H_2O$) which is much more soluble than celestite or barite, the dissolved Ba or Ra will be about two orders of magnitude less than that without excess gypsum.

The numerical reactive transport simulation results confirm this scenario. Fig. 3 shows the evolution of SO_4^{2-} and Ra^{2+} aqueous concentrations, Figs. 4b, 5 and 6 depict the mole fractions χ_j of $RaSO_4$ and $RaCO_3$, $BaSO_4$ and $BaCO_3$ as well as $SrSO_4$ and $SrCO_3$ end members in both solid solutions (($Ba,Sr,Ra)CO_3$ and ($Ba,Sr,Ra)SO_4$), respectively. At the beginning of simulation, both SO_4^{2-} and Ra^{2+} diffuse into the model domain, and a small fraction of the Ra is fixed in the form of Ra-containing Ba–Sr carbonates (see Fig. 4a where the very weak incorporation of Ra in calcite is neglected). At around 40 a, when the SO_4^{2-} front encounters the Ra^{2+} front, the carbonate solid solutions are transformed into the Ra-containing sulfate solid solutions (Fig. 4a and b). This causes a sharp decline of the aqueous Ra^{2+} concentration (Fig. 3). At the same time, Ba and Sr are also re-partitioned into the sulfate phase (Figs.

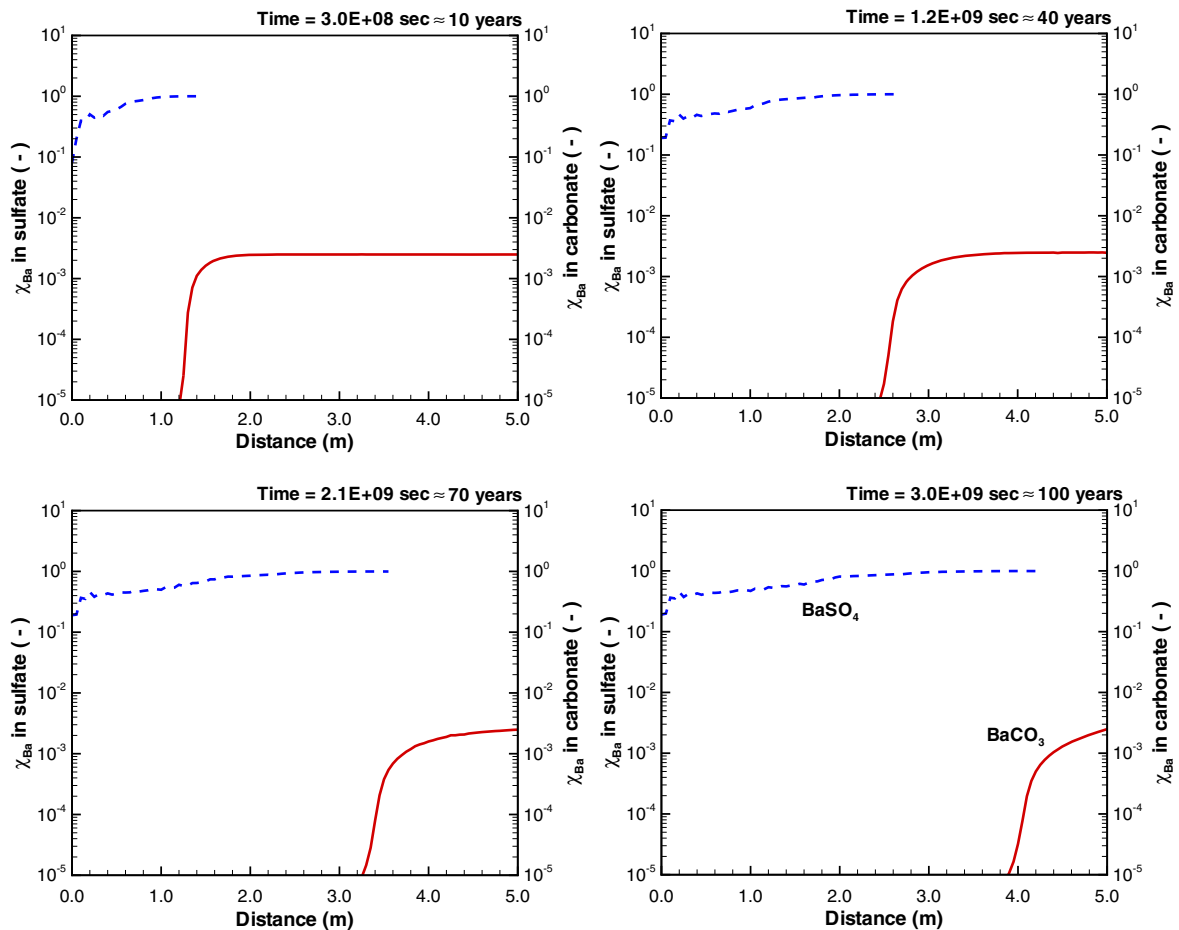**Fig. 5.** Temporal evolution of mole fractions χ_{Ba} of Ba end members in sulfate and carbonate solid solutions. Dashed lines are for χ_{Ba} in sulfate and solid lines for χ_{Ba} in carbonate phases.

5 and 6). As the SO_4^{2-} ingression proceeds, the mobile Ra^{2+} can no longer diffuse further into the tunnel. Instead, the dissolved aqueous Ra^{2+} is gradually fixed into stable sulfate solid solutions.

As a result of the numerical study, it can be shown that the formation of solid solutions and their transformations must strongly retard the transport of Ra. In Fig. 7 the reactive transport results are compared with analytical solutions for linear sorption effects (e.g. Fetter, 1999). The following set of Ra distribution coefficients $K_D = 0.0, 3.0 \times 10^{-4}, 2 \times 10^{-3}$ and 0.1 m^3/kg from Nagra (2002) was used for comparison. These values stand for no retardation, pessimistic, reference and optimistic estimation of the Ra sorption in compacted bentonite, respectively. It should be noted that the K_D values given in Nagra (2002) are based on a cation exchange mechanism. Details on the derivation of the values are given in Bradbury and Baeyens (2003) and Wersin and Schwyn (2004). According to Bradbury and Baeyens (2003), only very few experimental data for the sorption of Ra on clay minerals are available. Therefore, they assumed that Ra is present as a bivalent cation in solution and that it is sorbed by cation exchange in analogy to other alkali-earth metals e.g. Ca, Mg, Sr and Ba. If appropriate data for Ra are not available, Sr and Ba are often used as chemical analogues. Compared with the solid solution incorporation, cation exchange is a different sorption mechanism in which Ra^{2+} competes with major cations (Ca^{2+}, Na^+, K^+) for permanent-charge sites in clay present in the (large) amount limited by the cation exchange capacity. In general, both mechanisms are expected to compete for metal cations. However, in the present study, cation exchange was omitted from the chemical model in order to simplify the analysis of the effects of solid solutions on the transport of Ra.

At the initial stage of the simulation, as long as SO_4^{2-} has not reached the Ra front, only a negligibly small fraction of Ra is fixed in the form of Ra carbonates (Fig. 4a). Therefore, the concentration of Ra^{2+} follows the one calculated with analytical solutions where no sorption is included. After around 40 a, when the SO_4^{2-} starts binding aqueous alkali-earth cations and transforming carbonates into sulfates, the profile of Ra^{2+} is retarded, depending on the ingression of the SO_4^{2-} front. Because it is the specific chemical system and corresponding reactions that influence the sorption of radio nuclides, none of the single-K_D value estimations can predict the Ra^{2+} profile correctly, particularly in a long-time period. This is consistent with the work of Reardon (1981), who did the simulation based on ion-exchange and concluded that a constant K_D is not sufficient to characterize a dynamic chemical evolution.

To test the model sensitivity, the amounts of Ba, Sr and SO_4^{2-} were varied and the simulation results are compared. First, the amounts of Ba and Sr were scaled down by a factor of 10^2 and 10^4. Fig. 8 shows that Ra^{2+} is still heavily retarded even with 0.01% of the original Ba and Sr inventories. This means that the Ba–Ra or Sr–Ra solid solutions can be formed even with very limited amount of Ba and Sr, presuming there is enough SO_4^{2-} available. In addition, the influence of the SO_4^{2-} content on the incorporation of Ra in the solid solutions was tested. In the system of interest, the limiting dissolved concentration of SO_4^{2-} is expected to be set by the solubility of gypsum ($CaSO_4 \cdot 2H_2O$). Hence, five chemical setups of the backfill material were prepared containing 0.1%, 0.25%, 0.5%, 0.75% and 1% mass of gypsum, respectively. They were used as initial conditions in the reactive transport model. The SO_4^{2-}-rich left boundary was removed, to let only Ra^{2+} diffuse from
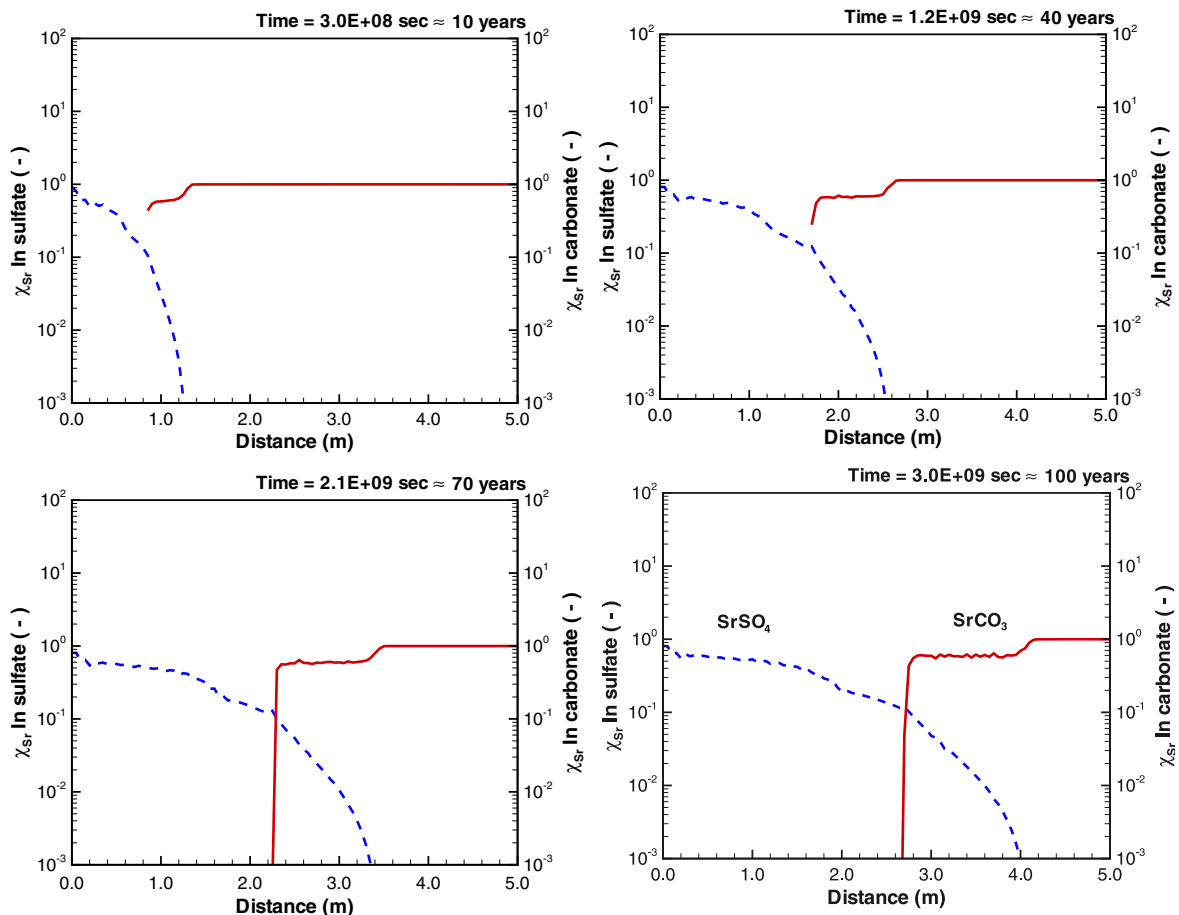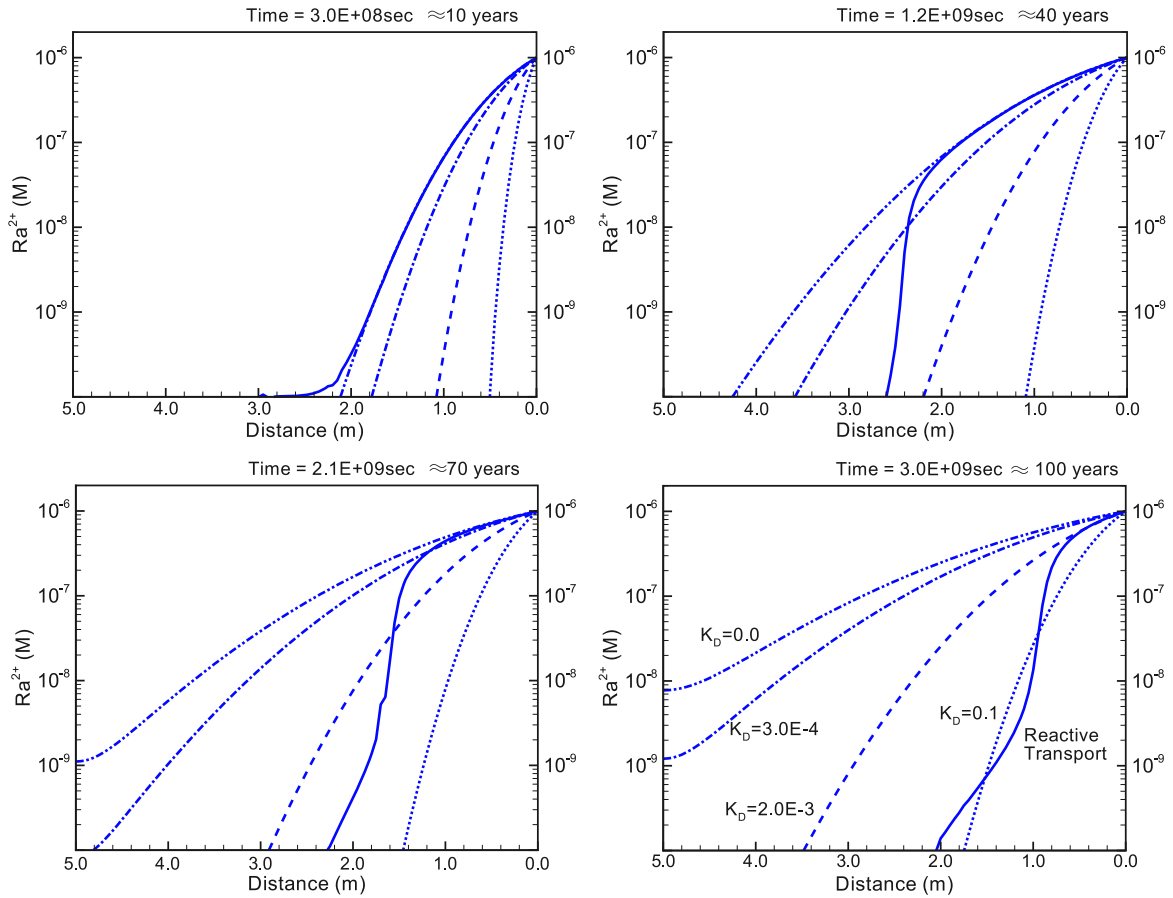

Fig. 6. Temporal evolution of mole fractions χSr of Sr end members in sulfate and carbonate solid solutions. Dashed lines are for χSr in sulfate and solid lines for χSr in carbonate phases.

Fig. 7. Comparison of the retardation behavior using solid solution and the traditional KD concept. Solid lines are concentration profiles of Ra^{2+} using the solid solution approach, dashed, double-dot ted lines, dashed-dotted lines, dashed lines and dotted lines are profiles calculated for KD values of 0.0, 3×10^{-4}, 2×10^{-3} and 0.1 m^3/kg, respectively.

right to left. Therefore the shape of the Ra front in Fig. 9 is different compared to Fig. 8. It is found that the amount of SO_4^{2-} heavily influences the formation of solid solutions. With 0.1% of gypsum

added, the calculated Ra^{2+} profile is close to the reference curve that has no retardation effect. The more SO_4^{2-} that is available, the more strongly Ra^{2+} is retarded. Therefore, the availability of SO_4^{2-} seems to be the most important factor for the retardation of Ra. It should be mentioned that the chemical system in this
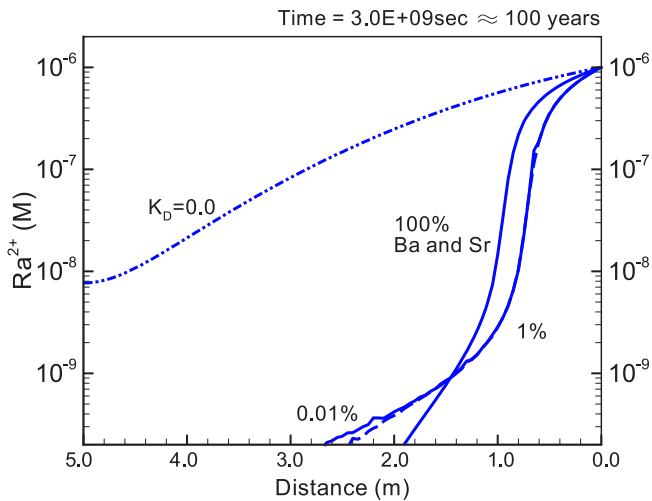
Fig. 8. Sensitivity of retardation effects regarding the available amounts of Ba and Sr. Solid lines are concentration of Ra^{2+} calculated for the chemical setup given in Table A3, dashed line and dotted line are Ra^{2+} concentration profiles with 1%, and 0.01% of Ba and Sr from the original setting, respectively. The dashed dotted line is the Ra^{2+} concentration profile calculated for the analytical solution with a KD value of zero.
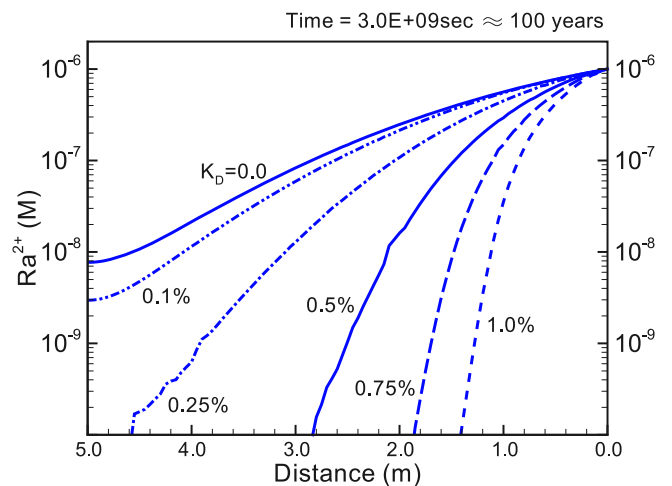
Fig. 9. Sensitivity of retardation effects regarding the available amount of SO_4^{2-}. From right to left, the curves are Ra^{2+} concentration profiles calculated for 1%, 0.75%, 0.5%, 0.25% and 0.1% of gypsum initially existing in the solid phase of the buffer material, compared to the amount of calcite, respectively. The leftmost solid line is the reference profile calculated for a KD value of zero.

Table A1
Chemical input data for the system totals and product species expressed in the form of mass actions (LMA approach, calcite–dolomite example).

			Master (primary) species							log K product
			H^+	H_2O	Ca^{2+}	Mg^{2+}	Cl^-	HCO_3^{3-}	e^-	
Product (secondary) species										
	Aqueous species									
		H_2	2						2	−3.11
		O_2	−4	2					−4	−85.99
		CH_4	9	−3				1	8	27.85
		OH^-	−1	1						−14.00
		CO_2	1	−1				1		6.35
		CO_3^{-2}	−1					1		−10.33
		$CaCO_3$	−1		1			1		−7.10
		$CaHCO_3^+$			1			1		1.11
		$CaOH^+$	−1	1	1					−12.78
		$MgCO_3$	−1			1		1		−7.35
		$MgHCO_3^+$				1		1		1.07
		$MgOH^+$	−1	1		1				−11.44
	Solids									
	Aragonite	$CaCO_3$	−1		1			1		1.99
	Brucite	$Mg(OH)_2$	−2	2		1				16.84
	Calcite	$CaCO_3$	−1		1			1		1.85
	Dolomite (disordered)	$CaMg(CO_3)_2$	−2		1	1		2		4.12
	Dolomite (ordered)	$CaMg(CO_3)_2$	−2		1	1		2		3.57
	Graphite	C	5	−3				1	−4	−21.82
	Portlandite	$Ca(OH)_2$	−2	2	1					22.80
Imposed total mass balance constraints (M)	At inflow boundary		0.00E+00	5.55E+01	1.00E−10	1.00E−03	2.00E−03	1.00E−10	0.00E+00	
	In column initially		0.00E+00	5.55E+01	1.22E−04	1.00E−12	1.00E−12	1.22E−04	1.22E−04	

simulation has a pH of about 8, and an Eh from −200 to −300 mV, which is consistent with the values predicted by Nagra (2002). In this redox environment, SO_4^{2-} is stable. Over a long term, i.e. >10 ka, redox might be altered due to canister corrosion, and SO_4^{2-} can be reduced to H_2S. However, that scenario is beyond the scope of this work, therefore not considered in this simulation.

At the temperature of 25 °C, some minerals may not maintain overall internal equilibrium with the aqueous phase. The crystals may precipitate over time from solutions with varying composition, and become zoned as they grow. Such heterogeneous crystals form commonly, for instance, in the case of carbonate minerals. However, Doerner and Hoskins (1925) observed that barite rapidly recrystallizes even at low temperatures. During this process (which they called "replacement"), large barite crystals grow at the expense of small (thermodynamically less stable) particles. As long as crystal growth continues, Ra will be incorporated in the growing crystals, continuously generating fresh surfaces for further Ra fixation. Such dynamic recrystallization will ultimately produce barite with homogeneously distributed Ra. In addition, because the amount of Ba–Sr sulfate in bentonite largely exceeds the amount of Ra, almost all of the Ra released from the waste will coprecipitate, even if part of the pre-existing sulfate minerals fails to react with the aqueous solution e.g. due to the presence of preferential pathways. This will result in a strong retardation effect for the Ra migration (as in Fig. 8).

As the K_D values from Nagra (2002) are based on a cation exchange model, the values depend on the cation exchange capacity of the clay rock. These values were given for pure compacted bentonite; for sand–bentonite mixtures, they have to be reduced according to the sand/bentonite ratio. However, the incorporation

Table A2a
Input thermodynamic and speciation data (GEM approach, calcite–dolomite example).

Phases and dependent components (DC)	DC chemical stoichiometry	Standard Gibbs energy (J/mol)
Dependent components		
Aqueous electrolyte	$Ca(CO_3)$	−10,99,176
	$Ca(HCO_3)^+$	−11,46,041
	Ca^{2+}	−552,790
	$CaOH^+$	−717,024
	$Mg(CO_3)$	−998,975
	$Mg(HCO_3)^+$	−10,47,022
	Mg^{2+}	−453,985
	$MgOH^+$	−625,868
	CO_2	−386,015
	CO_3^{2-}	−527,982
	HCO_3^-	−586,940
	CH_4	−34,354
	ClO_4^-	−8535
	Cl^-	−131,290
	H_2	17,729
	O_2	16,446
	OH^-	−157,270
	H^+	0
	H_2O	−237,181
Gas mixture	CO_2	−394,393
	CH_4	−50,659
	H_2	0
	O_2	0
Solid phase		
Aragonite	$CaCO_3$	−11,28,355
Brucite	$Mg(OH)_2$	−832,227
Graphite	C	0
Calcite	$CaCO_3$	−11,29,176
Dolomite (disordered)	$CaMg(CO_3)_2$	−21,57,149
Portlandite	$Ca(OH)_2$	−897,013

Table A2b
Initial bulk composition data used in calcite–dolomite example.

	On left inflow boundary	In the colomn initially
Bulk elemental compositions (mol)		
C	1.00E−16	3.30E−04
Ca	1.00E−16	3.30E−04
Cl	2.00E−03	2.00E−07
H	1.11E+02	1.11E+02
Mg	1.00E−03	1.00E−07
O	5.55E+01	5.55E+01
Charge	0	0

Table A3a
Thermodynamic and initial speciation data used in the Ra Aq-SS application example (1 bar, 25 °C).

Phases			Species stoichiometry composition	Standard Gibbs free energy (J/mol)	Initial in the column (mol)	On left boundary, sulfate rich (mol)	On right boundary, radium rich (mol)
Aquous phase components			$Ba(CO_3)$	−11,04,251	1.38E−07	1.33E−12	1.38E−07
			$Ba(HCO_3)^+$	−11,53,325	7.05E−07	1.21E−11	7.05E−07
			$Ba(SO_4)$	−13,20,652	2.15E−14	9.43E−09	6.04E−12
			Ba^{2+}	−560,782	4.90E−05	8.03E−09	4.90E−05
			$BaOH^+$	−721,077	1.14E−10	8.14E−15	1.14E−10
			$Ca(CO_3)$	−10,99,176	1.11E−06	1.11E−06	1.11E−06
			$Ca(HCO_3)^+$	−11,46,041	2.33E−06	4.15E−06	2.34E−06
			$Ca(SO_4)$	−13,10,378	2.13E−14	9.65E−04	5.99E−12
			Ca^{2+}	−552,790	1.22E−04	2.06E−03	1.22E−04
			$CaOH^+$	−717,024	1.39E−09	1.03E−08	1.39E−09
			$Pb(HS)_2$	−83,923	5.32E−18	4.96E−14	1.49E−15
			$Pb(HS)_3^-$	−79,375	0.00E+00	2.15E−17	0.00E+00
			Pb^{2+}	−23,891	1.42E−15	6.21E−19	5.10E−18
			PbO_2H^-	−338,904	0.00E+00	0.00E+00	0.00E+00
			PbO	−164,640	9.63E−17	0.00E+00	0.00E+00
			$PbOH^+$	−225,727	6.27E−14	1.19E−17	2.25E−16
			$Ra(CO_3)$	−11,03,745	3.43E−14	0.00E+00	3.43E−10
			$Ra(OH)^+$	−721,617	4.33E−17	0.00E+00	4.32E−13
			$Ra(SO_4)$	−13,21,649	0.00E+00	1.09E−16	2.76E−14
			Ra^{2+}	−561,493	1.99E−11	8.24E−17	1.99E−07
			$HSiO_3^-$	−10,14,598	2.70E−07	1.94E−07	2.70E−07
			SiO_2	−833,411	2.00E−05	2.00E−05	2.00E−05
			SiO_3^{2-}	−938,510	1.24E−12	8.22E−13	1.23E−12
			$Sr(CO_3)$	−11,07,830	6.83E−08	3.57E−09	6.83E−08
			$Sr(HCO_3)^+$	−11,57,538	4.52E−07	4.22E−08	4.52E−07
			$Sr(SO_4)$	−13,21,366	3.36E−15	7.99E−06	9.45E−13
			Sr^{2+}	−563,836	1.97E−05	1.75E−05	1.97E−05
			$SrOH_+$	−725,159	6.93E−11	2.69E−11	6.92E−11
			CO_2	−386,015	9.84E−06	2.36E−06	9.87E−06
			CO_{30}^{2-}	−527,982	1.75E−06	2.80E−07	1.74E−06
			HCO_3^-	−586,940	3.80E−04	6.57E−05	3.81E−04
			CH_4	−34,354	1.41E−06	2.90E−13	1.40E−06
			H_2	17,729	4.08E−10	1.24E−11	4.07E−10
			O_2	16,446	0.00E+00	0.00E+00	0.00E+00
			$S_2O_3^{2-}$	−519,989	0.00E+00	1.50E−11	0.00E+00
			HSO_3^-	−529,098	0.00E+00	1.19E−14	0.00E+00
			SO_3^{2-}	−487,886	0.00E+00	6.49E−14	0.00E+00
			HSO_4^-	−755,805	0.00E+00	2.20E−09	7.86E−17
			SO_4^{2-}	−744,459	2.81E−13	2.05E−03	7.90E−11
			H_2S	−27,930	7.24E−11	6.74E−07	2.02E−08
			HS^-	11,969	6.44E−10	4.32E−06	1.80E−07
			S^{2-}	120,422	0.00E+00	3.92E−17	1.76E−18
			OH^-	−157,270	1.74E−07	1.25E−07	1.74E−07
			H^+	0	2.59E−09	4.60E−09	2.59E−09
			H_2O	−237,181	1.11E+01	1.11E+01	1.11E+01
Gas phase components			CO_2	−394,393	0.00E+00	0.00E+00	0.00E+00
			CH_4	−50,659	0.00E+00	0.00E+00	0.00E+00
			H_2	0	0.00E+00	0.00E+00	0.00E+00
			O_2	0	0.00E+00	0.00E+00	0.00E+00
			H_2S	−33,752	0.00E+00	0.00E+00	0.00E+00
Solid solutions	$(Ra,Ba,Sr)CO_3$	Witherite	$BaCO_3$	−11,37,634	0.00E+00	0.00E+00	0.00E+00
		Ra-carbonate	$RaCO_3$	−11,36,851	0.00E+00	0.00E+00	0.00E+00
		Sr-carbonate	$SrCO_3$	−11,44,735	0.00E+00	0.00E+00	0.00E+00
	$(Ra,Sr,Ba)CO_3$[*]	Witherite	$BaCO_3$	−11,37,634	1.99E−07	0.00E+00	1.99E−07
		Ra-carbonate	$RaCO_3$	−11,36,851	4.43E−14	0.00E+00	4.43E−10
		Sr-carbonate	$SrCO_3$	−11,44,735	7.98E−05	0.00E+00	7.98E−05
	$(Ra,Ba,Sr)SO_4$	Ba-sulfate	$BaSO_4$	−13,62,152	0.00E+00	9.40E−04	0.00E+00
		Ra-sulfate	$RaSO_4$	−13,64,516	0.00E+00	1.88E−11	0.00E+00
		Sr-sulfate	$SrSO_4$	−13,46,150	0.00E+00	2.20E−04	0.00E+00
	$(Ra,Sr,Ba)SO_4$[*]	Ba-sulfate	$BaSO_4$	−13,62,152	0.00E+00	5.95E−05	0.00E+00
		Ra-sulfate	$RaSO_4$	−13,64,516	0.00E+00	1.19E−12	0.00E+00
		Sr-sulfate	$SrSO_4$	−13,46,150	0.00E+00	2.55E−04	0.00E+00
	$(Pb,Ca)CO_3$	Calcite	$CaCO_3$	−11,29,176	9.87E−03	1.10E−02	9.87E−03
		Cerussite	PbO_3	−629,148	6.97E−10	1.99E−14	2.50E−12
	Solid phases	Graphite	C	0	7.17E−06	0.00E+00	6.79E−06
		Portlandite	$Ca(OH)_2$	−897,013	0.00E+00	0.00E+00	0.00E+00
		Gypsum	$CaSO_4 \cdot 2H_2O$	−17,97,763	0.00E+00	0.00E+00	0.00E+00
		Cerussite	PbO_3	−629,148	0.00E+00	0.00E+00	0.00E+00
		Litharge	PbO	−189,200	0.00E+00	0.00E+00	0.00E+00
		Galenite	PbS	−81,846	1.00E−09	1.00E−09	9.96E−10
		Anlgesite	$PbSO_4$	−813,173	0.00E+00	0.00E+00	0.00E+00
		Ra-carbonate	$RaCO_3$	−11,36,851	0.00E+00	0.00E+00	0.00E+00
		Ra-sulfate	$RaSO_4$	−13,64,516	0.00E+00	0.00E+00	0.00E+00
		Sulfur	S	0	0.00E+00	0.00E+00	0.00E+00
		Quartz	SiO_2	−856,239	3.53E+01	3.53E+01	3.53E+01
			pH		7.91	7.72	7.91
			pe		−5.12	−4.17	−5.12

[*] Two solid solution phases were included to model miscibility gaps wherever appropriate.

Table A3b
Initial bulk composition data used in the Ra Aq–SS application example.

	Initial in the column	On left boundary (sulfate rich)	On right boundary (with radium)
Bulk elemental compositions (mol)			
Ba	5.00E−05	1.00E−03	5.00E−05
C	1.04E−02	1.10E−02	1.04E−02
Ca	1.00E−02	1.40E−02	1.00E−02
H	2.22E+01	2.21E+01	2.22E+01
O	8.17E+01	8.16E+01	8.17E+01
Pb	1.00E−09	1.00E−09	1.00E−09
Ra	2.00E−11	2.00E−11	2.00E−07
S	1.02E−09	4.50E−03	2.01E−07
Si	3.53E+01	3.53E+01	3.53E+01
Sr	1.00E−04	5.00E−04	1.00E−04
Charge	0	0	0

Table A4
Regular interaction parameters α_{ij} used in solid solution models.

End member binary	Carbonate solid solution	Sulfate solid solution
Ba–Sr	5.3[a]	2.34[b]
Ba–Ra	0[c]	0[c]
Sr–Ra	5.3[d]	2.34[d]
Ca–Pb	2.94[a]	–

Note: Ca end members in Ba–Sr–Ra carbonate and sulfate solid solutions, as well as Ba,Sr,Ra end members in Ca carbonate (calcite) and sulfate phases, have been omitted because of very limited miscibility (less than 1%) in order to simplify the example.

[a] Data (Glynn, 2000), Table 2, assumed regular mixing in Ba–Sr binary.
[b] Data (Glynn, 2000), Table 1c.
[c] Mixing between Ba^{2+} and Ra^{2+} was assumed ideal due to similar ionic radii.
[d] No direct data, interaction parameter assumed the same as for the Ba–Sr binary.

of cations in solid solutions does not depend directly on the amount of bentonite in the system. The effective retardation of Ra in the system scales mainly with the availability of SO_4^{2-} ions. The results show that the incorporation in solid solutions results in a retardation similar or stronger than that expected to result from cation exchange in compacted bentonite. This can partially be due to the fact that initial Sr and Ba inventories are also mainly located on cation exchange sites. For a more plausible evaluation of Ra^{2+} transport in such systems, both mechanisms (solid solution and cation exchange) need to be taken into account simultaneously. This is currently the work in progress.

7. Conclusions and outlook

In this study, a new coupled code GeoSys-GEM, which is capable of simulating reactive transport processes in complex aqueous–solid solution systems is presented. The codes are coupled at source code level, which provides a maximum efficiency for simulation and software maintenance. The coupling of the multi-component mass-transport code GeoSys with the chemical solver GEMIPM2K is verified by a widely used dissolution–precipitation benchmark test. Further tests and benchmarks are planned. Especially a comparison between LMA and GEM methods will be interesting for systems that involve highly redox sensitive phases and elements, as code comparison for such systems very often gives highly divergent results (De Windt et al., 2003).

The Gibbs Energy Minimization (GEM) method can find chemical equilibrium between several non-ideal and ideal solutions, and many pure condensed phases. Stable phases are found in a theoretically sound way within a single GEM run. This feature of GEM is important especially for the investigation of aqueous–solid solution systems. Such a chemical system is expected to exist e.g. at ce-

ment–clay interfaces that are common in designs for nuclear waste repositories. In the solid solution example, it was demonstrated that the SO_4^{2-} ingression into a carbonate-containing bentonite may significantly enhance the fixation of mobile Ra. This is caused by the re-partitioning of Ra from carbonate into sulfate solid solutions. In safety assessment of waste repositories, a linear K_D concept is often used to predict retardation during the transport of radionuclides. To be conservative, and in order not to overestimate the retardation, minimum or even zero-K_D values are chosen. However, these values do not always reflect properly the chemical buffering capacity of the back-filling material (i.e. compacted bentonite or bentonite–sand mixtures).

With the new reactive transport modeling code presented in this paper, it was possible to predict the transport of radionuclides more precisely, if provided with detailed chemical composition of the material. The ability to model complex interactions is a necessary prerequisite for the proper analysis of the experimental investigation of the transport experiments in such systems. Moreover, with this new simulation tool, it is possible to enhance the retardation effect of solid solutions by optimizing the chemical composition in the buffer system, i.e. by adjusting the Ba, Sr and SO_4^{2-} contents. The new tool will not replace existing performance assessment codes, but it should provide the possibility of gaining a more detailed system understanding and improving the concept used in performance assessment.

A disadvantage of reactive transport modeling using the GEM approach is that it is computationally more expensive than that with LMA based codes. Therefore, future work will also be focused on improving the computational efficiency of numerical algorithms.

Appendix A

A.1. Chemical system setups for calcite–dolomite and radium Aq-SS examples

See Tables A1–A4.

References

Bear, J., Bachmat, Y., 1990. Introduction to Modeling of Transport Phenomena in Porous Media. Springer, Berlin.

Bethke, C.M., 1996. Geochemical Reaction Modeling – Concepts and Applications. Oxford University Press, New York.

Bradbury, M.H., Baeyens, B., 2003. Near field sorption data bases for compacted MX-80 bentonite for performance assessment of a high-level radioactive waste repository in Opalinus clay host rock, PSI Bericht Nr. 03-07, Nagra NTB 02-18. Paul Scherrer Institut, Villigen Switherland. ISSN 1019-0643.

Bradbury, M.H., Baeyens, B., 2004. Project Opalinus Clay. Sorption data bases for Opalinus clay influenced by a high pH plume, PSI Bericht Nr. 04-07, Nagra NTB 03-12, Paul Scherrer Institut, Villigen Switzerland, ISSN 1019-0643.

Bruno, J., Bosbach, D., Kulik, D., Navrotsky, A., 2007. Chemical thermodynamics of solid solutions of interest in radioactive waste management: a state-of-the art report. In: Mompean, F.J., Illemassene, M., Perrone, J. (Eds.), Chemical Thermodynamics Series, vol. 10. OECD, Paris, pp. 6–100.

Clauser, C. (Ed.), 2003. Numerical Simulation of Reactive Flow in Hot Aquifers (SHEMAT and Processing SHEMAT). Springer, Berlin.

Cleverley, J.S., Hornby, P., Poulet, T., 2006. Reactive transport modelling in hydrothermal systems using the Gibbs minimisation approach. Geochim. Cosmochim. Acta 70, A106.

Davies, C.W., 1962. Ion Association. Butterworths, Washington, DC.

De Windt, L., Burnol, A., Montarnal, P., van der Lee, J., 2003. Intercomparison of reactive transport models applied to UO2 oxidative dissolution and uranium migration. J. Contam. Hydrol 61, 303–312.

Doerner, H.A., Hoskins, W.M., 1925. Co-precipitation of radium and barium sulfates. J. Am. Chem. Soc. 47, 662–675.

Engesgaard, P., Kipp, K.L., 1992. A geochemical transport model for redox-controlled movement of mineral fronts in groundwater-flow systems – a case of nitrate removal by oxidation of pyrite. Water Resour. Res. 28, 2829–2843.

Fetter, C.W., 1999. Contaminant Hydrogeology. Prentice Hall, Upper Saddel River, NJ.

Gaucher, E.C., Blanc, P., 2006. Cement/clay interactions – a review: experiments, natural analogues and modeling. Waste Manage. 26, 776–788.

Germann, F.E.E., 1921. Adsorption of radium by barium sulfate. J. Am. Chem. Soc. 43, 1615–1621.

Glynn, P.D., 2000. Solid solution solubilities and thermodynamics: sulfates, carbonates and halides. In: Jambor, J.L., Nordstrom, D.K. (Eds.), Sulfate Minerals: Crystallography, Geochemistry and Environmental Significance. Rev. Mineral. Geochem. 40, pp. 481–511.

Glynn, P.D., 2003. Modeling Np and Pu transport with a surface complexation model and spatially variant sorption capacities: implications for reactive transport modeling and performance assessments of nuclear waste disposal sites. Comput. Geosci. 29, 331–349.

Grandia, F., Merino, J., Bruno, J., 2008. Assessment of the radium-barium co-precipitation and its potential influence on the solubility of Ra in the near-field. SKB Technical Report TR-08-07. Swedish Nuclear Fuel and Waste Management Co. Stockholm, Sweden.

Guimarães, L., Gens, A., Olivella, S., 2007. Coupled thermo-hydro-mechanical and chemical analysis of expansive clay subjected to heating and hydration. Transport Porous Med. 66, 341–372.

Hummel, W., Berner, U., Curti, E., Pearson, F.J., Troenen, T., 2002. The Nagra/PSI Chemical Thermodynamic Data Base 01/01. Universal Publishers. <http://les.web.psi.ch/TDBbook/index.htm>.

Karpov, I.K., Chudnenko, K.V., Kulik, D.A., 1997. Modeling chemical mass transfer in geochemical processes: thermodynamic relations, conditions of equilibria, and numerical algorithms. Am. J. Sci. 297, 767–806.

Karpov, I.K., Chudnenko, K.V., Kulik, D.A., Avchenko, O.V., Bychinski, V.A., 2001. Minimization of Gibbs free energy in geochemical systems by convex programming. Geochem. Int. 39, 1108–1119.

Kolditz, O., Bauer, S., 2004. A process-orientated approach to compute multi-field problems in porous media. Int. J. Hydroinformat. 6, 225–244.

Kühn, M., Gessner, K., 2006. Reactive transport model of silicification at the Mount Isa copper deposit, Australia. J. Geochem. Explor. 89, 195–198.

Kulik, D.A., 2006a. Classic adsorption isotherms incorporated in modern surface complexation models: implications for sorption of actinides. Radiochim. Acta 94, 765–778.

Kulik, D.A., 2006b. Dual-thermodynamic estimation of stoichiometry and stability of solid solution end members in aqueous–solid solution systems. Chem. Geol. 225, 189–224.

Kulik, D., Berner, U., Curti, E., 2004. Modelling chemical equilibrium partitioning with the GEMS-PSI code. In: Smith, B., Gschwend, B. (Eds.), PSI Scientific Report 2003/Volume IV, Nuclear Energy and Safety. Paul Scherrer Institut, Villigen, pp. 109–122.

Kulik, D.A., Dmytrieva, S.V., Chudnenko, K.V., Thoenen, T., Wagner, Th., 2008. GEM-Selektor (GEMS-PSI) – Research Package for Thermodynamic Modeling of Aquatic (Geo)chemical Systems by Gibbs Energy Minimization. Paul Scherrer Institut, <http://gems.web.psi.ch/>.

Lagneau, V., Lagneau, A., Catalette, H., 2005. Reactive transport modeling of CO2 sequestration in deep saline aquifers. Oil Gas Sci. Technol. – Rev. IFP 60, 231–247.

Langmuir, D., Riese, A.C., 1985. The thermodynamic properties of radium. Geochim. Cosmochim. Acta 49, 1593–1601.

MacQuarrie, K.T.B., Mayer, K.U., 2005. Reactive transport modeling in fractured rock: a state-of-the-science review. Earth-Sci. Rev. 72, 189–227.

Martin, P., Akber, R.A., 1999. Radium isotopes as indicators of adsorption–desorption interactions and barite formation in groundwater. J. Envrion. Radioact. 46, 271–286.

Martin, A.J., Crusius, J., Jay McNee, J., Yanful, E.K., 2003. The mobility of radium-226 and trace metals in pre-oxidized subaqueous uranium mill tailings. Appl. Geochem. 18, 1095–1110.

Mayer, K.U., Benner, S.G., Frind, E.O., Thornton, S.F., Lerner, D.N., 2002a. Multicomponent reactive transport modeling of natural attenuation at the Four Ashes Research Site, UK. In: Thornton, S.F., Oswald, S.E. (Eds), Groundwater Quality: Natural and Enhanced Restoration of Groundwater Pollution. IAHS Publication, no. 275, pp. 479–484.

Mayer, K.U., Frind, E.O., Blowes, D., 2002b. Multicomponent reactive transport modeling in variably saturated porous media using a generalized formulation for kinetically controlled reactions. Water Resour. Res. 38, 1174.

Nagra (National Cooperative for the Disposal of Radioactive Waste) 2002. Nagra Technical Report 02-06: Models Codes and Data for Safety Assessment. Wettingen, Switzerland.

Parkhurst, D.L., Appelo, C.A.J., 1999. User's guide to PHREEQC (version 2) – a computer program for speciation, batch-reaction, one-dimensional transport, and transport, and inverse geochemical calculations. USGS Techniques and Methods 6-A11. Reston, Virginia. USGS.

Pfingsten, W., 1994. Modular coupling of transport and chemistry: theory and model applications. PSI-Bericht. Paul Scherrer Institute, Villigen. pp. 15–94.

Pfingsten, W., 2002. Experimental and modeling indications for self-sealing of a cementitious L&ILW repository by calcite precipitation. Nucl. Technol. 140, 63–82.

Pfingsten, W., Paris, B., Soler, J.M., Mäder, U.K., 2006. Tracer and reactive transport modelling of the interaction between high-pH fluid and fractured rock: field and laboratory experiments. J. Geochem. Explor. 90, 95–113.

Powell, R., Holland, T.J.B., 1993. On the formulation of simple mixing models for complex phases. Am. Mineral. 78, 1174–1180.

Prommer, H., 2002. A Reactive Multicomponent Transport Model for Saturated Porous Media, User's Manual Version 1.0, Contaminated Land Assessment and Remediation Research Centre. The University of Edinburgh, UK.

Pruess, K., Garcia, J., Kovscek, T., Oldenburg, C., Rutqvist, J., Steefel, C., Xu, T., 2004. Code intercomparison builds confidence in numerical simulation models for geological disposal of CO2. Energy 29, 1431–1444.

Reardon, E.J., 1981. Kd's – can they be used to describe reversible ion sorption reactions in contaminant migration? Ground Water 19, 279–286.

Schäfer, D., Schäfer, W., Kinzelbach, W., 1998. Simulation of reactive processes related to biodegradation in aquifers: 1. Structure of the three-dimensional reactive transport model. J. Contam. Hydrol. 31, 167–186.

Soler, J.M., 2003. Reactive transport modeling of the interaction between a high-pH plume and a fractured marl: the case of Wellenberg. Appl. Geochem. 18, 1555–1571.

Soler, J.M., Mäder, U.K., 2007. Mineralogical alteration and associated permeability changes induced by a high-pH plume: modeling of a granite core infiltration experiment. Appl. Geochem. 22, 17–29.

Spycher, N.F., Sonnenthal, E.L., Apps, J.A., 2003. Fluid flow and reactive transport around potential nuclear waste emplacement tunnels at Yucca Mountain, Nevada. J. Contam. Hydrol., 653–673.

Steefel, C.I., De Paolo, D.J., Lichtner, P.C., 2005. Reactive transport modeling: an essential tool and a new research approach for the Earth sciences. Earth Planet. Sci. Lett. 240, 539–558.

Van der Lee, J., De Windt, L., Lagneau, V., Goblet, P., 2003. Module-oriented modeling of reactive transport with HYTEC. Comput. Geosci. 29, 265–275.

Van Loon, L.R., Jakob, A., 2005. Evidence for a second transport porosity for the diffusion of tritiated water (HTO) in a sedimentary rock (Opalinus Clay – OPA): application of through and out-diffusion techniques. Transport Porous Med. 61, 193–214.

Wang, W., Kolditz, O., 2007. Object-oriented finite element analysis of thermo-hydro-mechanical (THM) problems in porous media. Int. J. Numer. Meth. Eng. 69, 162–201.

Wersin, P., Schwyn, B., 2004. Project Opalinus Clay: Integrated Approach for the Development of Geochemical Databases Used for Safety Assessment Nagra Technical Report NTB 03-06 NAGRA Wettingen, Switzerland.

Xie, M., Bauer, S., Kolditz, O., Nowak, T., Shao, H., 2006. Numerical simulation of reactive processes in an experiment with partially saturated bentonite. J. Contam. Hydrol. 83, 122–147.

Xie, M., Wang, W., Jonge, J.D., Kolditz, O., 2007. Numerical modelling of swelling pressure in unsaturated expansive elasto-plastic porous media. Transport Porous Med. 66, 311–339.

Xu, T., Pruess, K., 2001. Modeling multiphase non-isothermal fluid flow and reactive geochemical transport in variably saturated fractured rocks: 1 methodology. Am. J. Sci. 301, 16–33.

Xu, T., Apps, J.A., Pruess, K., 2004. Numerical simulation of CO2 disposal by mineral trapping in deep aquifers. Appl. Geochem. 19, 917–936.

Yabusaki, S.B., Steefel, C.I., Wood, B.D., 1998. Multidimensional, multicomponent, subsurface reactive transport in nonuniform velocity fields: code verification

using an advective reactive streamtube approach. Journal of Contaminant Hydrology 30, 299–331.

Yeh, G.-T., Tripathi, V.S., 1998. A model for simulating transport of reactive multispecies components: model development and demonstration. Water Resour. Res. 27, 3075–3094.

Zhu, C., 2004a. Coprecipitation in the barite isostructural family: 1. binary mixing properties. Geochim. Cosmochim. Acta 68, 3327–3337.

Zhu, C., 2004b. Coprecipitation in the barite isostructural family: 2. numerical simulations of reactions and mass transport. Geochim. Cosmochim. Acta 68, 3339–3349.

Enclosed Publication

[EP4] **Haibing Shao**, Dmitrii A. Kulik, Urs Berner, Georg Kosakowski and Olaf Kolditz (2009): Modeling the competition between solid solution formation and cation exchange on the retardation of aqueous radium in an idealized bentonite column, *Geochemical Journal* 43(6), e37-e42.

EXPRESS LETTER

Modeling the competition between solid solution formation and cation exchange on the retardation of aqueous radium in an idealized bentonite column

HAIBING SHAO,[1,3]* DMITRII A. KULIK,[2] URS BERNER,[2] GEORG KOSAKOWSKI[2,4] and OLAF KOLDITZ[1,3]

[1]Department of Environmental Informatics, UFZ-Helmholtz Centre for Environmental Research,
Permoserstr. 15, 04318 Leipzig, Germany
[2]Department of Nuclear Energy and Safety Research (NES), Waste Management Laboratory (LES), Paul Scherrer Institut,
CH-5232 Villigen PSI, Switzerland
[3]Applied Environmental System Analysis, Technische Universitaet Dresden, Helmholtzstraße 10, D-01069 Dresden, Germany
[4]University of Tübingen, Sigwartstraße 10, D-72076 Tübingen, Germany

Clays and clay rocks are considered viable geotechnical barriers in radioactive waste disposal. One reason for this is the propensity for cation exchange reactions in clay minerals to retard the migration of radionuclides. Although another retardation mechanism, namely the incorporation of radionuclides into sulfate or carbonate solid solutions, has been known for a long time, only recently has it been examined systematically. In this work, we investigate the competitive effect of both mechanisms on the transport of radium (Ra) in the near-field of a low- and intermediate level nuclear waste repository. In our idealized geochemical model, numerical simulations show that barium (Ba) and strontium (Sr) needed for Ra sulfate solid solutions also partition to the cation exchange sites of montmorillonite (Mont), which is the major mineral constituent of bentonite that is used for tunnel backfill. At high Mont content, most Ra tends to attach to Mont, while incorporation of Ra in sulfate solid solutions is more important at low Mont content. To explore the effect of the Mont content on the transport of radium, a multi-component reactive transport model was developed and implemented in the scientific software OpenGeoSys-GEM. It was found that a decrease of fixation capacity due to low Mont content is compensated by the formation of solid solutions and that the migration distance of aqueous Ra is similar at different Mont/water ratios.

Keywords: reactive transport, solid solutions, cation exchange, bentonite, radioactive waste repository, montmorillonite, OpenGeoSys, GEM-Selector

INTRODUCTION

Bentonite, comprised mainly of the clay mineral montmorillonite (Mont), is widely used in geotechnical applications to isolate hazardous wastes. In radioactive waste repositories, pure bentonite is suggested as a buffer material to seal waste canisters, while bentonite-sand mixtures are utilized as backfill for access tunnels (Nagra, 2002). The understanding of thermo-hydro-mechanical (THM) and chemical (C) processes in engineered barrier systems is of crucial importance for the long-term safety of subsurface waste repositories (Stephansson *et al.*, 2004; Wallner *et al.*, 2007; Rutqvist *et al.*, 2009). In such geotechnical systems, chemical interactions between radionuclides and clay minerals determine the retention

and possible release of radionuclides from the repository to the biosphere. Among all chemical processes, cation exchange (Reardon, 1981), surface complexation (Glynn, 2003) and the formation of solid solutions (Zhu, 2004) are considered to contribute most significantly to the retardation of radionuclides. Cation exchange reactions in bentonite, and in more general form, on clay minerals, have been well investigated (Bradbury and Baeyens, 1997; Huertas *et al.*, 2001; Fernandez *et al.*, 2004). The effect of solid solutions has also attracted some recent attention. Martin *et al.* (2003) evaluated experimentally the mobility of radium, and reported that dissolution of a $(Ba,Ra)SO_4$ solid solution controls the aqueous concentration of radium and barium in pore water released from nuclear waste repositories. Zhu (2004) provided a compilation of mixing parameters for Ra and Ba sulfate isostructural family. Grandia *et al.* (2008) found that the solubility of Ra in a repository environment should be in the range of 10^{-11} mol/L, in the presence of $(Ba,Ra)SO_4$

*Corresponding author (e-mail: haibing.shao@ufz.de)

co-precipitation, and that it will be three orders of magnitude higher if only a pure $RaSO_4$ phase is considered. Shao *et al.* (2009a) numerically analyzed non-ideal aqueous-solid solution systems with both Ba–Sr–Ra carbonate and Ba–Sr–Ra sulfate formations. They concluded that the re-partitioning of radium from carbonate to sulfate may cause a strong retardation effect on Ra. A shortcoming of their study is that the cation exchange process was not considered in their reactive transport model. In this work, we further develop their model and investigate how the radium-containing solid solutions may interact with the cation exchange in bentonite, and how these interactions may influence the transport of Ra.

MODEL

Governing equations

In this work, the reactive transport of chemical components is governed by an advection-dispersion mass balance, supplemented by source/sink from chemical reactions occurring at equilibrium. These relationships are respectively (Bear and Bachmat, 1990),

$$\begin{cases} \dfrac{\partial C_i}{\partial t} = -\nabla(vC_i) + \nabla(D_i \nabla C_i) + Q_i \\ \dfrac{\partial C_i}{\partial t} = \Gamma_i(C_1 \cdots C_m), \end{cases} \quad i = 1, 2, \ldots, m, \quad (1)$$

where C_i denotes the molar concentration of the i-th species of a m multi-species system; v is the pore water velocity of groundwater flow; D_i is the diffusion-dispersion coefficient of component i; Q_i is a source/sink term and $\Gamma_i(C_i \cdots C_m)$ is a source/sink term of species i due to equilibrium chemical reactions with other species. The above governing equations are simulated using the multicomponent reactive transport code OpenGeoSys-GEM. It employs the sequential non-iterative approach to couple the mass transport code OpenGeoSys (Wang *et al.*, 2009) with GEMIPM2K (Kulik *et al.*, 2008). For each time step, the advection-dispersion equation (ADE) is calculated first, and concentrations for each species are passed to the chemical solver, which calculates local equilibrium at each grid node. Resultant concentrations of chemical species are then passed to the subsequent time step. Details regarding code development and verification can be found in Shao *et al.* (2009a).

Representation of cation exchange processes

In reactive transport codes, cation exchange processes are usually calculated assuming that the clay mineral is represented by an X-"ligand" initially occupied with Na^+. We implemented a more chemically plausible solid solution model of ion exchange in clay. For such a model it is necessary to formulate each end member with exactly one negative charge per formula unit of *Mont*, according to the following exchange reaction

$$\frac{1}{2}M^{2+} + NaMont \Leftrightarrow Na^+ + M_{0.5}Mont. \quad (2)$$
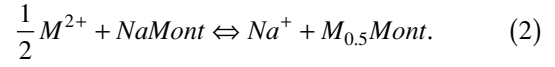
The corresponding equilibrium constant K_G (expressed in the Gapon convention in mole fractions) for the ideal mixing is

$$K_G = \frac{x_{M_{0.5}Mont}}{x_{NaMont}} \cdot \frac{a_{Na^+,aq}}{a_{M^{2+},aq}^{0.5}}, \quad (3)$$

where a stands for the activity of aqueous cation and x is the mole fraction of corresponding mineral end member. It is numerically the same as a Gaines-Thomas selectivity coefficient K^c_{GT} (Gaines and Thomas, 1953) or Vanselow (1932) selectivity coefficient K^c_V for the mono-to-monovalent exchange, but is related to them for mono-to-divalent exchange as

$$K_G = K_V^{0.5} = \left(K^c_{GT,M} \cdot \frac{\sum n}{2\sum zn} \right)^{0.5}. \quad (4)$$

Here $\sum n$ is the sum of the mole amounts and $\sum zn$ is the sum of equivalents of ions present on the exchanger.

Geochemical model

The geochemical model is constructed from compositional data on FEBEX bentonite (Huertas *et al.*, 2001; Fernandez *et al.*, 2004), which contains approximately 92% smectite. In order to focus on the competition of cation exchange and solid solutions, we do not consider the redox effect in our chemical system. Therefore the smectite is represented by a pure montmorillonite formula unit (referred to as Mont, $[MgAl_5(Si_4O_{10})_3(OH)_6]^-$) without any Fe. From this basis formula, a sodium montmorillonite with a composition of $Na[MgAl_5(Si_4O_{10})_3(OH)_6]$ (referred to as Na-Mont) was first set up as a dependent component. Other cation-exchange components, including K, Ca, Mg, Ba, Sr, and Ra end members, were defined using exchange reactions with Na-Mont in form of Eq. (2). An ideal solid solution phase was composed of K-, Ca-, Mg-, Ba-, Sr-, and Ra-Mont as end members, and exchange coefficients were converted from K^c_{GT} values given by Fernandez *et al.* (2004). The exchange equations and corresponding coefficients are listed in Table 1.

Because pore water composition for highly compacted bentonite is difficult to estimate, most available pore water

Table 1. Selectivity coefficients K^c_{GT}, equilibrium constants K_G for ion-exchange reactions, and standard Gibbs energies of end members representing the montmorillonite clay phase (-Mont stands for $[MgAl_5(Si_4O_{10})_3(OH)_6]$) at 298.15 K

End members	Reactions	K^c_{GT}*	K_G	$G°_{298}$ (J/mol)
Na-Mont				−15908267
K-Mont	$K^+ + Na\text{-}Mont \Leftrightarrow Na^+ + K\text{-}Mont$	10.6	10.6	−15934700
$Ca_{1/2}$-Mont	$1/2Ca^{2+} + Na\text{-}Mont \Leftrightarrow Na^+ + Ca_{1/2}\text{-}Mont$	12.8	2.2	−15924343
$Mg_{1/2}$-Mont	$1/2Mg^+ + Na\text{-}Mont \Leftrightarrow Na^+ + Mg_{1/2}\text{-}Mont$	10.7	2.0	−15874717
$Sr_{1/2}$-Mont	$1/2Sr^{2+} + Na\text{-}Mont \Leftrightarrow Na^+ + Sr_{1/2}\text{-}Mont$	12.8	2.5	−15930451
$Ba_{1/2}$-Mont	$1/2Ba^{2+} + Na\text{-}Mont \Leftrightarrow Na^+ + Ba_{1/2}\text{-}Mont$	12.8**	2.5**	−15928924
$Ra_{1/2}$-Mont	$1/2Ra^{2+} + Na\text{-}Mont \Leftrightarrow Na^+ + Ra_{1/2}\text{-}Mont$	12.8**	2.5**	−15929280

According to measurements by Fernandez et al. (2004).
**Assumed to be the same as for Sr.*

cation profiles are extrapolated from batch extraction tests. In this work, Mont phase composition is based on the initial cation loadings reported by Fernandez *et al.* (2004). The model system includes mineral phases of Mont, quartz, kaolinite and gibbsite, together with 3.2 mMol/L of NaCl to match the chloride inventory of FEBEX bentonite. An excess atmosphere with $\log P_{CO2}$ of −3.5 is built into the system. GEM simulation results were compared with the data from batch experiments at a solid/liquid ratio of 0.147. Initial guesses of $G°_j$ values were first obtained from thermodynamic databases (Bechtel SAIC Company, 2004; CTDP, 2009), or estimated by analytical method (Mattigod and Sposito, 1978). They are later adjusted such that trace amount of kaolinite precipitated in the presence of Mont and quartz, while Gibbsite remained undersaturated. Next, the solid/liquid ratio was varied from 0.147 to 25. The simulated pH value decreased from 8.6 to about 7.5, and dissolved Al drops from 3×10^{-7} to less than 4×10^{-8} molal at a solid/liquid ratio of 4.0. For higher solid/liquid ratios, the pore water composition is dominated by cation occupancies on clay and remained nearly constant. A more improved calibration would require comparison with measured Al concentrations, unfortunately such information was not provided by Fernandez *et al.* (2004).

Additionally, a sensitivity analysis was performed by increasing the stability of all Mont end members, i.e., decreasing their $G°_{298}$ values simultaneously with 30 kJ/mol. In terms of aqueous primary species, only the behavior of Al was noticeably altered. Total dissolved Al decreased to 1×10^{-8} molal, while kaolinite disappeared and gibbsite remained undersaturated. The pH and other dissolved cations remained nearly unaffected. From this we conclude that the ion distribution between ion exchanger (clay) and aqueous solution is largely unaffected by the solubility of the Mont phase as long as this phase is stable relative to gibbsite and kaolinite. Hence, we accepted the $G°_{298}$ values for Na-Mont. $G°_{298}$ values for all

other end-members are calculated using exchange reactions with Na-Mont. The exchange coefficients and subsequent $G°_{298}$ values are listed in Table 1.

After calibrating the Mont phase model, four non-ideal solid solutions, $(Ca,Ba,Sr)CO_3$, $(Ra,Ba,Sr)CO_3$, $(Ra,Ba,Sr)SO_4$ and $(Ra,Sr,Ba)SO_4$, were added to the definition of the chemical system. We assumed that Ba and Sr tend to form separate solid solution phases, while calcium is distributed between calcite and gypsum in the presence of sulfate. The $CaSO_4$ containing solid solutions were excluded from the present setup. Instead, the Ra–Ba–Sr sulfate system was set as two solid solution phases, one mainly celestite–$RaSO_4$ and another mainly barite–$RaSO_4$. Gypsum, magnesite and quartz were included as pure mineral phases. Details regarding the chemical system definition are provided in a separate Excel file (see supporting information Shao *et al.*, 2009b). During pre-processing, bentonite is usually exposed to the air, and the bentonite pore water alkalinity is then controlled by the partial pressure of CO_2. To reflect this, the system is maintained in equilibrium with atmospheric air so that the $\log P_{CO2}$ value is consistent at −3.5. With this setting, our calculated pH value (7.51) is similar to the one measured by Fernandez *et al.* (2004). A different $\log P_{CO2}$ value would be required to represent a closed and fully saturated repository (e.g., to −2.2 for typical groundwater). In FEBEX bentonite, the initial bentonite (solid)/liquid ratio is 19 kg/kg (Fernandez *et al.*, 2004). However, bentonite can be mixed with different proportions of sand for backfilling the access tunnels. This also results in a change of the solid/liquid ratio. For example, the tunnel backfilling material may contain 80 wt. % of sand and 20 wt. % of bentonite (that contains 75% Mont) for the dry material. At a porosity of 0.3, the solid/liquid ratio for Mont/water is about 1.35. In our model, we fix the amount of water at 1 kg, and scale the given amount of Mont proportionally. Total system volume is conserved through the addition of quartz, thus representing different propor-
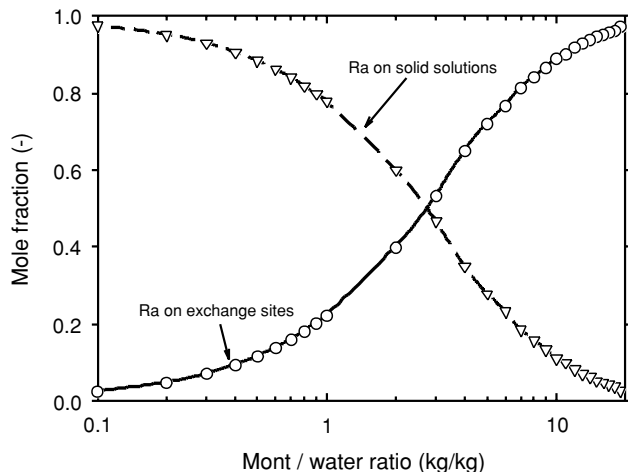
Fig. 1. Influence of Mont/water ratio on the radium distribution among cation exchange sites and solid solution formations.

Fig. 2. Aqueous phase radium profile after 1000 years, with clay content adjusted by Mont/water ratio of 10, 1.0 and 0.1 kg/kg.

tions of sand in the Mont-sand backfill. The Mont/water ratio was gradually lowered from 19 to 0.1, but with 2×10^{-7} M of Ra^{2+} remaining in the system. The Ra distribution between sulfate solid solutions and Mont phase was calculated in order to investigate the influence of clay content on retention mechanisms of Ra.

Model geometry and numerical setup

To demonstrate the impact of competition between the two mechanisms on the transport of mobile radium, we considered a simplified 5 m long one-dimensional column model, representing a tunnel connected to an intermediate level radioactive waste repository. Sensitivity analyses were conducted to ensure appropriate spatial and temporal discretizations. For a constant time step setting, grid sizes of 0.05, 0.025, and 0.0125 m were tested, with no observable influence on the radium profile. Therefore we have chosen a spatial discretization of 0.05m. On the other hand, an inappropriate choice of the time step size has a much bigger impact on the penetration depth of radium. An improperly calibrated time step (too large) results in overestimation of transport distance for radium. After several tests, we found that, at the conditions investigated here, the simulation result converges accurately for time steps equal to or smaller than 1×10^6 s (11.6 days). If we accept that time step size is governed theoretically by a relationship of the form $\Delta t = A * \Delta x^2 / D_e$, where D_e is effective diffusion coefficient, then these results suggest A is approximately 0.1 for the conditions explored here. Therefore, all of our reactive transport simulations adopt this setting.

Within a waste repository, the hydraulic gradient is usually flat and the bentonite has a very low hydraulic conductivity (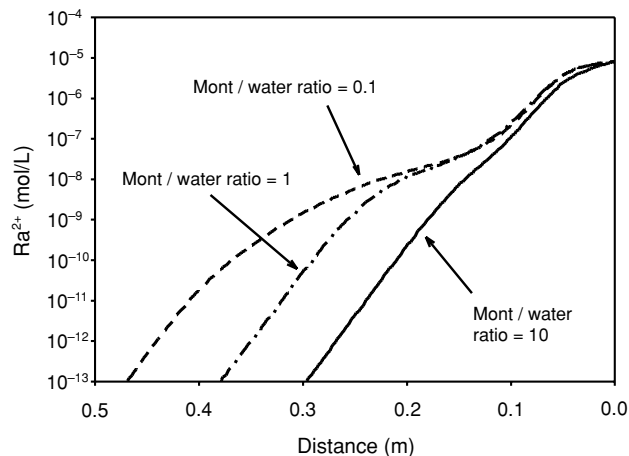up to 5.0×10^{-11} m/s), so that transport of aqueous species in the tunnel will be dominated by diffusion. We used for all species the same effective diffusion coefficient of 2.0×10^{-10} m^2/s. With a cation accessible porosity of 0.12 for a highly compacted bentonite (Nagra, 2002), the pore diffusion coefficient for all mobile chemical components is set to 1.7×10^{-9} m^2/s. The temperature and pressure were assumed to be 25°C and 1 bar, respectively. The imposed chemical boundary condition is a constant radium concentration, representing the leakage of the radionuclides out of the waste matrix at the right end of the tunnel backfill. The source term, i.e., aqueous concentration of Ra^{2+}, was fixed at 1.0×10^{-6} mol/L. Such a radium concentration can be estimated in the cement backfill material for intermediate level waste (Nagra, 2002). To keep the model simple, the radioactive decay of radium was not considered.

RESULTS

Figure 1 depicts the partitioning of Ra between the ion exchanger and solid solutions subject to the amount of clay in the system (in terms of the Mont/water ratio). At a Mont/water ratio of 19, bentonite is in a compacted form, which is used to seal the high level waste canister. Cation exchange sites in the Mont phase attract most of the Ba and Sr in the system so that, while carbonate and sulfate are abundant in the aqueous phase, insufficient Ba and Sr restrains the formation of Ra sulfate solid solutions. Sufficient Ba and Sr remain for sulfate formation only when the Mont/water ratio is lowered to approximately unity. Despite the fact that the limited clay content lowers the total amount of Ra bound in the Mont phase, the sulfate solid solutions compensate for this and provide a secondary fixation mechanism. When the ratio
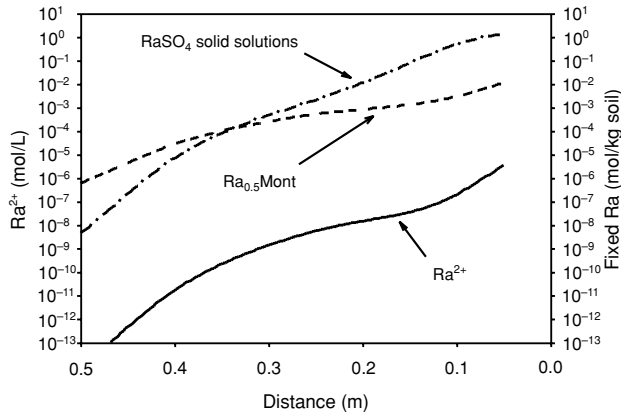
Fig. 3. Amount of Ra distributed between sulfate solid solutions, clay cation exchange, and pore water. Simulation results after 1000 years, at Mont/water ratio of 0.1.

is about 0.1, only a minor proportion of Ra is retained in the montmorillonite, and the incorporation in sulfate solid solution becomes the major retardation mechanism for the transport of radium.

Figure 2 shows the concentration profile for aqueous Ra^{2+} after 1000 years. The shape and extension of the profiles are similar at three different Mont/water ratios of 0.1, 1.0, and 10 kg/kg. The aqueous radium concentrations is lowered by 2~3 orders of magnitude, as soon as it diffuses into the column. Both sulfate and Mont solid solutions provide the capacity to fix radium. Figure 3 shows the amount of radium in solution and on both types of fixation sites, at a Mont/water ratio of 0.1. The sulfate solid solution provides the major fixation capacity, due to the low Mont content in the solid phase. These results agree well with the case study presented by Martin *et al.* (2003), where Ra transport was monitored in a sandy/gravel aquifer contaminated by leakage from a mining waste deposit.

DISCUSSIONS

In order to simulate cation exchange reactions, models based on the Law of Mass Action (LMA) such as PhreeqC (Parkhurst and Appelo, 1999, Xie *et al.*, 2004) and MINSORB (Bradbury and Baeyens, 1997) are often used. In such models, the real stoichiometry of clay minerals (Al, Mg, Si, H and O) is usually not included, and is replaced by "sorption site capacities". However, the GEM-Selektor package based on Gibbs Energy Minimization simplifies the thermodynamic consideration of cation exchange reactions in the form of solid solutions with full stoichiometry of the clay mineral, whose solubility can be calibrated according to cation profiles measured in batch extraction tests. In the experiment of Fernandez *et*

al. (2004), it was observed that the measured aqueous concentrations of K, Mg, Ca and Sr increase together with the S/L ratio (table 5 in their paper), while the pH of the aqueous solution decreased accordingly. These phenomena are both qualitatively reproduced in our model.

In this work, the equilibrium exchange constant for Ra was assumed to be the same as for Sr. To test the sensitivity of this parameter, we decreased the stability of the exchange component $Ra_{1/2}Mont$, by increasing its $G°_{298}$ value 7000 J/mol (17 times weaker K_G). This correction is well above the range of selectivity coefficients for alkali earth cations on montmorillonite (Benson, 1982; Bruggenwert and Kamphorst, 1979). However, the model result basically remains the same and the trend in Fig. 1 is intact, suggesting that it is the availability of Ba, Sr, and sulfate in competition with the availability of clay ion exchange sites that govern the formation of solid solutions, rather than a particular value of the exchange constant of radium on montmorillonite. Therefore, the distribution of Ra among the clay ion exchange and the sulfate solid solution is far more influenced by the Mont/water ratio than by the value of cation exchange constant.

A comparison of the Ra profile in Fig. 2 with previous results (Shao *et al.*, 2009a) shows that the mobility of aqueous radium is considerably lower if cation exchange reactions in addition to solid solution formation is considered. Even with a limited amount of clay (Mont/water ratio of 0.1 in Fig. 3), Ra^{2+} can penetrate less than 1.5 m into the column after 1000 years. The Ra profile shown in Fig. 2 suggests that the diminishing fixation capacity of the Mont phase can be compensated for by incorporation into sulfate solid solution. However, the chemical system presented here is simplified. In a real bentonite-sand mixture, it is possible that some portion of carbonate and sulfate will be unavailable to solid solution formation and that the cation exchange reactions may be influenced by the competition with other cations.

SUMMARY

In this work, the impact of competition between the cation exchange on montmorillonite and the formation of sulfate solid solutions on the retardation of radium is investigated. Both mechanisms are built in an idealized geochemical model and simulation shows that both of them can fix the mobile radium into the solid phase. The distribution of radium in sulfate solid solutions is mainly influenced by the amount of Ba and Sr available, which can also undergo cation exchange on clay minerals like montmorillonite. At high clay content, the cation exchange dominates the whole system and is the major process that retards the transport of Ra, whereas at low clay content, the incorporation in sulfate solid solutions fixes most of the Ra.

REFERENCES

Bear, J. and Bachmat, Y. (1990) *Introduction to Modeling of Transport Phenomena in Porous Media*. Springer, Berlin, 584 pp.

Bechtel SAIC Company (2004) *Qualification of Thermodynamic Data for Geochemical Modeling of Mineral-Water Interactions in Dilute Systems*. U.S. Department of Energy, DOE Scientific and Technical Information.

Benson, L. (1982) A tabulation and evaluation of ion exchange data on smectites. *Environ. Geol.* **4**(1), 23–29.

Bradbury, M. H. and Baeyens, B. (1997) A mechanistic description of Ni and Zn sorption on Na-montmorillonite Part II: modelling. *J. Contaminant Hydrol.* **27**(3), 223–248.

Bruggenwert, M. G. M. and Kamphorst, A. (1979) Chapter 5: Survey of experimental information on cation exchange in soil systems. *Developments in Soil Science*, Volume 5, Part 2 (Bolt, G. H., ed.), 141–203, Elsevier.

CTDP (2009) Common Thermodynamic Database Project. Available at http://www.ctdp.org/

Fernandez, A. M., Baeyens, B., Bradbury, M. and Rivas, P. (2004) Analysis of the porewater chemical composition of a Spanish compacted bentonite used in an engineered barrier. *Phys. Chem. Earth* **29**(1), 105–118.

Gaines, G. L. and Thomas, H. C. (1953) Adsorption studies on clay minerals. II. A formation of the thermodynamics of exchange adsorption. *J. Chem. Phys.* **21**(4), 714–718.

Glynn, P. (2003) Modeling Np and Pu transport with a surface complexation model and spatially variant sorption capacities: implications for reactive transport modeling and performance assessments of nuclear waste disposal sites. *Comput. Geosci.* **29**(3), 331–349.

Grandia, F., Merino, J. and Bruno, J. (2008) Assessment of the radium-barium co-precipitation and its potential influence on the solubility of Ra in the near-field. SKB Technical Report TR-08-07, Swedish Nuclear Fuel and Waste Management Co, Stockholm.

Huertas, F. J., Carretero, P., Delgado, J., Linares, J. and Samper, J. (2001) An experimental study on the ion-exchange behavior of the smectite of Cabo de Gata (Almería, Spain): FEBEX bentonite. *J. Colloid Interface Sci.* **239**(2), 409–416.

Kulik, D. A., Dmytrieva, S. V., Chudnenko, K. V., Thoenen, T. and Wagner, T. (2008) GEM-Selektor (GEMS-PSI) Research Package for Thermodynamic Modeling of Aquatic (Geo)chemical Systems by Gibbs Energy Minimization.

Paul Scherrer Institute. Available at http://gems.web.psi.ch/

Martin, A. J., Crusius, J., McNee, J. J. and Yanful, E. K. (2003) The mobility of radium-226 and trace metals in preoxidized subaqueous uranium mill tailings. *Appl. Geochem.* **18**(7), 1095–1110.

Mattigod, S. V. and Sposito, G. (1978) Improved method for estimating the standard free energies of formation ($\Delta G°_{f,298.15}$) of smectites. *Geochim. Cosmochim. Acta* **42**(12), 1753–1762.

Nagra (2002) Models, Codes and Data for Safety Assessment. Nagra Technical Report 02-06, Swiss National Cooperative for the Disposal of Radioactive Waste, Wettlingen, Switzerland.

OpenGeoSys (2009) www.opengeosys.net

Parkhurst, D. L. and Appelo, C. A. (1999) *User's guide to phreeqc (version 2)—A computer program for speciation, batch-reaction, one-dimensional transport, and inverse geochemical calculations*. USGS Techniques and Methods 6-A11. USGS. Reston, Virginia.

Reardon, E. J. (1981) Kd's—Can they be used to describe reversible ion sorption reactions in contaminant migration? *Ground Water* **19**(3), 279–286.

Rutqvist, J., Barr, D., Birkholzer, J. T., Fujisaki, K., Kolditz, O., Liu. Q.-S., Fujita, T., Wang, W. and Zhang, C.-Y. (2009) A comparative simulation study of coupled THM processes and their effect on fractured rock permeability around nuclear waste repositories. *Environ. Geol.* **57**(6), 1347–1360.

Shao, H., Dmytrieva, S. V., Kolditz, O., Kulik, D. A., Pfingsten, W. and Kosakowski, G. (2009a) Modeling reactive transport in non-ideal aqueous-solid solution system. *Appl. Geochem.* **24**(7), 1287–1300.

Shao, H., Kulik, D. A., Berner, U., Kosakowski, G. and Kolditz, O. (2009b) Chemical system definition and input values for the reactive transport simulation. Geochemical Journal Database, TERRAPUB, http://www.terrapub.co.jp/journals/GJ/archives/

Stephansson, O., Hudson, J. and Jing, L. (eds.) (2004) Coupled thermo-hydro-mechanical-chemical processes in geosystems: Fundamentals, modelling, experiments, and applications. *Geo-Engineering Book Series*, Vol. 2, Elsevier, London, U.K., 852 pp.

Vanselow, A. P. (1932) Equilibria of the base-exchange reactions of bentonites, permutites, soil colloids, and zeolites. *Soil Sci.* **33**(2), 95–114.

Wallner, M., Lux, K.-H. and Minley, W. (eds.) (2007) *The Mechanical Behavior of Salt: Understanding of THMC Processes in Salt*. Routlegde Chapman & Hall.

Wang, W., Kosakowski, G. and Kolditz, O. (2009) A parallel finite element scheme for thermo-hydro-mechanical (THM) coupled problems in porous media. *Comput. Geosci.* **35**(8), 1631–1641.

Xie, M., Agus, S. S., Schanz, T. and Kolditz, O. (2004) An upscaling method and numerical modelling of swelling/shrinking processes in compacted bentonite/sand mixtures. *Int. J. Numer. Anal. Meth. Geomech.* **28**(15), 1479–1502.

Zhu, C. (2004) Coprecipitation in the barite isostructural family: 1. Binary mixing properties. *Geochim. Cosmochim. Acta* **68**(16), 3327–3337.